

**Dissertation zur Erlangung des Doktorgrades  
der Fakultät für Chemie und Pharmazie  
der Ludwig-Maximilians-Universität München**



**Molecular characterization of the interaction between  
peripherin-2 and opsins in rod and cone photoreceptors**

**Ong Nam Phuong Nguyen  
aus München  
2016**

## **Erklärung**

Die Dissertation wurde im Sinne von § 7 der Promotionsordnung vom 28. November 2011 von Herrn Prof. Dr. Martin Biel betreut.

## **Eidesstattliche Versicherung**

Die Dissertation wurde eigenständig und ohne unerlaubte Hilfsmittel erarbeitet.

München, den .....

.....

(Ong Nam Phuong Nguyen)

Dissertation eingereicht am: 29.01.2016

1. Gutachter: Prof. Dr. Martin Biel

2. Gutachter: PD Dr. Stylianos Michalakis

Mündliche Prüfung am: 24.02.2016

## Table of contents

<b>Table of contents</b> .....	<b>I</b>
<b>1 Introduction</b> .....	<b>1</b>
1.1 Anatomy of the retina .....	1
1.2 Anatomy of photoreceptors .....	2
1.3 Signaling transduction in photoreceptors.....	3
1.4 Topology and function of retinal opsins .....	5
1.5 Peripherin-2.....	8
1.5.1 Topology and function of peripherin-2 .....	8
1.5.2 Mutations in the PRPH2 gene .....	11
1.6 Degenerative retinal dystrophies .....	12
1.6.1 Retinitis pigmentosa .....	12
1.6.2 Adult vitelliform macular dystrophy .....	12
1.7 Aims of this study .....	14
<b>2 Materials and methods</b> .....	<b>15</b>
2.1 Chemicals, solutions and buffers.....	15
2.2 Molecular biology .....	15
2.2.1 Plasmids .....	15
2.2.2 Polymerase chain reaction (PCR) .....	16
2.2.3 Precipitation of DNA fragments .....	16
2.2.4 Restriction analysis .....	17
2.2.5 Agarose gel electrophoresis and DNA fragment isolation .....	17
2.2.6 Dephosphorylation and ligation .....	18
2.2.7 Transformation of bacterial cells.....	18
2.2.8 Inoculation of bacterial cells and isolation of plasmid DNA .....	19
2.2.9 DNA quantification and sequencing.....	20
2.2.10 Introduction of mutations into DNA constructs .....	20
2.2.11 Cloning of peripherin-2 constructs .....	21
2.3 Cell culture .....	21
2.3.1 Cultivation of mammalian cell lines.....	21
2.3.2 Transfection .....	21
2.4 Animals .....	22
2.5 Protein biochemistry .....	22
2.5.1 Isolation and quantification of proteins.....	22
2.5.2 Membrane preparations .....	23

2.5.3	Co-immunoprecipitation.....	24
2.5.4	SDS-polyacrylamide gel electrophoresis .....	25
2.5.5	Western blotting and immunodetection.....	26
2.6	Production and purification of rAAVs .....	28
2.6.1	Transfection and harvest .....	28
2.6.2	Purification of rAAVs via iodixanol gradient centrifugation .....	29
2.6.3	Purification of rAAVs via anion exchange chromatography.....	31
2.6.4	Concentration of rAAVs .....	31
2.6.5	rAAV titer determination via quantitative real-time PCR.....	32
2.7	Subretinal injection .....	33
2.8	Retina preparation and immunohistochemistry .....	34
2.9	Confocal microscopy .....	35
2.10	Isolation of rod and cone photoreceptor outer segments .....	36
2.11	Fluorescence resonance energy transfer (FRET) .....	37
2.12	Statistics.....	39
<b>3</b>	<b>Results .....</b>	<b>40</b>
3.1	Analysis of the peripherin-2 and rhodopsin interaction in outer segments of rod photoreceptors .....	40
3.1.1	Confirmation of the CNGB1a-interacting proteins in the mouse retina .....	40
3.1.2	Analysis of the rod opsin/peripherin-2/CNGB1a complex in HEK293 cells.....	41
3.1.3	FRET analysis of the rod opsin/peripherin-2/CNGB1a interaction in HEK293 cells.	42
3.1.4	Identification of the rod opsin-binding region in peripherin-2.....	43
3.1.5	Analysis of rod opsin and peripherin-2 binding characteristics.....	44
3.1.6	FRET analysis of the peripherin-2/rhodopsin interaction in isolated rod outer segments.....	45
3.1.7	Effects of the adRP-linked G266D mutation on the peripherin-2/rod opsin interaction.....	47
3.2	Analysis of the peripherin-2 and cone opsin interaction in outer segments of cone photoreceptors .....	50
3.2.1	Interaction analysis of WT and V268I peripherin-2 with cone opsins in HEK293 cells.....	50
3.2.2	Analysis of the peripherin-2/cone opsin interaction in WT murine retinas .....	53
3.2.3	rAAV-mediated expression of the V268I mutant in cones .....	54
3.2.4	FRET analysis of the WT and V268I peripherin-2/cone opsin interaction in cone outer segments .....	56
<b>4</b>	<b>Discussion .....</b>	<b>58</b>

4.1	Analysis of the peripherin-2 and rhodopsin interaction in outer segments of rod photoreceptors .....	58
4.2	Analysis of the peripherin-2 and cone opsin interaction in outer segments of cone photoreceptors .....	61
<b>5</b>	<b>Summary</b> .....	<b>64</b>
	<b>Zusammenfassung</b> .....	<b>66</b>
<b>6</b>	<b>Literature</b> .....	<b>68</b>
6.1	Cited publications .....	68
6.2	Own publications .....	77
<b>7</b>	<b>Appendix</b> .....	<b>78</b>
7.1	List of primers used for cloning and sequencing .....	78
7.2	List of CNGB1a-binding proteins identified via LC-MS/MS .....	79
7.3	Abbreviations .....	80
7.4	Danksagung .....	84

# 1 Introduction

## 1.1 Anatomy of the retina

The retina is the most inner layer of the eye and represents the light sensing part. It lies above the choroid layer and spans the back part of the eye. Vertebrates characteristically possess an inverse retina, that is, the light detecting cell layer is averted from the light. The light sensing cells are referred to as photoreceptors. Photoreceptors are subdivided into rods and cones. As shown in Figure 1.1.1, atop lies the pigment epithelium in which the photoreceptor outer segments (OS) are embedded. The subjacent rod and cone cell bodies form the outer nuclear layer (ONL). The synapses of photoreceptors as well as the upper synapses of bipolar and horizontal cells build up the outer plexiform layer (OPL). Next is the inner nuclear layer (INL) harboring the cell bodies of bipolar, horizontal, and amacrine cells. The bipolar cell terminals form synapses with ganglion cells in the inner plexiform layer (IPL). The ganglion cell bodies shape the ganglion cell layer (GCL). The axons of ganglion cells converge to the optic nerve and transmit the signal output to the visual centers of the brain.

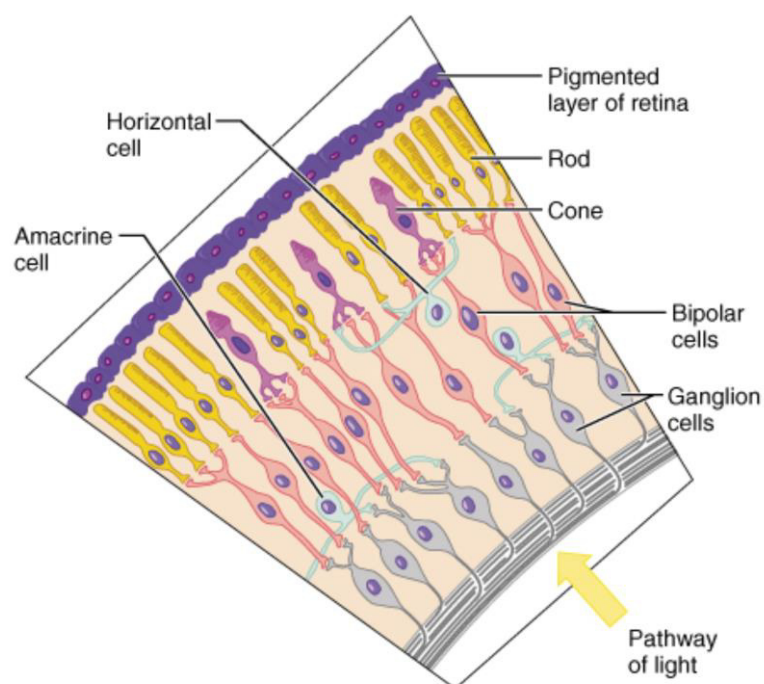


**Figure 1.1.1. Illustration of the retinal structure.** Adapted from Benjamin Cummings, an imprint of Addison Wesley Longman, Inc.

## 1.2 Anatomy of photoreceptors

Rod and cone photoreceptors are the primary light sensing cells of the retina. Rods are specialized in dim light and night vision (scotopic system), whereas cones mediate daylight vision and color discrimination (photopic system). Rods and cones share many common morphological features which are summarized in Figure 1.2.1. Photoreceptors contain four principal compartments: the outer segment, the inner segment, the soma, and the synaptic terminal. Outer segment and inner segment are connected via a cilium, which is the traffic bottleneck through which the components from the cell body are transported to the outer segment. The structure of outer segments differs between rods and cones. Rod outer segments are long and cylindrical comprising approximately a thousand membrane stacks referred to as discs. The disc membrane is physically separated from the plasma membrane (Cohen, 1960; Nickell *et al.*, 2007; Sung and Chuang, 2010). By contrast, cone outer segments are generally shorter and conical in shape. The cone membrane structures corresponding to the discs in rods are designated as lamellae. The membrane of lamellae is at least partly fused with the plasma membrane resulting in an intradiscal space that is continuous with the extracellular environment (Carter-Dawson and LaVail, 1979; Carter-Dawson and LaVail, 1979; Eckmiller, 1987; Mustafi *et al.*, 2009).

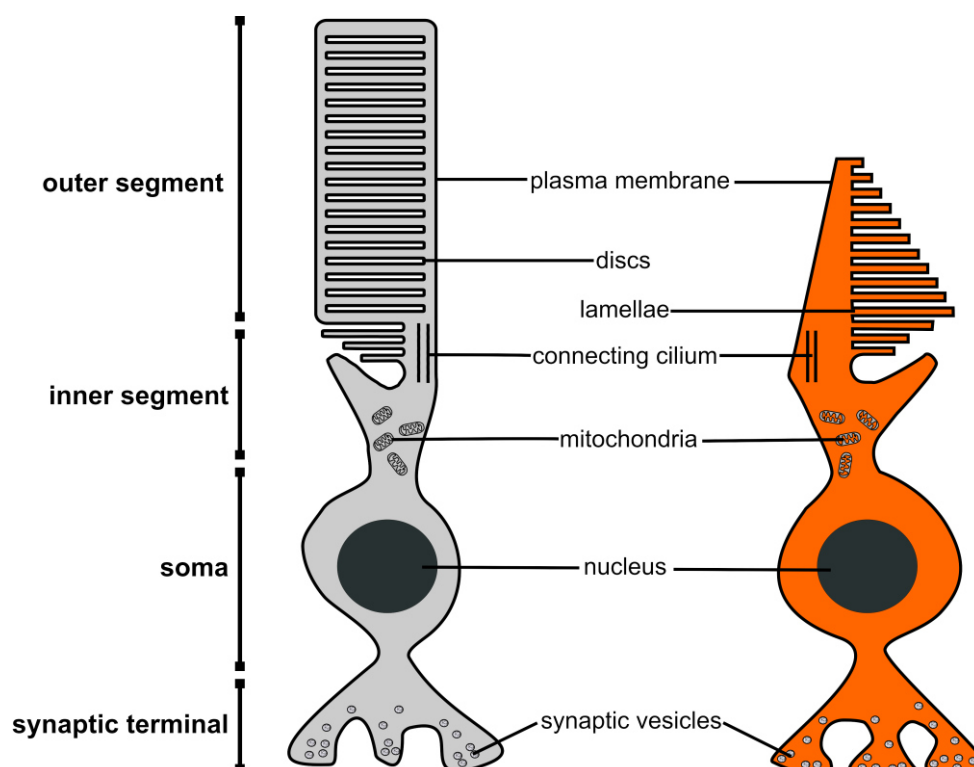


**Figure 1.2.1. Schematic representation of rod and cone photoreceptors.** Both cell types contain an outer segment, a connecting cilium, an inner segment, a soma (cell body), and the synaptic

terminal. Rod outer segments consist of stacks of discs that are separated from the plasma membrane. By contrast, cone outer segments have lamellae that are partially fused with the plasma membrane.

### 1.3 Signaling transduction in photoreceptors

Light-induced signaling transduction takes place in the outer segments. In the dark, the constitutively active guanylyl cyclases E and F (GC-E/F) generate high levels of cyclic guanosine monophosphate (cGMP), which binds to the cyclic nucleotide-gated (CNG) channel to preserve its open state. Open CNG channels maintain the influx of  $\text{Na}^+$  and  $\text{Ca}^{2+}$  cations into the photoreceptor resulting in the "dark current". This dark current depolarizes the plasma membrane up to -40 mV. The change in the membrane potential ensures opening of the voltage-gated calcium channel (Cav1.4) at the synaptic terminal. The resulting influx of  $\text{Ca}^{2+}$  cations through the Cav1.4 channel gives rise to a continuous transmitter release from the synaptic vesicles.

When photons are absorbed by the chromophore retinal, which is covalently bound to rhodopsin in rods or the cone opsins in cones (see chapter 1.4), retinal isomerizes from its 11-*cis* state to the all-*trans* state resulting in conformational changes of the opsin apoprotein. This causes transducin to activate the cGMP phosphodiesterase 6 (PDE6), which in turn hydrolyzes cGMP to GMP. Decrease in cGMP evokes closure of the CNG channel thus leading to hyperpolarization of the photoreceptor plasma membrane to -70 mV (Barnes, 1994). The subsequent termination of transmitter release evokes the transmission of the light signal information to the visual centers of the brain. Rods possess a higher light sensitivity than cones and can detect single photons, which is only possible due to pronounced signal amplification in the phototransduction cascade (Baylor *et al.*, 1979; Gunkel *et al.*, 2015).

The dark current is restored by re-increasing the cGMP concentration to dark level. Responsible for this regulation is the intracellular  $\text{Ca}^{2+}$  level that mediates GC-E/F activity. GC-E/Fs are regulated by guanylyl cyclase-activating proteins (GCAPs) that are inactive when bound to  $\text{Ca}^{2+}$ . Under light condition, the CNG channel is closed which leads to low  $\text{Ca}^{2+}$  levels (Fain *et al.*, 2001). This in turn induces GCAPs, which increase the cGMP production by activating the GC-E/Fs. The high cGMP concentration re-opens CNG channels restoring the dark current (Figure 1.3.1A).

The termination of the signaling transduction cascade and the photoresponse kinetics are controlled by further processes including inactivation of the meta II intermediate of opsin apoproteins by phosphorylation. In case of rods, metarhodopsin II ( $\text{Rh}^*$ ) is inactivated by the

rhodopsin kinase 1 (GRK1) (Chen *et al.*, 1999). Furthermore, a protein referred to as arrestin binds to phosphorylated rhodopsin to prevent it from activating transducin (Xu *et al.*, 1997). Finally, to restore the GPCR back to its inactive and excitable state, all-*trans* retinal is replaced by its 11-*cis* form and rhodopsin is dephosphorylated (Figure 1.3.1B).

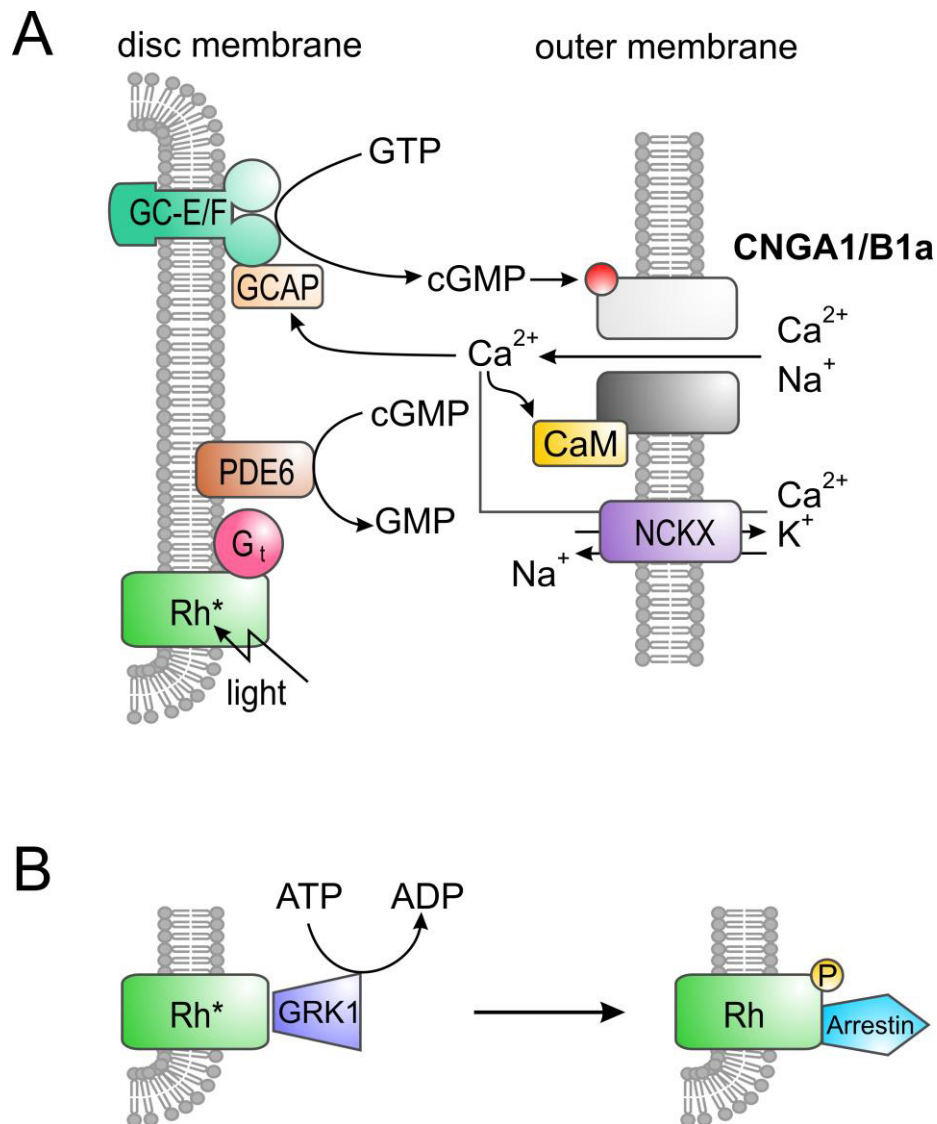


**Figure 1.3.1. Signaling transduction cascade in rod photoreceptors.** A) Components and molecular mechanisms that play a role during light-induced rhodopsin activation. B) Prevention of sustained transducin activation via phosphorylation of Rh\* by rhodopsin kinase (GRK1) and subsequent binding of arrestin. For details, see text. GC-E/F, guanylyl cyclase E/F; GCAP, guanylyl cyclase-activating protein; PDE6, phosphodiesterase 6;  $G_t$ , transducin; CaM, calcium-calmodulin; NCKX, Na<sup>+</sup>/Ca<sup>2+</sup>/K<sup>+</sup> exchanger.

## 1.4 Topology and function of retinal opsins

Retinal opsins are the light sensors of the phototransduction cascade. Rod photoreceptors exclusively express rhodopsin, which is mainly localized to the disc membrane and possesses an absorption maximum at 495 nm. Cone photoreceptors are further divided into subtypes each expressing one or more cone-specific opsins. Trichromats like catarrhines and humans have three different cone types and consequently three different cone opsins to cover their visual spectrum. Accordingly, the short wavelength-sensitive cone opsin (S-opsin) has an absorption maximum at 420 nm, the medium wavelength-sensitive cone opsin (M-opsin) at 535 nm, and the long wavelength-sensitive cone opsin (L-opsin) at 565 nm. The majority of mammals are dichromats and possess only S- and M-opsin. As prototypical members of the GPCR superfamily, rod and cone opsins consist of seven transmembrane domains, which are alternately connected via three cytoplasmatic and three extracellular (intradiscal in case of rhodopsin) loops. The N-terminus is extracellular (intradiscal) and the C-terminus is located to the cytoplasmatic side (Figure 1.4.1A). A recent study unveiled the crystal structure of bovine rhodopsin with bound chromophore as illustrated in Figure 1.4.1B (Choe *et al.*, 2011). The sequence homology differs between the single opsins (Figure 1.4.2). For human opsins, the highest homology exists between M-opsin and L-opsin (95.9 %). Rhodopsin and M-opsin share a 40.9 % homology, whereas that of rhodopsin and S-opsin is 43.9 %. Finally, S-opsin and M-opsin share a 40.6 % homology (Nathans *et al.*, 1986). According to studies, rhodopsin is considered to have evolved from cone opsins during photoreceptor evolution (Okano *et al.*, 1992), while M-opsin and L-opsin derived from gene duplication of a common ancestral gene, which explains their high homology (Hunt *et al.*, 1998).

Mouse models revealed that rod photoreceptors fail to form outer segments in absence of rhodopsin (Lem *et al.*, 1999). Mutations in the gene encoding rhodopsin account for approximately 25 % of autosomal-dominant retinitis pigmentosa (adRP). The genes coding for M- and L-opsin are located on the X-chromosome (Xq28 in humans). Mutations in these genes cause X-linked retinal diseases affecting M- and L-cones and thus leading to various forms of red-green visual impairment. However, progressive cone dystrophies are also associated with mutations in the M-/L-opsin gene (Gardner *et al.*, 2010; Neitz and Neitz, 2011). In humans, the gene coding for S-opsin is located on chromosome 7 (7q32) and mutations in this gene affect males and females to an equal extent (Nathans *et al.*, 1986).

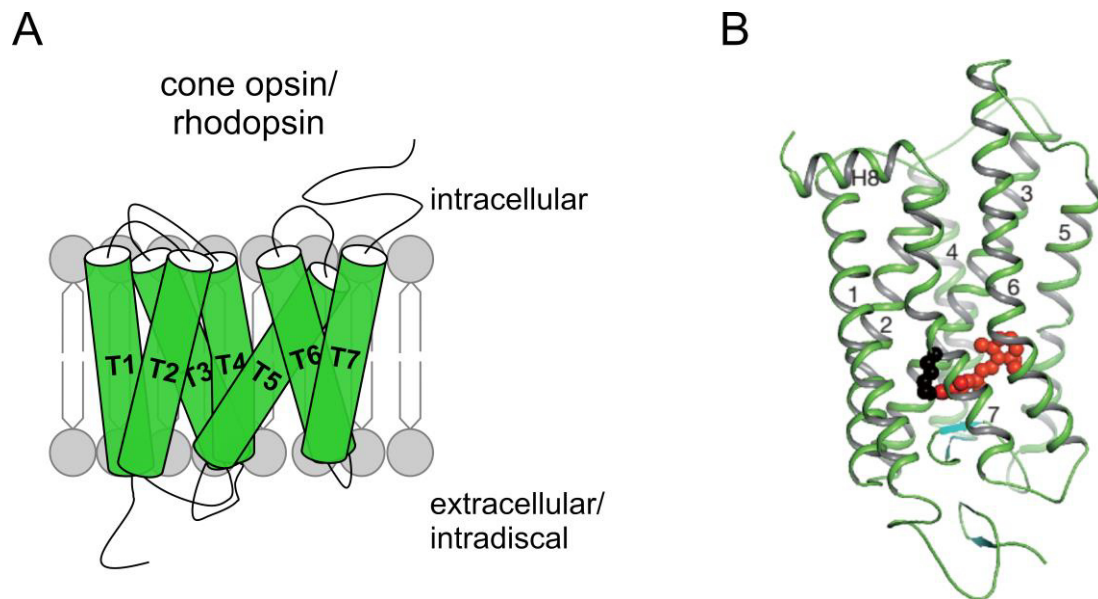


**Figure 1.4.1. Schematic topology of rod and cone opsins.** A) Opsins consist of an extracellular (for cone opsins) or intradiscal (for rhodopsin) N-terminus, an intracellular C-terminus, and seven transmembrane domains (T1-T7) that are connected by six loop regions. B) Crystal structure of inactive bovine rhodopsin consisting of the apoprotein opsin in its inactive conformation and the chromophore 11-*cis*-retinal (shown as red spheres), which is covalently bound to lysine 296 (shown as black spheres) via a Schiff base. Transmembrane helices (numbered 1-7) are followed by an intracellular helix H8. The C-terminus of rhodopsin is not shown. The  $\beta$ -strands in the intradiscal domain are depicted as cyan arrows. Image from Choe *et. al*, 2011.

## Introduction

```

S-opsin  -----MRKMS-EEEFYLF---KNISSVGPWDGPQYHIAPVWAFYLQA 38
M-opsin  MAQQWSQLRLAGRHPQDSYEDSTQSSIFTYT---NSNSTRGPFEGPNYHIAPRWVYHLTS 57
L-opsin  MAQQWSQLRLAGRHPQDSYEDSTQSSIFTYT---NSNSTRGPFEGPNYHIAPRWVYHLTS 57
rhodopsin -----MNGTEGPNFYVPFSNATGVVRSPPFEYPQYYLAEPWQFSMLA 41
          . : * . . * : : :

S-opsin  AFMGTVFLIGFPLNAMVLVATLRYKCLRQPLNYILVNVSFSGFLLCIFSVFPVAVASCNG 98
M-opsin  VWMIFVVIASVFTNGLVLAATMKFKLRHPLNWILVNLAVADLAETVIASTISVNVQVYG 117
L-opsin  VWMIFVVTASVFTNGLVLAATMKFKLRHPLNWILVNLAVADLAETVIASTISIVNQVSG 117
rhodopsin AYMFLLVLVGFPINFLTLYVTVQHKKLRTPNLNYILLNLAVADLFMVLGGFTSTLYTSLHG 101
          .:* .. . * :.* .*:.* **:*:*:*:.. : : . . *

S-opsin  YFVFGRHVCALEGFLGTVAGLVGTGWSLAFLAERYIVICKPFGNFRFSSKHALTVVLATW 158
M-opsin  YFVLGHPMCYLEGYTVSLCGITGLWSLAIISWERWMVCKPFGNVRFDAKLAIVGIAFSW 177
L-opsin  YFVLGHPMCYLEGYTVSLCGITGLWSLAIISWERWLVCVCKPFGNVRFDAKLAIVGIAFSW 177
rhodopsin YFVFGPTGCNLEGGFATLGGEIALWSLVLAIERVYVVCVCKPMSNFRFGENHAIMGVAFTW 161
          ***:* * ***: : * ***...: ***:*:*:*:*:*:* : * : : *

S-opsin  TIGIGVSIPPFEGWSRFIPEGLQCSCGPDWYTVGTKYRSESYTWFLFIFCFIVPLSLICF 218
M-opsin  IWAAVWTAPPIFGWSRYWPHGLKTSVCGPDVFSGSSYPGVQSYMIVLMVTCCITPLSIIVL 237
L-opsin  IWSAVWTAPPIFGWSRYWPHGLKTSVCGPDVFSGSSYPGVQSYMIVLMVTCCIIPLAIIIML 237
rhodopsin VMALACAAPPLAGWSRYIPEGLQCSCGIDYYTLKPEVNNESFVIYMFVVHFTIPMIIIF 221
          . : ** :***: *.*: *** * : : :* : : : * : * :

S-opsin  SYTQLLRALKAVAAQQQESATTQKAEREVSRMVVVMVGSFCVCYVPYAAFAMVMVNNRNH 278
M-opsin  CYLQVWLAIRAVAKQQKESESTQKAEKEVTRMVVVMVLAFCFCWGPYAFFACFAAANPGY 297
L-opsin  CYLQVWLAIRAVAKQQKESESTQKAEKEVTRMVVVMIFAYCVCWGPYTFACFAAANPGY 297
rhodopsin CYGQLVFTVKEAAAQQQESATTQKAEKEVTRMVIIMVIAFLICWVPYASVAFYIFTHQGS 281
          . * * : : : * **:* :*****:*:*:*:*:*: : : . * : * : * :

S-opsin  GLDLRLVTIPSFSSKSAIYNPIIYCFMNKQFQACIMKMVCGKAMTDESDTCS--SQKTE 336
M-opsin  PFHPLMAALPAFFAKSATIYNPVIYVFMNRQFRNCILQLF-GKKVDDGSELSS--ASKTE 354
L-opsin  AFHPLMAALPAYFAKSATIYNPVIYVFMNRQFRNCILQLF-GKKVDDGSELSS--ASKTE 354
rhodopsin NFGPIFMTIPAFFAKSAAIYNPVIYIMMNKQFRNCMLTTICCGKNPLGDDEASATVSKTE 341
          : : :*:*:*:* **:*:* :**:*:* * : : . . : * .***

S-opsin  VSTVSSTQVGPN 348
M-opsin  VSSVSSVSPA-- 364
L-opsin  VSSVSSVSPA-- 364
rhodopsin TSQVAPA----- 348
          . * * : .

```

**Figure 1.4.2. Sequence homology between human rhodopsin, S-opsin, M-opsin, and L-opsin.**

Using the Clustal Omega (1.2.1) program to align amino acid sequences of human retinal opsins, the results show an overall sequence identity of 28.0 % with a total number of 104 conserved amino acids (asterisks) and 111 similar positions (periods and colons). Approximate sequence homology between the following opsins is: M-opsin and L-opsin, 95.9 %; rhodopsin and M-opsin, 40.9 %; rhodopsin and S-opsin, 43.9 %; M-opsin and S-opsin, 40.6 %.

## 1.5 Peripherin-2

### 1.5.1 Topology and function of peripherin-2

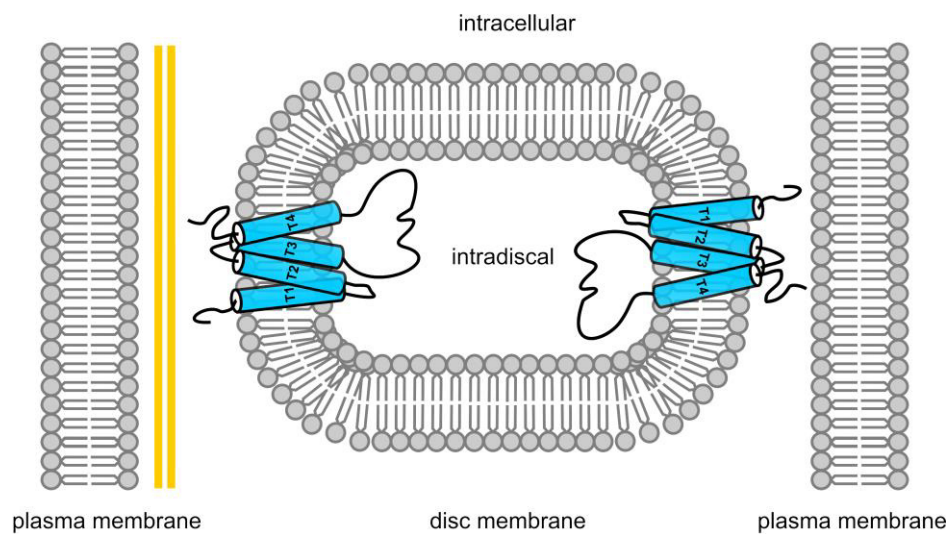
Peripherin-2 is a glyco-membrane protein and belongs to the tetraspanin family. Tetraspanins are transmembrane proteins found in multicellular eukaryotes. In humans, 33 different tetraspanins have been identified so far. They act as scaffolding proteins anchoring many other proteins to the cell membrane and are involved in multiple cellular processes including cell signaling, adhesion, and motility (Hemler, 2005; Goschnick *et al.*, 2006; Andreu and Yanez-Mo, 2014).

Rod and cone photoreceptors express two tetraspanins, peripherin-2 and its non-glycosylated homologue rom-1. Characteristically for a tetraspanin, peripherin-2 is composed of four transmembrane  $\alpha$ -helical domains and both the N- and the C-terminus are located to the intracellular side. Peripherin-2 comprises a large extracellular (intradiscal in rods) D2 loop region between the third and the fourth transmembrane domain. (Connell and Molday, 1990; Vos *et al.*, 2010). As depicted in Figure 1.5.1.1, peripherin-2 is located in the rim region of the disc membrane in rod outer segments (Molday *et al.*, 1987; Arikawa *et al.*, 1992). In cone outer segments, peripherin-2 is proposed to exclusively localize to the region of the lamellae adjacent to the axoneme and surrounded by the plasma membrane (Arikawa *et al.*, 1992; Han *et al.*, 2012). Together with its interaction partners, peripherin-2 is essential for the morphogenesis and structural integrity of photoreceptor outer segments (Stuck *et al.*, 2016). The hitherto known outer segment binding partners of peripherin-2 are the B-subunit of the rod CNG channel (CNGB1a), the glutamic acid-rich protein (GARP) that is exclusively expressed in rods, the retinal outer segment membrane protein rom-1, melanoregulin, and calmodulin (Goldberg *et al.*, 1995; Poetsch *et al.*, 2001; Boesze-Battaglia *et al.*, 2007; Edrington *et al.*, 2007; Michalakis *et al.*, 2011). Peripherin-2 can also form homodimers and homotetramers as well as higher order oligomers (Goldberg *et al.*, 1995; Goldberg and Molday, 1996; Loewen and Molday, 2000). Tetramerization is mediated via disulfide bridges between the cysteine residues within the large D2 loop region. The domain essential for dimerization is so far unknown, however, it is suggested also to be localized within the D2 loop (Loewen *et al.*, 2001). In addition, it was demonstrated that peripherin-2 and rom-1 can associate to heteromeric oligomers (Goldberg *et al.*, 1995; Goldberg and Molday, 1996).

Mouse models showed that absence of peripherin-2 causes impairment of outer segment formation indicating that peripherin-2 is crucial for outer segment biogenesis (Sanyal and Jansen, 1981). Peripherin-2 has also been shown to induce membrane curvature, a process suggested to be essential for generation of discs. (Kevany *et al.*, 2013; Khattree *et al.*, 2013). Another important function of peripherin-2 is its involvement in membrane fusion

processes (Boesze-Battaglia *et al.*, 1997; Boesze-Battaglia *et al.*, 1998; Stefano *et al.*, 2002). The disc-stabilizing function of peripherin-2 is proposed to be mediated via interaction with other outer segment proteins. This hypothesis is supported by studies showing that peripherin-2 binds to CNGB1a as well as the other two soluble isoforms, GARP1 and GARP2 (Poetsch *et al.*, 2001; Ritter *et al.*, 2011). Corroborating this idea, further work revealed that deletion of GARP in rods results in disorganized and disoriented discs (Zhang *et al.*, 2009). Although the precise mechanisms are still elusive, peripherin-2 seems to play a differential role in rods and cones. Rods lacking peripherin-2 are incapable of forming outer segments (Sanyal and Zeilmaker, 1984). However, the relatively low number of cones in the murine retina hampered the investigation of cone outer segment formation in absence of peripherin-2. This issue was solved when crossing the peripherin-2 knockout mouse (*rds*<sup>-/-</sup>) with a cone-dominant mouse model (*nr1*<sup>-/-</sup>). Cones of *rds*<sup>-/-</sup>/*nr1*<sup>-/-</sup> mice displayed two important differences from rods: significant visual function was preserved and the cone outer segments still developed albeit balloon-shaped and lacking lamellae (Farjo *et al.*, 2006). These findings proposed that, in contrast to rods, the outer segment and lamellae morphogenesis in cones does not primarily require peripherin-2, but peripherin-2 is rather needed in second place for rim formation.

### A rod outer segment



### B cone outer segment

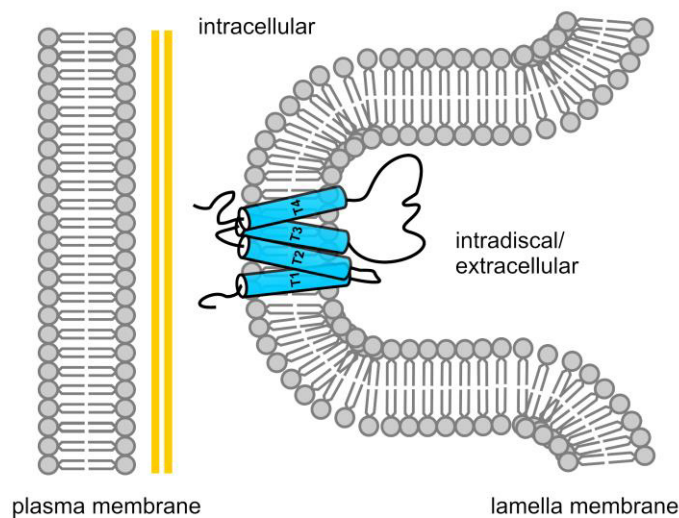


**Figure 1.5.1.1. Schematic topology and localization of peripherin-2 in rod and cone outer segments.** A-B) Peripherin-2 encompasses four transmembrane domains (T1-T4). The N-, C-terminus, and second loop region are intracellular. The first and the large third loop region are located on the intradiscal side in rods (A) and on the intradiscal/extracellular side in cones (B). Peripherin-2 is localized to the rim region of the disc membrane in rods (A) and the rim region of the lamella membrane adjacent to the axoneme (yellow lines) and surrounded by the plasma membrane in cones (B), respectively.



**Figure 1.5.2.1. Exon 2-specific disease-associated point mutations in PRPH2.** Left, the region of peripherin-2 encoded by exon 2 is marked with a dashed rectangle. Right, schematic magnification of the exon 2-encoded part with currently known positions of point mutations highlighted in red.

## 1.6 Degenerative retinal dystrophies

Degenerative retinal dystrophies can be subdivided into diseases that primarily lead to loss of rod photoreceptors designated as different forms of retinitis pigmentosa, and diseases that cause degeneration of cone photoreceptors, such as adult vitelliform macular dystrophy.

### 1.6.1 Retinitis pigmentosa

The prevalence of retinitis pigmentosa (RP) is worldwide 1:4,000, which makes it the most common form of inheritable dystrophies (Ammann *et al.*, 1965; Boughman *et al.*, 1980; Jay, 1982; Puech *et al.*, 1991; Berson *et al.*, 1993). The most prevalent subtype of RP is rod-cone dystrophy that characteristically primarily leads to degeneration of rod photoreceptors. As a secondary effect, this also causes loss of cones and thus, a premature loss of photoreceptors. Primary symptoms of patients suffering from this disease are night blindness followed by a progressive loss of peripheral vision at daylight (referred to as tunnel vision). When cones start to degenerate, dysfunctions in contrast perception and color discrimination emerge, while visual acuity diminishes. In the final state, most patients suffer from complete blindness. Furthermore, RP leads to degeneration of the retinal pigment epithelium that subsequently causes pigment deposits in the retina (Hamel, 2006). This attribute is eponymous for the disease. The different hereditary forms of RP can vary from autosomal-dominant (adRP), autosomal-recessive, X-chromosomal, to digenic (Boughman and Fishman, 1983; Ferrari *et al.*, 2011). After autosomal-recessive RP, the second most prevalent form is adRP that covers 30-40 % of RP cases (Bunker *et al.*, 1984; Ayuso *et al.*, 1995; Hartong *et al.*, 2006). Mutations in the PRPH2 gene account for approximately 10 % of adRP (Ferrari *et al.*, 2011; Manes *et al.*, 2015).

### 1.6.2 Adult vitelliform macular dystrophy

Adult vitelliform macular dystrophy (AVMD) belongs to a heterogeneous group of macular dystrophies that are designated as pattern dystrophy and affect the retinal pigment

epithelium. This group of disorders is autosomal-dominantly inherited and the course of disease is very variable. Generally, the phenotype encompasses mild defects in visual acuity and color discrimination that can affect one or both eyes. Patients suffering from AVMD display cone degeneration in the area of the macula (Epstein and Rabb, 1980). Typically, the loss of cones is accompanied by yellow-brown, egg yolk-like (vitelliform) pigment deposits in the foveal or parafoveal region of the retina (Epstein and Rabb, 1980; Renner *et al.*, 2004). The disease occurs only in adult individuals (Renner *et al.*, 2004). Mutations in the PRPH2 gene account for 18 % of AVMD (Felbor *et al.*, 1997).

## 1.7 Aims of this study

This study deals with the analysis of rod and cone opsins as hitherto unidentified interaction partners of peripherin-2 in rod and cone photoreceptors.

Studies have suggested a differential role of peripherin-2 in the two photoreceptor cell types. Corroborating this hypothesis, mutations in the PRPH2 gene are either associated with rod diseases or linked to cone defects. However, the underlying mechanisms causing this differential function of peripherin-2 in rods and cones have not been elucidated. A possibility to illuminate this issue would be to analyze the interaction partners of peripherin-2 in the native environment. One known peripherin-2-binding protein in rods is CNGB1a, a component of the phototransduction cascade. However, it is conceivable that peripherin-2 also interacts with other proteins of the phototransduction cascade such as retinal opsins, phosphodiesterase 6, and guanylyl cyclase E/F in the respective photoreceptor type. Importantly, based on the mass spectrometry analysis conducted in preliminary unpublished work to identify putative binding partners of CNGB1a, it was postulated that rhodopsin, the rod CNG channel, and peripherin-2 are part of the same complex. In this context, the following questions should be addressed:

- 1) Is the protein complex comprising rhodopsin, peripherin-2, and the rod CNG channel present in the rod outer segment? To investigate this question, a set of different methodical approaches *in vitro* and *in vivo* was applied.
- 2) Does a similar protein complex also exist in the outer segment of cone photoreceptors?
- 3) If there is an interaction between peripherin-2 and rod/cone opsins, do some disease-linked point mutations in the PRPH2 gene interfere with this binding?

## 2 Materials and methods

### 2.1 Chemicals, solutions and buffers

All used chemicals had the quality "*pro analysi*" or "for molecular biological use" and were obtained by the companies VWR, Sigma-Aldrich, Merck, Biorad or Roth if not stated otherwise. For all solutions, high pure and deionized water from the Milli-Q Plus System (Millipore) was used. All solutions and buffers used in experiments that required high purity were autoclaved (Sterilisator, Münchner Medizin Mechanik).

### 2.2 Molecular biology

#### 2.2.1 Plasmids

##### pcDNA3.1

The pcDNA3.1 plasmid (Invitrogen) is a commonly used mammalian expression vector containing a cytomegalovirus (CMV) promoter which enables heterologous gene expression in mammalian cell lines, a simian virus origin of replication (SV40 ori) for replication in mammalian cells, a colicinogenic factor (ColE1) ori for replication in prokaryotes, a filamentous phage (f1) ori for recovery of single-stranded plasmids in prokaryotes, a multiple cloning site (MCS) for insertion of a gene or gene fragment of interest into the vector, a polyadenylation signal of the bovine growth hormone (pA BGH), a neomycin resistance gene (Neo<sup>R</sup>) under the control of the SV40 promoter for selection of stable mammalian cells, and an ampicillin resistance gene (Amp<sup>R</sup>) for selection of transformed bacterial cells.

##### pAAV2.1

The pAAV2.1 *cis* plasmid is used for expression of genes delivered by recombinant adeno-associated viruses (rAAV). In this work, human rhodopsin promoter (hRHO) and murine short-wavelength opsin promoter (mSWS) were used for specific gene expression in mouse rod and cone photoreceptors, respectively. The vector further contains two inverted terminal repeats (ITR) encoding all *cis*-acting elements for efficient replication (rep) and packaging (cap) of rAAVs in the presence of helper plasmids. Between the two flanking ITRs, the packaging capacity is approximately 5.2 kilobase pairs (kb). The plasmid also contains a MCS for introduction of a gene or gene fragment of interest between the ITRs, a woodchuck hepatitis virus posttranscriptional regulatory element (WPRE) to enhance gene expression, a

pA BGH, and Amp<sup>R</sup> for selection of recombinant prokaryotes. The two helper plasmids used in combination with pAAV2.1 vectors for the generation rAAVs were pAD Helper plasmid and pAAV2/8-YF rep/cap plasmid which contains rep gene of serotype AAV2 and cap gene of serotype AAV8 for enhanced specific transduction of photoreceptors (Allocca *et al.*, 2007; Vandenberghe and Auricchio, 2012). The serotypes contain mutations (YF) substituting tyrosine (Y) with phenylalanine (F) residues at exposed sites of the capsid surface to allow for a high transduction efficiency in host retinal cells (Petrus-Silva *et al.*, 2009; Petrus-Silva *et al.*, 2011).

## 2.2.2 Polymerase chain reaction (PCR)

The PCR pipetting schemes and reaction conditions for the different polymerases used in this study were adjusted according to the manual of the respective manufacturer and application. An overview of the standard PCR condition for each polymerase is shown in Table 2.2.2.1. All used primers were purchased by Eurofins MWG Operon.

**Table 2.2.2.1. Standard PCR conditions for polymerases used in this study.**

Polymerase	Taq (in-lab production)		Herculase II (Agilent)		Kapa Hifi (Peqlab)	
<b>Initial denaturation</b>	95 °C	2 min	95 °C	2 min	95 °C	3 min
<b>*Denaturation</b>	95 °C	30 sec	95 °C	20 sec	98 °C	20 sec
<b>*Annealing</b>	X °C	30 sec	X °C	15 sec	X °C	15 sec
<b>*Elongation</b>	72 °C	30-60 sec/kb	72 °C	30 sec/kb	72 °C	30 sec/kb
<b>Final elongation</b>	72 °C	5 min	72 °C	3 min	72 °C	1 min/kb
<b>Storage</b>	10 °C	∞	10 °C	∞	10 °C	∞

The optimal annealing temperatures (X) were applied according to the respective manufacturer's manual and melting temperatures of the used primers. \*These steps were repeated in 35 cycles.

## 2.2.3 Precipitation of DNA fragments

For further applications after amplification, the PCR products were precipitated and reconstituted in H<sub>2</sub>O to remove PCR buffer and reaction contents. First, H<sub>2</sub>O was added to

the PCR product to a final volume of 100  $\mu$ l. 10  $\mu$ l of 3 M sodium acetate buffer pH 5.2 and 275  $\mu$ l of chilled ethanol were added before cooling the mixture at -80  $^{\circ}$ C for 10 min. The mixture was then centrifuged at 16,000x *g*, 4  $^{\circ}$ C for 15 min and the supernatant was subsequently removed. The DNA pellet was washed with 70 % (v/v) ethanol and was centrifuged at 16,000x *g*, 4  $^{\circ}$ C for another 5 min. The pellet was air-dried prior to reconstitution in a suitable amount of H<sub>2</sub>O (10-30  $\mu$ l).

#### 2.2.4 Restriction analysis

Restriction enzymes used in this study were purchased from the companies New England Biolabs (NEB) and Thermo Fisher Scientific (formerly Fermentas). The reaction conditions were conducted according to the respective manufacturer's protocols. The amount of DNA used for cloning was 3-5  $\mu$ g, whereas 0.5  $\mu$ g of DNA or 2  $\mu$ l of minipreparation of plasmid DNA (see 2.2.8) were used for restriction analysis.

#### 2.2.5 Agarose gel electrophoresis and DNA fragment isolation

After restriction digest, DNA fragments were mixed with 6x loading dye and loaded on agarose gels depending on the desired fragment size (0.7 % for fragments higher than 500 bp and 2 % for fragments of 500 bp or smaller). Agarose gels were made by boiling the respective amount of agarose (peqGOLD Universal-Agarose, peqlab) in 1x TBE buffer. After cooling down to approximately 50  $^{\circ}$ C, peqGREEN dye (peqlab) was added to the agarose solution (5  $\mu$ l/100 ml) before pouring it into the tray for hardening. The dye enables detection of DNA fragments under UV light. GeneRuler 1 kb plus DNA ladder (Thermo Fisher Scientific) was also loaded to determine the fragment sizes. Gels were run at 150 V in a gel apparatus (peqlab) until sharp bands could be cut off the gel under UV light using Geldoc 2000 imager (BioRad). The DNA fragment within the cut gel slice was extracted by using the QIAquick Gel Extraction Kit (Qiagen) according to the manufacturer's protocol. The DNA bound to the extraction column was eluted by adding 30  $\mu$ l of elution buffer (provided in the kit). To check for proper purification, 2  $\mu$ l of the eluted DNA were loaded on an agarose gel.

10x TBE

---

0.5 M EDTA pH 8.0	200 ml
boric acid	275 g

## Materials and methods

---

tris	540 g
H <sub>2</sub> O	ad 5 l

### 1x TBE

---

10x TBE	1 l
H <sub>2</sub> O	ad 10 l

### 6x loading dye

---

0.5 M EDTA pH 8.0	24 ml
10x TBE	60 ml
xylene cyanol 50 mg/ml	3 ml
bromophenol blue 50 mg/ml	3 ml
ficoll type 400	18 g
H <sub>2</sub> O	ad 100 ml

### 2.2.6 Dephosphorylation and ligation

Dephosphorylation of the vector was done to avoid re-closing before introduction of the insert, which mainly occurs when the used enzymes for restriction digest generate blunt ends or identical sticky end overhangs. The Rapid DNA Dephosphorylation Kit (Roche) was used for this purpose and the dephosphorylation conditions were applied according to the manufacturer's manual.

Ligation was performed using T4 DNA ligase (NEB). The vector to insert ratio should be 1:3 to 1:5. Therefore, the amount of the vector and insert DNA fragments was calculated for each ligation reaction. Pipetting scheme and reaction conditions were applied according to the manufacturer's manual. The reaction was incubated overnight at 16 °C.

### 2.2.7 Transformation of bacterial cells

Chemically treated, competent  $\beta$ 10 *Escherichia coli* (*E. coli*) strain was used for transformation with either isolated DNA plasmids or ligation reactions. 100  $\mu$ l aliquots of competent cells stored at -80 °C were thawed on ice prior to addition of 5  $\mu$ l of ligation reaction or 10 ng of plasmid DNA. The cell suspension was then gently mixed by tapping at the tube wall and was incubated on ice for 10 min. A subsequent heat shock at 42 °C for 45

sec was performed in a heat block and cells were re-incubated on ice for 2 min. The cell suspension was plated on the LB(+) selection agar plate containing 100 µg/ml ampicillin (resistance provided by the used plasmids) and was incubated overnight at 37 °C.

### LB(+) medium

peptone	10 g
NaCl	5 g
yeast extract	5 g
glucose	1
H <sub>2</sub> O	<i>ad 1 l</i>
adjust pH to 7.2-7.5 and autoclave	

### LB(+) agar

agar	15 g
LB(+) medium	<i>ad 1 l</i>
ampicillin	100 mg

## 2.2.8 Inoculation of bacterial cells and isolation of plasmid DNA

Single bacterial clones were picked from the plate and were transferred into tubes with 5 ml LB(+) medium plus ampicillin (100 µg/ml). The suspension was incubated over night at 37 °C with shaking at 225 rpm. On the next day, the suspension was centrifuged at 3500 rpm and room temperature (RT) for 10 min and the supernatant was removed. The pellet was resuspended in 250 µl resuspension buffer before transferring into 2 ml Eppendorf tubes. After adding 250 µl lysis buffer, the cell suspension was inverted 5 times and was incubated for 5 min at RT. Afterwards, 250 µl neutralization buffer was added and the mixture was inverted 5 times before incubation for 5 min at RT. The suspension was then centrifuged at 13,000 rpm and 4 °C for 15 min. The supernatant containing the plasmid DNA was transferred into a fresh 1.5 ml Eppendorf tube. To precipitate the DNA, 525 µl isopropanol was added to the mix. After vortexing, the mixture was centrifuged at 13,000 rpm and 4 °C for 15 min. Subsequently, the pellet was washed with 70 % (v/v) ethanol by centrifugation at 13,000 rpm and 4 °C for 5 min. The supernatant was discarded and the pellet was air-dried before resuspension in 30 µl of H<sub>2</sub>O.

For large scale and high purity plasmid isolation, PureLink® HiPure Plasmid Midiprep or Megaprep Kit (Invitrogen) was used, following the instructions from the manufacturer's manual.

### Resuspension buffer

tris	6.06 g
EDTA	3.72 g
RNAse A	100 mg
H <sub>2</sub> O	<i>ad</i> 1 l
adjust pH to 8.0 with 37 % HCl	

### Lysis buffer

NaOH	8 g
10 % (w/v) SDS solution	100 ml
H <sub>2</sub> O	<i>ad</i> 1 l

### Neutralization buffer

3 M potassium acetate pH 5.5	500 ml
H <sub>2</sub> O	<i>ad</i> 1 l

## 2.2.9 DNA quantification and sequencing

Quality and relative quantity of the isolated DNA was determined by agarose gel electrophoresis (see 2.2.5). In addition, the Nanodrop<sup>TM</sup> 2000c spectrophotometer with inbuilt instrument settings and software (Thermo Scientific) was used to determine the absolute amount of DNA via measuring its absorption at 260 nm. The 260 nm/280 nm ratio provided information about protein contamination and should be higher than 1.8, whereas phenol contamination was given by the 260 nm/230 nm ratio which should be at 2-2.3.

All DNA sequencing services were done by Eurofins MWG Operon and the sent samples and corresponding primers were diluted to concentrations proposed by the company.

## 2.2.10 Introduction of mutations into DNA constructs

Mutations were introduced via site-directed mutagenesis. The PCR was done using the QuikChange II XL Site-Directed Mutagenesis Kit (Agilent) according to the manufacturer's manual. The specific primers for this purpose were ordered from Eurofins MWG Operon. After the PCR, the DNA template was digested with DpnI restriction enzyme at 37 °C for 1 h.

The amplified plasmids carrying the mutation were purified via precipitation (see 2.2.3) and 2-3  $\mu$ l were used for transformation of competent cells (see 2.2.7).

### 2.2.11 Cloning of peripherin-2 constructs

Murine Prph2 was PCR amplified from retinal cDNA and sub-cloned into pcDNA3.1 vector. It was C-terminally tagged with myc-tag for co-immunoprecipitation (co-IP) experiments (see 2.5.3) or cerulean and citrine for FRET analysis, respectively (see 2.5.11). Murine Prph2 C-terminally fused with cerulean or citrine was also sub-cloned into pAAV2.1 vector containing either the human rhodopsin (hRHO) or mouse S-opsin (mSWS) promoter (Michalakis *et al.*, 2010; Koch *et al.*, 2012) for rAAV production and transduction of mouse rod or cone photoreceptors, respectively (see chapters 2.6. and 2.7).

## 2.3 Cell culture

### 2.3.1 Cultivation of mammalian cell lines

HEK293 cells were used for *in vitro* transfections and were cultivated in DMEM + GlutaMAX<sup>TM</sup>-I medium (+1 g/l glucose, +pyruvate, +10 % fetal bovine serum (FBS), +1 % penicillin/streptomycin (Life technologies)). For generation of rAAVs, HEK293T cell line was used and cultivated in DMEM + GlutaMAX<sup>TM</sup>-I medium (+4.5 g/l glucose, -pyruvate, +10 % fetal bovine serum (FBS), +1 % penicillin/streptomycin (Life technologies)). Cells were kept at 37 °C and 10 % CO<sub>2</sub>.

### 2.3.2 Transfection

HEK293 and HEK293T cells were transiently transfected using the calcium phosphate technique (Graham and van der Eb, 1973). For transfection of 10 cm dishes, the following reagents were added to a 15 ml Falcon tube:

DNA	15 $\mu$ g
2.5 M calcium chloride	50 $\mu$ l
H <sub>2</sub> O	<i>ad</i> 500 $\mu$ l

While vortexing the mixture, 500  $\mu$ l of 2x BBS solution was added dropwise, followed by incubation for 5 min at RT to allow homogenous formation of DNA complexes. The transfection mixture was then added dropwise to the cells (40-70 % confluence). Transfected cells were incubated at 37 °C and 5 % CO<sub>2</sub> for 8-16 h before replacing the medium with fresh medium and transferring the cells back to 37 °C and 10 % CO<sub>2</sub>. Cells were harvested 48 h post-transfection. The amounts of the reagents given above were scaled up to the following, if 15 cm dishes were used:

DNA	30 $\mu$ g
2.5 M calcium chloride	100 $\mu$ l
H <sub>2</sub> O	<i>ad</i> 1 ml
2x BBS	1 ml

### 2x BBS

---

BES	10.65 g
NaCl	16.35 g
Na <sub>2</sub> HPO <sub>4</sub> x 2H <sub>2</sub> O	210 mg
H <sub>2</sub> O	<i>ad</i> 1 l

adjust pH to 6.95 with NaOH,  
sterile filtrate

## 2.4 Animals

All mice used in this study possessed the C57BL/6 genetic background. All procedures involving animals were performed with permission of the local authority (Regierung von Oberbayern). All mice had *ad libitum* access to food (Ssniff; regular feed: R/M-H, breeding feed: M-Z Extrudat) and water. Mice were maintained on a 12 h light/dark cycle.

## 2.5 Protein biochemistry

### 2.5.1 Isolation and quantification of proteins

Isolation of proteins from transfected mammalian cells was performed in the following procedure:

Cells were harvested 48 h post-transfection by removing the medium and transferring the cells to a 2 ml Eppendorf tube. The suspension was centrifuged at 1000x *g* and 4 °C for 10 min. Afterwards, the supernatant was removed and the cell pellet was resuspended in an appropriate volume of lysis buffer (300 µl for cells cultivated in 10 cm dishes, 600 µl for cells cultivated in 15 cm dishes). Cell suspensions were tumbled at 4 °C for 30 min before centrifugation at 4 °C and maximum rpm for 10 min. The supernatant was collected into a fresh 1.5 ml Eppendorf tube and could be stored at -20 °C until further use.

Bradford assay (Bradford, 1976) was used to determine protein concentration of the isolated proteins by transferring 5 µl of the protein lysate into 1 ml poly(methyl methacrylate) (PMMA) cuvettes and addition of 95 µl 0.15 M NaCl solution (5 µl of lysis buffer served as blank control). 1 ml of coomassie blue solution was added and incubated for 2 min at RT. Protein concentration was measured using the BioPhotometer (Eppendorf).

### Lysis buffer

Triton X-100	2.5 ml
5 M NaCl	15 ml
2.5 M CaCl <sub>2</sub>	400 µl
H <sub>2</sub> O	<i>ad</i> 500 ml

### Coomassie blue solution

coomassie brilliant blue G250	50 mg
95 % (v/v) ethanol	25 ml
85 % (v/v) phosphoric acid	50 ml

## 2.5.2 Membrane preparations

Membrane Preparations were performed for enrichment of membrane proteins from transfected mammalian cells or transduced murine retina. Therefore, 1 ml of 1x membrane preparation buffer with complete EDTA-free protease inhibitor cocktail (Roche) was added to the cell pellet or the retina tissue prior to the breakup using the Potter S homogenizer (B. Braun). The homogenized cells were centrifuged at 5,000x *g*, 4 °C for 10 min and the supernatant was collected in to a 6.5 ml clean thick wall polycarbonate tube (16 x 64 mm, Beckman Coulter). 1x membrane preparation buffer was added to a total volume of 4 ml before ultracentrifugation was performed at 30,000 rpm and 4 °C for 45 min in a Sorvall Discovery90 ultra centrifuge with a 45Ti rotor (Beckman). The pellet was then resuspended

in 50-100  $\mu$ l of 1x membrane preparation buffer depending on the pellet size and 5  $\mu$ l were used for protein quantification (see 2.5.1).

3x membrane preparation buffer	
MOPS	3.15 g
sucrose	77 g
0.5 M EDTA (pH 7.4)	6 ml
H <sub>2</sub> O	<i>ad</i> 250 ml

### 2.5.3 Co-immunoprecipitation

Co-IP experiments were performed to analyze protein-protein interactions. For this, 5  $\mu$ g of antibody was added to 30  $\mu$ l of protein G dynabeads (novex by Life Technologies) per sample and PBS was added to a total volume of 500  $\mu$ l. The solution was tumbled at 4 °C for 30 min. Optionally, antibodies could be cross-linked to the beads by adding BS<sup>3</sup> (Thermo Scientific) to a final concentration of 5 mM and tumbling for another 30 min at RT. The cross-linker was inactivated by adding 25  $\mu$ l of 1 M tris-HCl buffer pH 7.5 to a final concentration of 50 mM and tumbling for 30 min at RT. The suspension was then washed twice with 200  $\mu$ l PBS by shortly spinning and retaining the beads with a magnetic separator. Afterwards, the beads were resuspended in 200  $\mu$ l PBS and the suspension was split into equal volumes to all samples. The samples were tumbled at 4 °C for 1-2 h before being washed five times with 200  $\mu$ l PBS. In the final step, the bound proteins were separated from the bead-antibody complexes by resuspending in 10  $\mu$ l PBS, 6x Lämmli buffer with dithiothreitol (DTT) and heating at 75 °C for 10 min before retaining the beads with the magnetic separator. The sample solutions were then ready to be analyzed via SDS-PAGE (see 2.5.4).

An additional de-glycosylation step was done for glycoproteins as they often appear as a smear in the Western blot analysis (see 2.5.5). To obtain sharp protein bands, the samples were resuspended in 10  $\mu$ l of PBS without addition of 6x Lämmli buffer in the final step. Denaturation and deglycosylation with PNGase F (NEB) were performed as described in the manufacturer's manual.

6x Lämmli	
tris-HCl pH 6.8	7 ml
glycerol	3 ml
SDS	1 g

bromophenol blue	1.2 mg
H <sub>2</sub> O	<i>ad</i> 10 ml

6x Lämmli + DTT

---

6x Lämmli	10 ml
DTT	930 mg

## 2.5.4 SDS-polyacrylamide gel electrophoresis

SDS-polyacrylamide gel electrophoresis (SDS-PAGE) was used to separate isolated proteins according to their molecular weight. Therefore, a gradient polyacrylamide gel consisting of a stacking gel and a 6-12 % separation gel was prepared using the Mini Protean 3 gel system (BioRad). PageRuler Prestained Protein Ladder (Thermo Scientific) was loaded to determine the protein sizes. Electrophoresis was run at 140 V and until the protein ladder bands were clearly separated.

10x electrophoresis buffer

---

tris	30 g
glycin	144 g
SDS	10 g
H <sub>2</sub> O	<i>ad</i> 1 l

4x tris-HCl/SDS pH 6.8 buffer

---

tris-HCl	0.5 M
SDS	0.4 %
adjust pH to 6.8	

4x tris-HCl/SDS pH 8.8 buffer

---

tris-HCl	1.5 M
SDS	0.4 %
adjust pH to 8.8	

Stacking gel (for 2 gels)

---

30 % acrylamide/bis-acrylamide	1 ml
4x tris-HCl/SDS pH 6.8 buffer	1.9 ml

## Materials and methods

---

H <sub>2</sub> O	4.6 ml
APS	37.5 µl
TEMED	7.5 µl

gradient separation gel (for 2 gels)

	6 %	12 %
30 % acrylamide/bis-acrylamide	2.3 ml	4.6 ml
4x tris-HCl/SDS pH 8.8 buffer	2.8 ml	2.8 ml
H <sub>2</sub> O	6.2 ml	3.9 ml
APS	22.5 µl	22.5 µl
TEMED	7.5 µl	7.5 µl

use a 10 ml pipette to aspire 4.25 ml 6 % gel solution followed by 4.25 ml 12 % gel solution. Gently mix by aspirating one air bubble before pouring the gradient gel solution into the gel system.

### 2.5.5 Western blotting and immunodetection

Western blotting procedure was performed at 100 V for 90 min using the Mini Trans-Blot Cell (BioRad), polyvinylidene fluoride (PVDF) membrane and transfer buffer. The setup of the blotting device was done according to the manufacturer's manual. After protein transfer, the membrane was incubated in a blocking solution at RT for 1 h before incubation in primary antibody solution at RT for another 1 h or at 4 °C over night, depending on the sensitivity of the primary antibody. The membrane was then washed thrice for five min with TBST by slight agitation prior to incubation in secondary antibody solution at RT for 1 h. After incubation, the membrane was washed thrice for five min with TBST and once in H<sub>2</sub>O. For chemiluminescence detection, the membrane was incubated with Western Blotting Luminol Reagent (Santa Cruz) prepared after manufacturer's protocol. The signal of the protein bands was detected using the Chemidoc MP Imaging system (BioRad) and ImageLab software.

Transfer buffer

tris	3 g
glycin	14.4 g
H <sub>2</sub> O	ad 1 l

## Materials and methods

---

### 10x TBS

tris	12.1 g
NaCl	80.2 g
H <sub>2</sub> O	ad 1 l

### TBST

10x TBS	100 ml
Tween 20	1 ml
H <sub>2</sub> O	ad 1 l

### Blocking solution

TBST	15 ml
non-fat dried milk powder	0.75 g
H <sub>2</sub> O	ad 1 l

### primary/secondary antibody solution

TBST	5 ml
non-fat dried milk powder	0.05 g
antibody stock solution	X

X is the used dilution according to Table 2.5.5.1.

**Table 2.5.5.1. Antibodies and respective dilutions used for Western blotting.**

Antibody	Source	Dilution
rb anti-CNGB1a	in-lab production	1:5000
ms anti-GFP JL-8	Clontech	1:2000
ms anti-myc 9B11	Cell Signaling	1:2000
ms anti-peripherin-2 2B7	Gift from Dr. Muna Naash, Department of Cell Biology, University of Oklahoma Health Sciences Center	1:2000
ms anti-rhodopsin 1D4	Thermo Scientific	1:2000
gt anti-mouse HRP	Santa Cruz	1:2000
gt anti-rabbit HRP	Santa Cruz	1:2000

## 2.6 Production and purification of rAAVs

### 2.6.1 Transfection and harvest

HEK293T cell line was used for transfection of the pAAV2.1 vector plus the helper plasmids pAD Helper and pAAV 2/8 (YF) via calcium phosphate transfection method as described in chapter 2.3.2. In addition to the regular components of the transfection reagent, dextran 500 and polybrene were added to achieve higher transfection efficiencies (Wu and Lu, 2007). 24 h before transfection, confluent 15 cm dishes of HEK293T cells were split 1:6 into 15x 15 cm dishes for each construct. The following two equations were used to calculate the necessary amount of pAD Helper and pAAV2/8 (YF) for the transfection solution:

$$\underline{\text{*amount of pAD Helper}} = \frac{270\mu\text{g} \times MM(\text{pADHelper})}{MM(\text{transgene\_pAAV2.1\_vector})} = \frac{270\mu\text{g} \times 9509\text{g/mol}}{X\text{g/mol}}$$

$$\underline{\text{**amount of AAV 2/8 (YF)}} = \frac{270\mu\text{g} \times MM(\text{pAAV2/8(YF)})}{MM(\text{transgene\_pAAV2.1\_vector})} = \frac{270\mu\text{g} \times 4523\text{g/mol}}{X\text{g/mol}}$$

MM = molar mass of double stranded plasmid

#### Transfection solution

pAAV2.1 vector	270 $\mu\text{g}$
pAD Helper	* $\mu\text{g}$
pAAV 2/8 (YF)	** $\mu\text{g}$
2.5 M CaCl <sub>2</sub>	1.75 ml
8 mg/ml polybrene	17.5 $\mu\text{l}$
10 mg/ml dextran	1.75 ml
H <sub>2</sub> O	ad 17.5 ml

The transfection solution was vortexed while adding 17.5 ml 2x BBS dropwise before adding to all 15 dishes with each 70-80 % cell confluence. Medium replacement was done 24 h post-transfection. After another 24 h, cells were harvested by scraping them with a cell scraper from each 15 cm dish and collecting cell suspensions from all dishes in a 500 ml centrifuge tube. The cell suspension was centrifuged at 2000x g and 4 °C for 15 min (4000 rpm in a J2-MC Beckman centrifuge using a JA-10 rotor). The medium was decanted from

the cell pellet before resuspending in 7.5 ml lysis buffer and subsequent transferring into a 50 ml polystyrene tube.

Lysis buffer for AAVs

NaCl	150 mM
tris-HCl pH 8.5	50 mM
sterile filtrate	

## 2.6.2 Purification of rAAVs via iodixanol gradient centrifugation

The cell suspension was shock-frozen in liquid nitrogen and thawed at 37 °C in a water bath for three times. Benzonase was added to the thawed cell suspension to a final concentration of 50 U/ml and the suspension was incubated at 37 °C for 30 min. The cells were pelleted via centrifugation at 2000x *g* and 4 °C for 25 min and the virus-containing supernatant was transferred into a Beckman Quick-Seal polypropylene tube (Beckman). The virus-containing phase was underlain with 7 ml 15 % iodixanol, followed by 5 ml 25 %, 5 ml 40 %, and at last by 6 ml 60 % iodixanol. Using a sterile, long glass pipette and a Gilson MINIPULS3 pump the iodixanol underlayers were made without mixing of the layers. The polypropylene tubes were balanced with PBS-MK before sealing them with the Beckman Tube Topper. Gradient centrifugation was carried out at 361,000x *g* and 18 °C for 1 h 45 min (70,000 rpm in an Optima LE-80K Beckman ultracentrifuge using a 70 Ti rotor). In the following step, the tube was pierced multiple times at the top near the seal for pressurization. To collect the 40 % phase containing the virus, a 21-gauge needle with a 5 ml syringe was used to pierce the tube through the side at the lower end of the 40-60 % interface. Approximately 5 ml of the 40 % phase were collected until the interface was close below the 25 % phase.

Tween/PBS-MK

10x PBS	50 ml
1 M MgCl <sub>2</sub>	500 µl
2.5 M KCl	500 µl
Tween 20	0.014 % (v/v)
H <sub>2</sub> O	<i>ad</i> 500 ml
sterile filtrate	

## Materials and methods

---

### 15 % iodixanol

10x PBS	5 ml
1 M MgCl <sub>2</sub>	50 µl
2.5 M KCl	50 µl
5 M NaCl	10 ml
Optiprep	12.5 ml
1 %(v/v) phenol red	37.5 µl
H <sub>2</sub> O	<i>ad</i> 50 ml
sterile filtrate	

### 25 % iodixanol

10x PBS	5 ml
1 M MgCl <sub>2</sub>	50 µl
2.5 M KCl	50 µl
Optiprep	20.9 ml
1 %(v/v) phenol red	50 µl
H <sub>2</sub> O	<i>ad</i> 50 ml
sterile filtrate	

### 40 % iodixanol

10x PBS	5 ml
1 M MgCl <sub>2</sub>	50 µl
2.5 M KCl	50 µl
5 M NaCl	10 ml
Optiprep	33.3 ml
H <sub>2</sub> O	<i>ad</i> 50 ml
sterile filtrate	

### 60 % iodixanol

1 M MgCl <sub>2</sub>	50 µl
2.5 M KCl	50 µl
Optiprep	50 ml
1 %(v/v) phenol red	37.5 µl
sterile filtrate	

### 2.6.3 Purification of rAAVs via anion exchange chromatography

For further virus purification, the ÄKTAprime plus chromatography system (GE Healthcare Life Sciences), HiTrap Q FF sepharose column (GE Healthcare Life Sciences), and PrimeView software (GE Healthcare Life Sciences) were used according to manufacturer's manual. The column was equilibrated with 25 ml of buffer A at 10 ml/min flow rate. The following manual run was selected with 1.0 ml/min flow rate and 1 ml fraction size. The virus phase was diluted 1:1 with buffer A prior to injection with a 10 ml syringe to the superloop. Injection of the virus dilution from the superloop into the system was started and 1 ml fractions were collected in 1.5 ml Eppendorf tubes. UV- and conductance curves were observed via the PrimeView software. When the conductance curve returned to base value, a switch to 100 % buffer B was performed at 10 ml/min flow rate and 0 ml fraction size to purge the sepharose column from remaining virus. It was then switched to sterile H<sub>2</sub>O to wash remaining salt from the column and system at 10 ml/min flow rate. When the conductance curve reached zero, washing was continued for 20 min. All 1 ml fractions within the plateau phase of the conductance curve were combined and stored at -20 °C until virus concentration as described in chapter 2.6.4.

#### Buffer A

tris	20 mM
NaCl	15 mM
H <sub>2</sub> O	ad 1 l
adjust pH to 8.5 and sterile filtrate	

#### Buffer B

NaCl	2.5 M
H <sub>2</sub> O	ad 1 l
adjust pH to 8.5 and sterile filtrate	

### 2.6.4 Concentration of rAAVs

4 ml of the purified virus fraction was applied to an Amicon centrifugal filter unit (Millipore) and centrifugation was done at 2000x *g* and 20 °C for 20 min (4000 rpm in a Beckman centrifuge using a JA-10 rotor). The flow-through was discarded and the residual virus fraction was applied to the Amicon filter. Centrifugation was continued until 500 µl remained in the filter unit. Washing was done with 1 ml 0.014 % Tween/PBS-MK by pipetting up and

down five times. Centrifugation in 10 min steps was continued until 100  $\mu$ l of concentrated virus suspension remained in the filter unit. It was then split into 10  $\mu$ l aliquots and stored in 1.5 ml tubes with screw cap. Virus suspensions were stored at -80 °C until determination of virus titer and subretinal injection.

### 2.6.5 rAAV titer determination via quantitative real-time PCR

To determine the genomic titer of the virus preparation by quantitative real-time PCR, a standard curve was generated using a serial dilution of the WPRE fragment which was amplified from the pAAV2.1 vector with the following primers:

WPREq\_F: AGTTCCGCCGTGGCAATAGG

WPREq\_R: CAAGGAGGAGAAAATGAAAGCC

After amplification, the fragment was purified as described in chapter 2.2.5. Its concentration was determined as described in chapter 2.2.9. The concentration of the standard for  $10^{10}$  genomic copies per 5  $\mu$ l was calculated with the following equation:

$$c(\text{pg}/\mu\text{l}) = \frac{10^{10} \times 660 \times 10^{12} \text{ pg/mol} \times \text{WPRE\_fragment\_size}}{6.022 \times 10^{23} \text{ /mol} \times 5\mu\text{l}}$$

c = concentration of the standard for  $10^{10}$  copies per 5  $\mu$ l

$660 \times 10^{12}$  pg/mol = mean molar mass of a base pair (deoxyribosyladenosine with deoxyribosylthymidine or deoxyribosylcytidine with deoxyribosylguanosine)

$6.022 \times 10^{23}$  /mol = Avogadro constant

Afterwards, a tenfold serial dilution was generated in which the first dilution contained  $1 \times 10^{10}$  copies/5  $\mu$ l and the last dilution contained  $1 \times 10$  copies/5  $\mu$ l. 5  $\mu$ l of H<sub>2</sub>O was used for blank. Each dilution was amplified in two samples by qPCR using the Light Cycler LC480 (Roche). The SYBR green I (Roche) fluorescence intensity was analyzed for each cycle. The LightCycler software LC-Run (version 5.32, Roche) was used to generate a fluorescence curve and subsequently to calculate the crossing points ( $C_p$ ) value which points out the cycle in which the fluorescence rises significantly above the background signal. The standard curve could then be formed from the logarithmized dilutions plotted against the  $C_p$  value.

The purified and concentrated rAAV preparations were diluted 1:500 in H<sub>2</sub>O before two of each sample were amplified via qPCR. Fluorescence was measured as described above

and a fluorescence curve was generated. The software then calculated the genomic titers by correlating the  $C_p$  values of the rAAV samples to the standard curve.

### Pipetting scheme for qPCR

WPRE_F (10 $\mu$ M)	1 $\mu$ l
WPRE_R (10 $\mu$ M)	1 $\mu$ l
SYBR green I master mix	10 $\mu$ l
template	5 $\mu$ l
H <sub>2</sub> O	<i>ad</i> 20 $\mu$ l

### qPCR conditions

Initial denaturation	95 °C	10 min
*Denaturation	95 °C	10 sec
*Annealing	60 °C	5 sec
*Elongation	72 °C	20 sec
Final elongation	72 °C	5 min

\*These steps were repeated in 40 cycles.

## 2.7 Subretinal injection

Subretinal injections were performed to transduce murine rod or cone photoreceptors with the rAAV transgene. First, a NanoFil 34-gauge beveled needle (World Precision Instruments) was sterilized and the 10  $\mu$ l glass syringe was preloaded with the virus preparation without any bubble formation. The 2 weeks old mouse (P14) was anaesthetized by intraperitoneal injection of xylazine (20 mg/kg) and ketamine (40 mg/kg). 5 % dexpanthenol eye salve was applied to the uninjected eye and the mouse was placed on a 37 °C heat plate. The eye chosen for injection was dilated with 1 % atropine and 0.5 % tropicamide eye drops for 5 min. Using a stereomicroscope the eye fundus was focused until blood vessels were clearly visible. The outer layers of the eye were penetrated by the needle at a 60 ° angle until it was visible beneath the retina. After slow injection of 1  $\mu$ l of virus suspension containing titer-matched rAAV copies ( $10^9$ ), the formation of a clear subretinal bleb confirmed the correct application into the subretinal space. The needle was carefully withdrawn and the injected eye was treated with gentamicin 5 mg/g and dexamethasone 0.3 mg/g eye salve. The anaesthetized mouse was placed under a heat lamp and was kept under supervision until it awakened from the narcosis. Minimum 10 days were required for sufficient protein expression in the retina. Three weeks post injection, all injected retinas

were analyzed for the fluorescence using scanning laser ophthalmoscopy (Spectralis, Heidelberg Eye Instruments).

## 2.8 Retina preparation and immunohistochemistry

The subretinally injected mouse was euthanized and the eyeball was collected. Under a stereomicroscope (Stemi 2000, Zeiss), the eyeball was perforated with a 0.8 mm needle at the *ora serrata* and subsequently pre-fixed for 5 min in 4 % paraformaldehyde (PFA) on ice. The eyeball was then cut with a micro-scissor (Mini Vanas, 3 mm, Frohnhäuser) along the *ora serrata* into two parts and the half containing cornea, lens and vitreous body was removed. The retina-containing cup was incubated in 4 % PFA for 45 min followed by 3 washing steps by incubation for 5 min in 0.1 M PB. The eye cup was then incubated in 30 % sucrose, under slight agitation overnight at 4 °C. The eye cup was embedded using Tissue Freezing Medium (Electron Microscopy Sciences) which was then frozen on dry ice. A cryostat (Leica CM3050 S, Leica) was used to make transversal sections from the embedded tissue with a section size of 10 µm. The retinal cryosections were mounted carefully onto glass slides and were stored at -80 °C until further use.

For Immunohistochemistry, glass slides with retinal cryosections were surrounded by a hydrophobic barrier using PAP pen Liquid blocker (Science Services). Each was re-hydrated with 0.1 M PB for 5 min followed by fixing in 4 % PFA in 0.1 M PB for 10 min. The cryosections were then washed thrice with 0.1 M PB for 5 min. Subsequently, incubation in primary antibody diluted in 0.1 M PB with 5 % ChemiBlocker (Millipore) and 0.3 % Triton X-100 was performed overnight at 4 °C. Afterwards, retinal cryosections were washed thrice with 0.1 M PB for 5 min followed by incubation in secondary antibody diluted in 0.1 M PB with 3 % ChemiBlocker for 1.5 h at RT. Afterwards, the cryosections were washed once with 0.1 M PB for 5 min prior to nuclear staining with Hoechst 33342 solution (5 µg/µl) for 5 min. After the final washing with 0.1 M PB for 5 min, one drop of Fluoromount-G™ Slide Mounting Medium (Thermo Scientific) was added on top of each cryosection before mounting a cover slip on the glass slide. Dried slides were stored at 4 °C in the dark until further analysis.

### 0.1 M PB

Na <sub>2</sub> HPO <sub>4</sub> x 2H <sub>2</sub> O	28.48 g
NaH <sub>2</sub> PO <sub>4</sub> x H <sub>2</sub> O	5.52 g
H <sub>2</sub> O	ad 2 l

adjust pH to 7.4

4 % PFA

PFA 6 g

0.1 M PB *ad* 150 ml

dissolve at 60 °C, sterile filtrate, store at -20 °C

**Table 2.8.1. List of primary and secondary antibodies used for immunohistochemistry.**

Antibody	Source	Dilution
ms anti-rhodopsin	Pierce	1:1000
rb anti-CNGB1a	in-lab production	1:5000
rb anti-M-opsin	Millipore	1:400
rb anti-S-opsin	Millipore	1:300
gt Cy-3 anti-mouse	Jackson Laboratories	1:400
dk Cy-3 anti-rabbit	Jackson Laboratories	1:400

## 2.9 Confocal microscopy

The Leica TCS SP8 confocal microscope (Leica) equipped with 4 solid state lasers (448 nm, 488 nm, 514 nm, 552 nm) was used for *in vitro* imaging of transfected HEK293 cells as well as for immunohistochemically stained retinal cryosections. The LAS-AF software modules (Leica) were used for capturing and processing the images. The Zeiss LSM 510 Meta (Zeiss) confocal microscope was especially used for immunohistochemically stained retinal cryosections to additionally visualize nuclear staining. It was equipped with 4 lasers (UV (251 nm), Argon2 (488 nm), HeNe/1 (543 nm), HeNe/2 (633 nm)). The images were captured and processed with the Zeiss LSM software. All images made with both microscopes consisted of an overlay of 3 scans (Z-stack).

**Table 2.9.1. Excitation and emission maxima of the used fluorescent proteins and dyes provided by Thermo Fisher Scientific.**

Visual color range	Fluorescent protein/dye	Excitation (nm)	Emission (nm)
yellow	citrine	516	529
cyan	cerulean	433	475

red	cy3	550	570
ultraviolet	Hoechst 33342	460	490

Source: <https://www.thermofisher.com/de/de/home/life-science/cell-analysis/labeling-chemistry/fluorescence-spectraviewer.html>

## 2.10 Isolation of rod and cone photoreceptor outer segments

An in-house developed quick protocol was used for isolation of transduced murine rod and cone photoreceptor outer segments as depicted in Figure 2.10.1. For this, mice were euthanized and the eyeball was proptosed by placing a Winkler forceps around the optic nerve and closing it behind its exit from the eye. The globe was transected along the equator using a sharp razor blade or scalpel and the vitreous body was removed by carefully pushing it out of the incision with a thin needle. The Winkler forceps was then gradually pressed upwards to sever the attachment of the optic nerve to the retina. The upward movement was continued until the retina lay free on the forceps. Afterwards, the retina was transferred into a petri dish filled with PBS and remaining pigment epithelium and ciliary body were removed using a stereomicroscope (Stemi 2000, Zeiss) and two fine forceps. The retina was placed into a 1.5 ml Eppendorf tube with 50-100  $\mu$ l PBS before vortexing for 15-30 sec and subsequent centrifugation at 500x  $g$  for 30 sec. The supernatant containing the rod and cone outer segments could be analyzed under the fluorescence microscope by adding 5  $\mu$ l on a glass slide with a cover slip. If the amount of transduced outer segments was sufficient, the supernatant was used for FRET measurements (see 2.11).

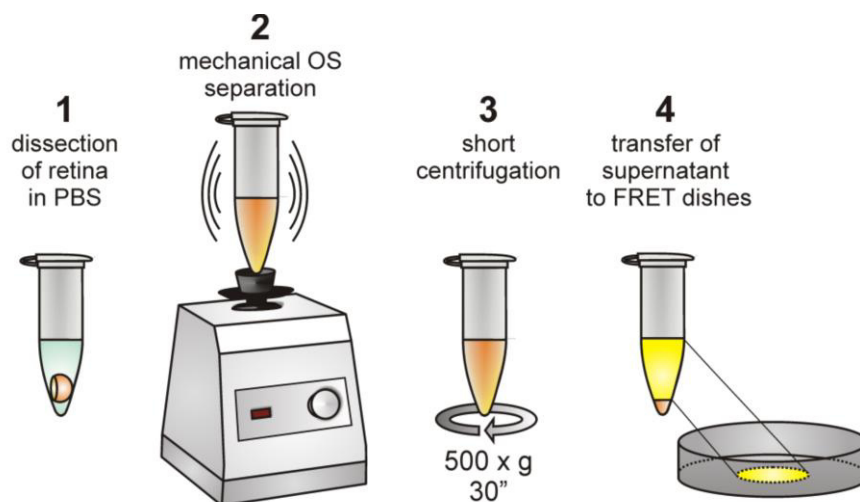


**Figure 2.10.1. Schematic overview of the quick protocol for isolation of photoreceptor outer segments.** OS, outer segments.

## 2.11 Fluorescence resonance energy transfer (FRET)

FRET analysis enables detection of protein-protein interactions and investigation of interaction dynamics. For this purpose, the putative interaction partners need to be fused to fluorophores with one being coupled to the donor-fluorophore and the other coupled to the acceptor-fluorophore with an excitation spectrum that should overlap with the emission spectrum of the donor-fluorophore (Figure 2.11.1). If the two proteins fulfill this requirement and if there is an interaction, FRET occurs via donor excitation and subsequent radiation-less energy transfer to the acceptor. As a requirement, the interaction partners need to be ideally within the Förster distance in which the transfer efficiency is at 50 %. The Förster distance is averagely 5 nm for most of the fluorophore pairs. To obtain comparable data, donor and acceptor emission intensities are measured to calculate the intensity ratios.

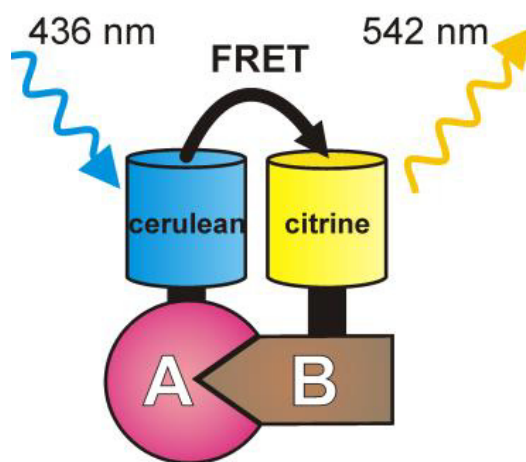


**Figure 2.11.1. Scheme of FRET principle.** Protein A is fused to cerulean (donor fluorophore) and protein B is fused to citrine (acceptor fluorophore). The interaction between A and B and excitation of cerulean at 436 nm lead to radiation-free transfer of energy to citrine, which in turn emits fluorescence at 542 nm.

For FRET measurements, HEK293 cells were grown in  $\mu$ -dishes for FRET (35 mm, low, ibidi) and were transiently transfected using the calcium phosphate method (see 2.3.2). After 24-48 h, the cells were washed and maintained in 37 °C pre-warmed FRET bath solution. In case of isolated rod and cone outer segments (see 2.10), the outer segment suspension was

transferred to a  $\mu$ -dish containing the pre-warmed FRET bath solution and was incubated at RT for 15-20 min to let the outer segments attach to the dish surface. Cells or outer segments were imaged using a Leica DMI6000B inverted fluorescent microscope with a 40x oil objective. Fluorescence intensity was detected by a photometric system (FEI Company) consisting of a photodiode detector head and a control unit for signal integration. The excitation source was a Polychrome V monochromator with a 150 W xenon high stability lamp which allowed for intensity and bandwidth control. The microscope was further equipped with a motorized filter wheel enabling cube switches within 300 msec as well as a donor filter cube (CFP excitation filter, T455LP dichroic mirror, and CFP emission filter), an acceptor filter cube (YFP excitation filter, T515LP dichroic mirror, and YFP emission filter), and a FRET filter cube (CFP excitation filter, T455LP dichroic mirror, and YFP emission filter). The excitation source and excitation parameters (e.g. wavelength, bandwidth, intensity) were controlled by the PolyCon 3.2 and the AxoScope 10.3 softwares and the filter switch was done manually. The fluorescence intensity signals were digitized via an analog digitizer (MiniDigi 2b) and were acquired with clampfit 10.3, part of pClamp 10.3 software. The image-plane pinhole was set to an appropriate size for capturing one single cell or outer segment which was placed in the center of the axial beam path for measurement. Fluorescence intensities of at least 10-15 individual cells or outer segments were measured with each cube (CFP, FRET, YFP). This was done for cells transfected/outer segments transduced with donor and acceptor fusion proteins (FRET sample) as well as for cells transfected/outer segments transduced with either donor or acceptor only which was necessary for later correction of donor bleed through, acceptor cross excitation, and donor cross talk. In addition, at least 5 cells/outer segments were analyzed which do not express any fluorescence protein to subtract auto-fluorescence from the intensities. After transfer of the data to MathLab and Microsoft Excel softwares, FRET ratios (FR) were calculated according to the three-cube-FRET equation:

$$FR = \frac{F_{DA}}{F_A} = \frac{S_{FRET,DA} - R_{D1} \times S_{CFP,DA}}{R_{A1} \times (S_{YFP,DA} - R_{D2} \times S_{CFP,DA})}$$

$F_{DA}$  =total citrine emission

$F_A$  = citrine emission corrected by acceptor cross excitation and donor cross talk

$S_{FRET}$  = FRET filter

$S_{CFP}$  = cerulean filter

$S_{YFP}$  =citrine filter

$D$  = cell expressing only donor for calibration

$A$  = cell expressing only acceptor for calibration

$D_A$  = cell expressing donor and acceptor for FRET

$R_{D1} = S_{FRET, D} / S_{CFP, D}$  (absolute term for correction of donor bleed through)

$R_{A1} = S_{FRET, A} / S_{YFP, A}$  (absolute term for correction of acceptor cross excitation)

$R_{D2} = S_{YFP, D} / S_{CFP, D}$  (absolute term for correction of donor cross talk)

The overall FRET ratio is the mean value of FRs calculated with the equation shown above. For all measurements, cerulean (FRET-optimized CFP derivative) or citrine (FRET-optimized YFP derivative) were N- or C-terminally fused to the proteins of interest (Griesbeck *et al.*, 2001; Zacharias *et al.*, 2002; Rizzo *et al.*, 2004).

### FRET bath solution

NaCl	140 mM
KCl	5 mM
MgCl <sub>2</sub>	1 mM
CaCl <sub>2</sub>	2 mM
glucose	10 mM
Na-HEPES	10 mM
H <sub>2</sub> O	<i>ad</i> 50 ml
adjust pH to 7.4	

## 2.12 Statistics

For the results in section 3.1, all values were calculated as mean  $\pm$  standard error of the mean (SEM) and  $n$  is the number of animals or trials. For comparison between two groups, unpaired Student's t-test was used. Statistical significance is given as follows: \*,  $p < 0.05$ ; \*\*,  $p < 0.01$ ; \*\*\*,  $p < 0.001$ .

Statistical analyses in chapter 3.2 were conducted using one-way ANOVA followed by Tukey's multiple comparison test to compare FRET ratios (FRs) between wild-type and mutant peripherin-2 with S-opsin and M-opsin. To compare between wild-type and mutant peripherin-2 with rod opsin, unpaired two-tailed t-test was used. All values were calculated as mean  $\pm$  standard error of the mean (SEM). \*,  $p < 0.05$ ; \*\*,  $p < 0.01$ ; \*\*\*,  $p < 0.001$ .

### 3 Results

#### 3.1 Analysis of the peripherin-2 and rhodopsin interaction in outer segments of rod photoreceptors

In preliminary work, to identify novel CNG channel-interacting proteins, immunoprecipitation from murine WT retinal lysates using a CNG channel B-subunit (CNGB1a)-specific antibody was performed in combination with a subsequent quantitative LC-MS/MS mass spectrometry analysis. Lysates of age-matched CNGB1-deficient mice served as negative control. Among the list of outer segment-specific putative CNGB1a-interacting proteins, rhodopsin and peripherin-2 were identified (see list in chapter 7.2). This finding implies that in rod photoreceptors, rhodopsin, the rod CNG channel subunit CNGB1a, and peripherin-2 assemble to one complex. To investigate this hypothesis in detail, *in vitro* and *in vivo* protein biochemical, imaging, and FRET experiments were conducted.

##### 3.1.1 Confirmation of the CNGB1a-interacting proteins in the mouse retina

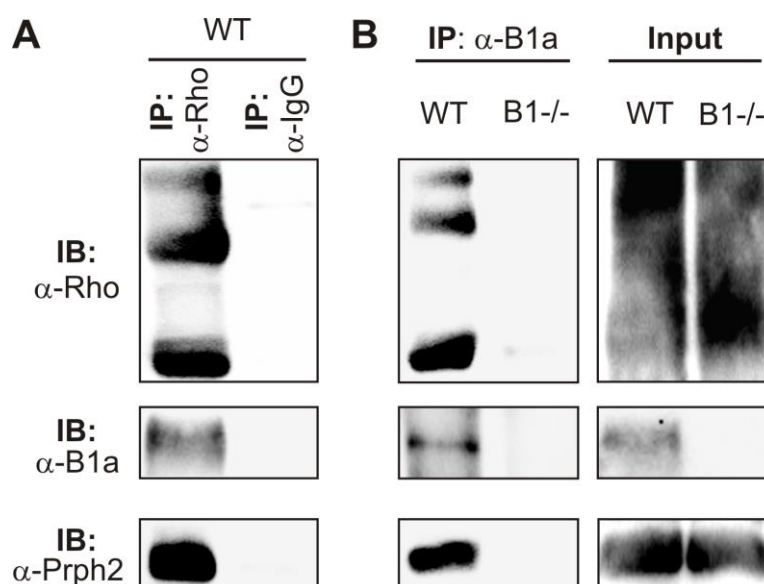


**Figure 3.1.1.1. CNGB1a, peripherin-2, and rhodopsin form a complex in the retina.** A) Retinal lysates of wild-type (WT) mice were immunoprecipitated (IP) with an anti-rhodopsin antibody ( $\alpha$ -Rho) or a non-specific control antibody ( $\alpha$ -IgG). The samples were analyzed in immunoblots (IB) using  $\alpha$ -Rho and antibodies directed against CNGB1a ( $\alpha$ -B1a) and peripherin-2 ( $\alpha$ -Prph2). B) *Left*, retinal lysates of WT and CNGB1 knockout mice (B1<sup>-/-</sup>) were immunoprecipitated with  $\alpha$ -B1a and probed

with  $\alpha$ -Rho,  $\alpha$ -B1a, and  $\alpha$ -Prph2. *Right*, loading control which contains 10 % of the retinal lysate used for the IP in the left panel.

Reciprocal co-immunoprecipitations (co-IP) from retinal lysates using either an anti-rhodopsin antibody (Figure 3.1.1.1A) or an anti-CNGB1a antibody (Figure 3.1.1.1B) revealed that rhodopsin, peripherin-2, and CNGB1a are present in the same channel complex. Importantly, no specific bands were observed when performing the co-IPs with retinal lysates from CNGB1 knockout mice (Figure 3.1.1.1B, lane 2) or when a control IgG was used instead of the anti-CNGB1a antibody (Figure 3.1.1.1A, lane 2). In addition to monomeric rhodopsin, the anti-rhodopsin antibody detected bands corresponding to rhodopsin oligomers (i.e. dimers, trimers, and tetramers) pointing to a tight interaction between rhodopsin molecules, which persisted under SDS-PAGE conditions.

### 3.1.2 Analysis of the rod opsin/peripherin-2/CNGB1a complex in HEK293 cells

In previous studies, it was shown that peripherin-2 binds to the N-terminal GARP domain of CNGB1a (Poetsch *et al.*, 2001; Ritter *et al.*, 2011). However, an interaction between peripherin-2 and rhodopsin or between rhodopsin and CNGB1a has not been reported so far. To address this issue, I performed co-IPs in HEK293 cells expressing different combinations of the chromophore-free rod apo-opsin (herein referred to as rod opsin), peripherin-2, and the rod CNG channel subunits (Figure 3.1.2.1A, B).

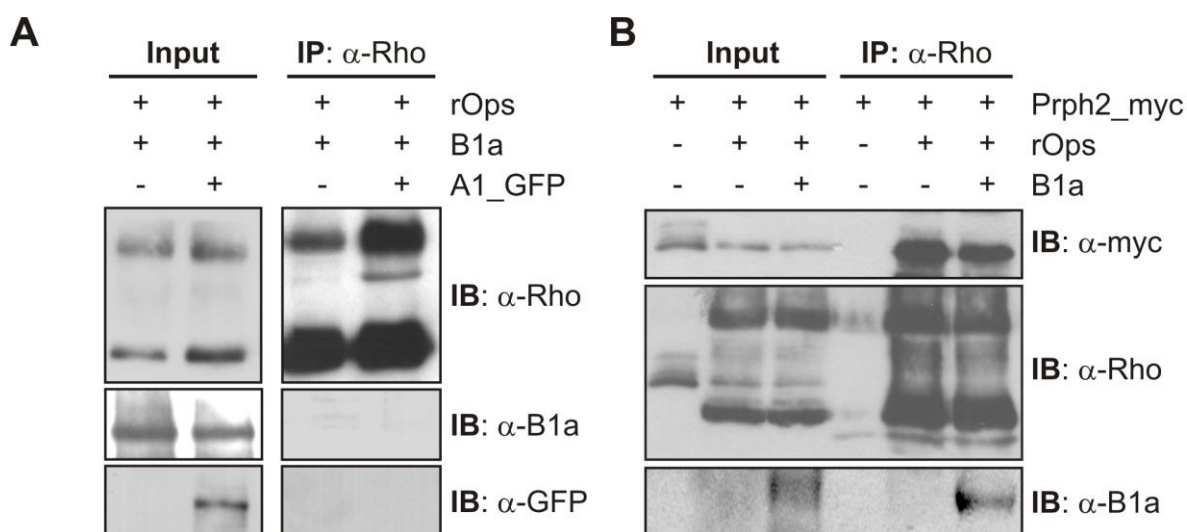


**Figure 3.1.2.1. Peripherin-2 binds to both, rod opsin and CNGB1a.** A) Lysates from HEK293 cells were co-transfected with rod opsin (rOps), CNGB1a (B1a), and GFP-tagged CNGA1 (A1\_GFP) as

indicated, prior to co-immunoprecipitation (IP) with  $\alpha$ -Rho. The immunoblot (IB) was probed with  $\alpha$ -Rho,  $\alpha$ -B1a, and an antibody directed against GFP ( $\alpha$ -GFP). The input contains 10 % of the cell lysate used for the IP. B) Lysates from HEK293 cells were co-transfected with rOps, B1a, and myc-tagged peripherin-2 (Prph2\_myc) as indicated, prior to IP with  $\alpha$ -Rho. The IB was analyzed with an antibody recognizing myc-tag ( $\alpha$ -myc),  $\alpha$ -Rho, and  $\alpha$ -B1a. The input contains 10 % of the cell lysate used for the IP. Single transfection of Prph2\_myc served as a negative control for non-specific binding to the beads used for the IP (third lane from the right).

In the absence of peripherin-2, rod opsin did not assemble with CNGB1a nor did it interact with this subunit when both subunits of the native CNG channel (CNGB1a + CNGA1) were present (Figure 3.1.2.1A). By contrast, when peripherin-2 was co-expressed together with rod opsin and CNGB1a, the CNGB1a subunit could be co-immunoprecipitated with the anti-rhodopsin antibody (Figure 3.1.2.1B, lane 6). Moreover, peripherin-2 was binding to rod opsin in the absence of CNGB1a (Figure 3.1.2.1B, lane 5). Taken together, the co-IP experiments indicate that rod opsin requires peripherin-2 to interact with CNGB1a. A model explaining this is that peripherin-2 physically links rod opsin and CNGB1a by simultaneously binding to both proteins.

### **3.1.3 FRET analysis of the rod opsin/peripherin-2/CNGB1a interaction in HEK293 cells**

To confirm the interaction described in chapter 3.1.2 with another method, FRET experiments were applied that allow detection and quantification of protein-protein interactions. For this purpose, the proteins were C-terminally tagged with either cerulean or citrine. The respective fusion protein pairs were transiently co-transfected in HEK293 cells that were subsequently used for FRET measurements.

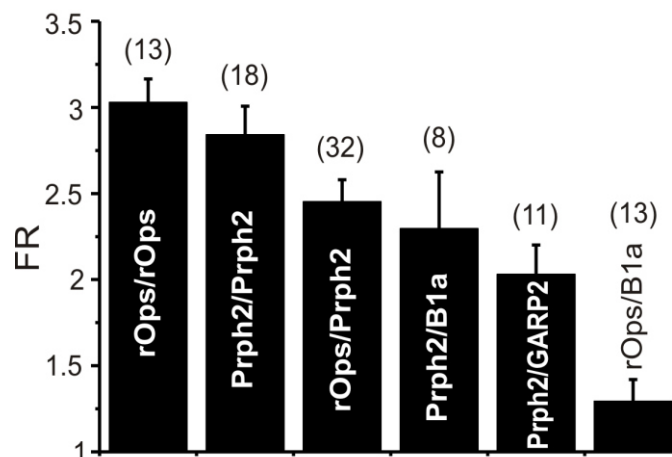


**Figure 3.1.3.1. The peripherin-2/rod opsin and peripherin-2/CNGB1a interaction is confirmed by FRET.** HEK293 cells were co-transfected with different fusion protein pairs. Subsequent FRET measurements were performed to detect and quantify homomeric and heteromeric protein-protein interactions. Rod opsin (rOps), peripherin-2 (Prph2), CNGB1a (B1a), and soluble GARP were C-terminally tagged with either cerulean (donor fluorophore of the pair) or citrine (acceptor fluorophore of the pair), as indicated. The calculated FRET ratios (FR) for the single FRET pairs are as follows: rOps/rOps, FR =  $3.03 \pm 0.14$ ; Prph2/Prph2, FR =  $2.84 \pm 0.17$ ; rOps/Prph2, FR =  $2.45 \pm 0.13$ ; Prph2/B1a, FR =  $2.30 \pm 0.33$ ; Prph2/GARP, FR =  $2.03 \pm 0.17$ ; rOps/B1a, FR =  $1.29 \pm 0.13$ . Numbers of independent measurements (n) are given in brackets.

In agreement with the immunoprecipitation data, robust FRET signals were obtained for rod opsin/peripherin-2 and as well as for peripherin-2/CNGB1a. Quantitatively, FRET ratios of these pairs were in a similar range. However, these FRET ratios were somewhat lower than those obtained for rod opsin or peripherin-2 homodimers. In agreement with previous findings (Poetsch *et al.*, 2001; Ritter *et al.*, 2011), the FRET data also revealed a robust interaction between peripherin-2 and the soluble GARP2, which corresponds to the N-terminal portion of CNGB1a. Importantly, the FRET ratio obtained for the rhodopsin/CNGB1a FRET pair was only slightly above background confirming that there is no specific interaction between these two proteins.

### 3.1.4 Identification of the rod opsin-binding region in peripherin-2

To narrow down the region in peripherin-2 which is essential for the interaction with rod opsin, citrine-tagged peripherin-2 constructs with different C-terminal truncations (Figure 3.1.4.1A) were generated and co-expressed with cerulean-tagged rod opsin in HEK293 cells. The results from the FRET measurements are illustrated in Figure 3.1.4.1B.

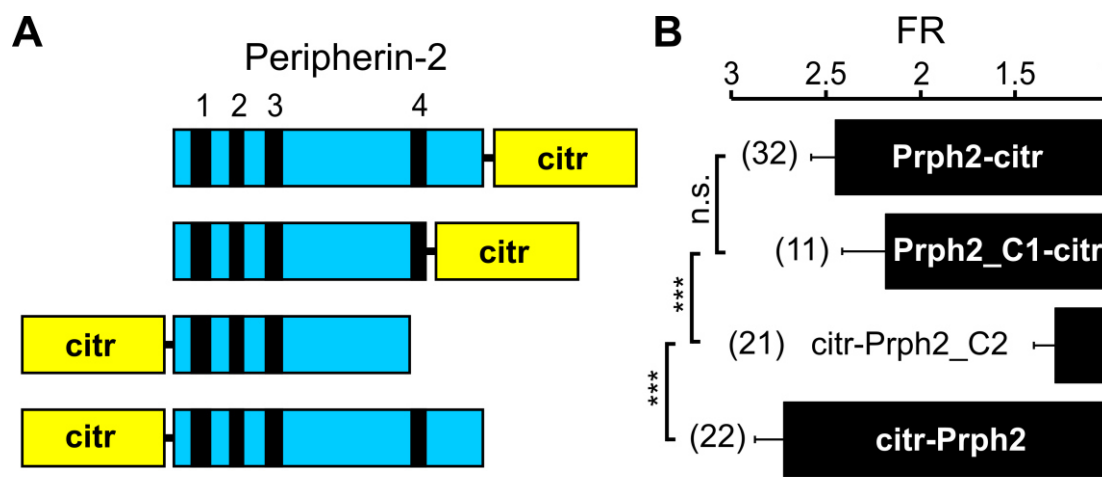


**Figure 3.1.4.1. The fourth transmembrane domain of peripherin-2 is required for interaction with rod opsin.** A) Illustration of peripherin-2 constructs used for determination of FRs in B. Citrine (citr) was fused to either the N- or C-terminus of peripherin-2. The numbered black boxes (1-4) depict the transmembrane domains of peripherin-2. B) FRs of the peripherin-2 constructs co-expressed with rod opsin-cerulean (rOps). Full-length peripherin-2 (Prph2-citr, citr-Prph2), truncated C-terminus (Prph2\_C1-citr), and truncated fourth transmembrane domain and C-terminus (citr-Prph2\_C2). FRs for the single FRET pairs are as follows: rOps/Prph2-citr, FR =  $2.45 \pm 0.13$ ; rOps/Prph2\_C1-citr, FR =  $2.19 \pm 0.23$ ; rOps/citr-Prph2\_C2, FR =  $1.29 \pm 0.11$ ; rOps/citr-Prph2, FR =  $2.73 \pm 0.15$ . Numbers of independent measurements (n) are given in brackets.

Truncation of the C-terminus downstream of the fourth transmembrane domain (Prph2\_C1-citr) did not interfere with the binding to rod opsin. By contrast, additional deletion of TM4 (citr-Prph2\_C2) disrupted the interaction with rod opsin. To ensure that citrine is located to the cytoplasmic side of the cell (like in the C-terminally tagged peripherin-2 constructs containing all four transmembrane domains), it was fused to the N-terminus of the truncation mutant containing only three transmembrane domains. Importantly, the position of citrine did not affect the principal peripherin-2/rod opsin interaction as the FRs of the FRET pairs were in a similar range for N- or C-terminally tagged peripherin-2 (citr-Prph2 and Prph2-citr, Figure 3.1.4.1B).

### 3.1.5 Analysis of rod opsin and peripherin-2 binding characteristics

For specific examination of protein interactions in the plasma membrane and determination of binding properties for the rod opsin/peripherin-2 interaction, confocal FRET experiments were carried out in HEK293 cells (Figure 3.1.5.1).

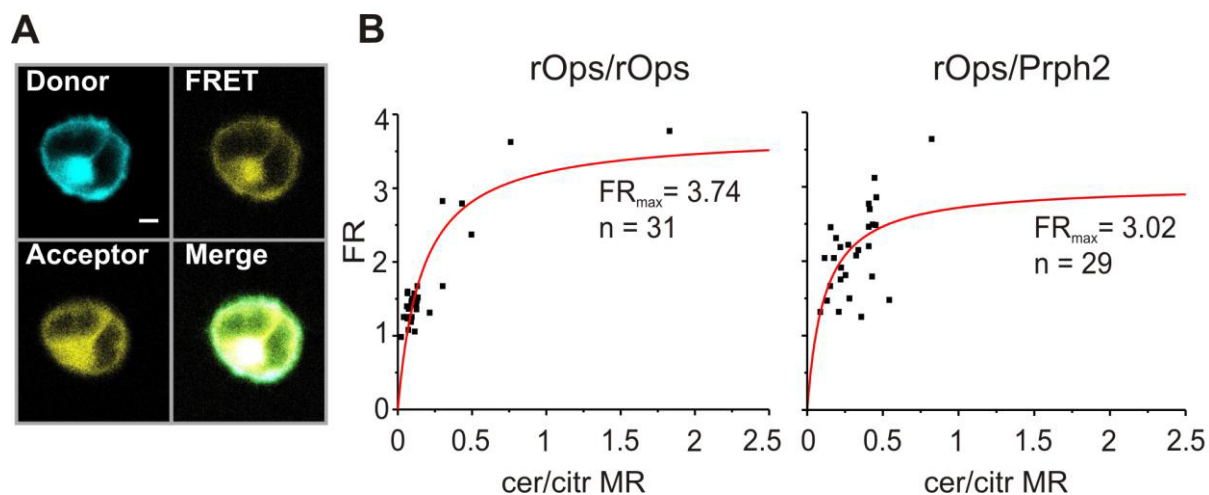


**Figure 3.1.5.1. FRET-based determination of the binding characteristics of the rod opsin/peripherin-2 interaction.** A) Representative confocal images of FRET channels (Donor, FRET, Acceptor, and Merge) of single HEK293 cells co-transfected with FRET pairs for determination of FRs shown in B. Scale bar represents 3  $\mu\text{m}$ . B) Data obtained from confocal FRET measurements of plasma membrane-restricted regions of single cells (black squares). The analyzed FRET pairs were rod opsin-cerulean and rod opsin-citrine (rOps/rOps) or rod opsin-cerulean and peripherin-2-citrine (rOps/Prph2). FR was plotted against the cerulean/citrine molar ratio (cer/citr MR) to calculate maximal FR values ( $\text{FR}_{\text{max}}$ ) and binding curves (red).

The respective maximal FR values ( $\text{FR}_{\text{max}}$ ) were determined for rod opsin/rod opsin and rod opsin/peripherin-2 pairs and were in compliance with the FRs obtained from standard (non-confocal) FRET experiments described in chapter 3.1.3. Based on  $\text{FR}_{\text{max}}$  and the binding curves, the relative binding affinity of the rod opsin/peripherin-2 interaction was calculated to be approximately 80 % of the homomeric rod opsin interaction.

### 3.1.6 FRET analysis of the peripherin-2/rhodopsin interaction in isolated rod outer segments

In order to verify that rhodopsin binds to peripherin-2 in native rod photoreceptors, the respective FRET constructs were cloned into rAAV vectors that contain a human rhodopsin promoter for specific expression in rod outer segments (Figure 3.1.6.1A).

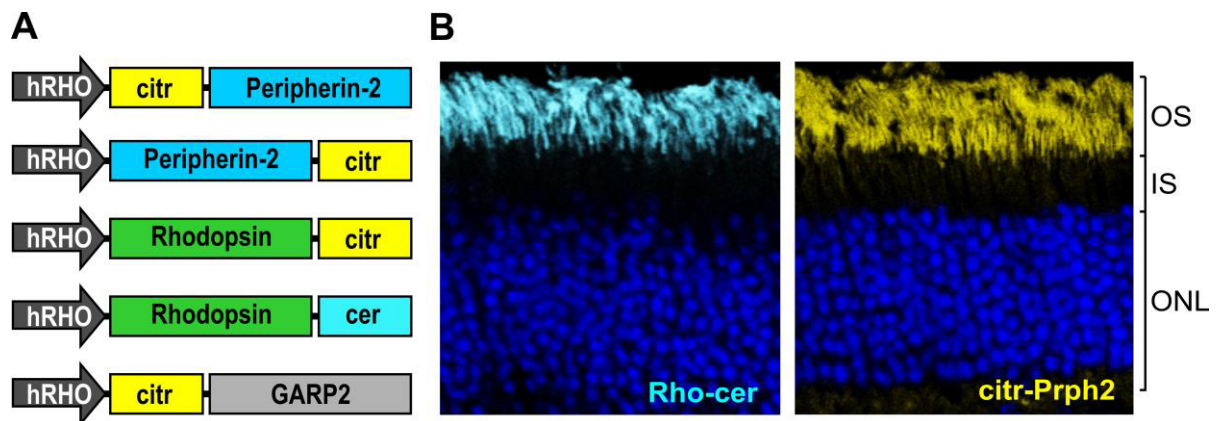


**Figure 3.1.6.1. Expression of rAAV constructs in the outer segments of transduced murine retinas.** A) Schematic presentation of the constructs used for rAAV-mediated transduction of retinas from two week-old C57BL/6N WT mice. hRHO, human rhodopsin promoter. B) Representative confocal images of retinal sections from mice three to four weeks after subretinal delivery of the generated viral vectors. Rhodopsin-cerulean (Rho-cer) is expressed in the left image and citrine-peripherin-2 (citr-Prph2) expression is shown in the right image. OS, outer segment; IS, inner segment; ONL, outer nuclear layer.

The representative images in Figure 3.1.6.1B show robust expression of individual cerulean- or citrine-tagged constructs in retinal sections three to four weeks after subretinal delivery of the viral vectors. The expressed fusion proteins were correctly localized to the rod outer segments indicating that the fluorophores did not affect the ciliary transport.

Rod outer segments were isolated using a self-designed quick protocol that allowed for preservation of outer segment structure and shape (Figure 3.1.6.2A). Figure 3.1.6.2B shows co-expression of a representative FRET pair (rhodopsin-cerulean and peripherin-2-citrine) in an isolated rod outer segment.

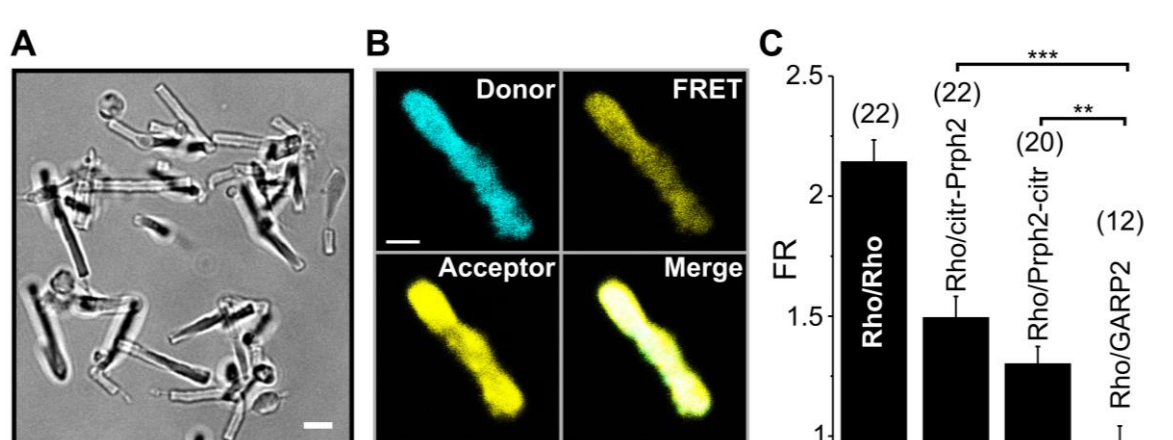


**Figure 3.1.6.2. FRET in isolated rod outer segments from WT mice injected with various rAAV construct pairs.** A) Bright-field of outer segments isolated from mouse retina. Scale bar represents 3

µm. B) Representative confocal image of a single rod outer segment used for FRET measurements. It co-expresses rhodopsin-cerulean (Donor) and peripherin-2-citrine (Acceptor). Scale bar represents 2 µm. C) FRs determined from the FRET measurements for each FRET pair are as follows: rhodopsin-cerulean/rhodopsin-citrine (Rho/Rho), FR =  $2.14 \pm 0.09$ ; rhodopsin-cerulean/citrine-peripherin-2 (Rho/citr-Prph2), FR =  $1.49 \pm 0.09$ ; rhodopsin-cerulean/peripherin-2-citrine (Rho/Prph2-citr), FR =  $1.30 \pm 0.07$ ; rhodopsin-cerulean/GARP2 (Rho/GARP2), FR =  $0.97 \pm 0.07$ . Numbers of independent measurements (n) are given in brackets.

As expected for the native system, FRs were consistently lower than those determined from heterologous expression in HEK293 cells. This can be most probably attributed to the presence of unlabeled endogenous WT proteins that interfere *in vivo* with the FRET constructs thus causing a decrease in the absolute FRET signal. Nevertheless, qualitatively, the results in rod outer segments were comparable with the results obtained from HEK293 cells (Figure 3.1.6.2C). Consistent with the data from HEK293 cells, the FR for N-terminally tagged peripherin-2 was slightly higher than for the C-terminally tagged protein, and the highest FR was observed for the rhodopsin homodimer. Additionally, no FRET was detectable for rhodopsin and rod-specific soluble GARP2 protein, which is in good agreement with previous studies (Korschen *et al.*, 1999; Ritter *et al.*, 2011).

### **3.1.7 Effects of the adRP-linked G266D mutation on the peripherin-2/rod opsin interaction**

As described in chapter 1.6.2, a certain number of peripherin-2 mutations have been associated with adRP. This raises the question whether some of these mutations may cause an impairment in the rhodopsin binding. To address this issue, I analyzed if some adRP-linked mutations are localized in the fourth transmembrane domain (TM4) of peripherin-2, which was demonstrated to be crucial for the interaction with rhodopsin (chapter 3.1.4). One adRP-associated mutation (G266D) was found in the part of TM4 that was most proximal to the intradiscal loop of peripherin-2, as depicted in Figure 3.1.7.1A. The interaction of this PRPH2 mutant and rod opsin was analyzed in transfected HEK293 cells using FRET and co-IP experiments.

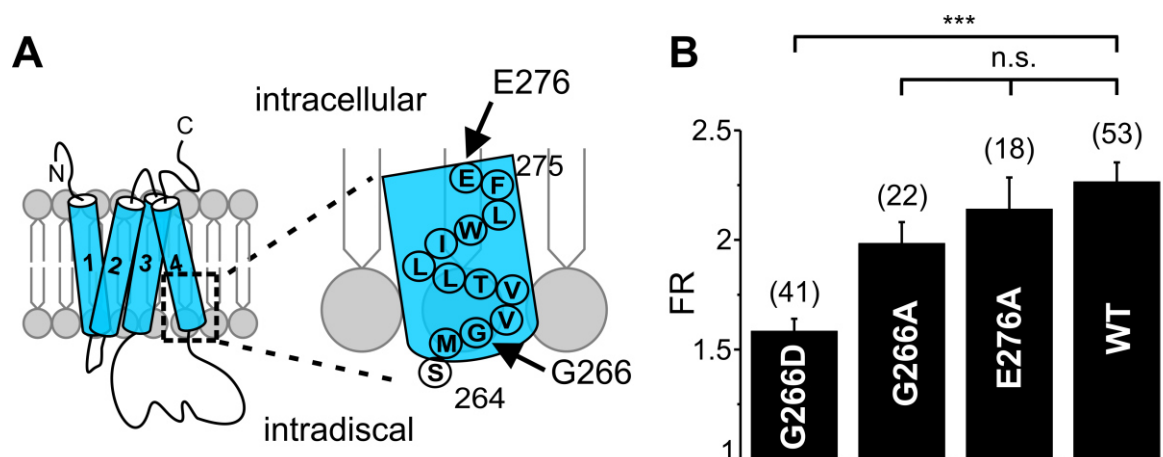


**Figure 3.1.7.1. The G266D mutation in TM4 of peripherin-2 abolishes binding to rod opsin.** A) Schematic illustration of the positions of mutations within TM4 of peripherin-2 that were analyzed in B (black arrows). Transmembrane domains are numbered (1-4). The dashed rectangle on the left depicts the magnified image of the proximal part of TM4 on the right. B) FRET experiments in HEK293 cells co-transfected with rod opsin (rOps) and WT or mutant peripherin-2 constructs, as indicated. FRs for the single FRET pairs are as follows: rOps/G266D, FR =  $1.58 \pm 0.05$ ; rOps/G266A, FR =  $1.98 \pm 0.09$ ; rOps/E276A, FR =  $2.14 \pm 0.14$ ; rOps/WT, FR =  $2.26 \pm 0.08$ . Numbers of independent measurements (n) are given in brackets.

The results from the FRET measurements in HEK293 cells illustrated in Figure 3.1.7.1B indicated that the G266D mutation disrupted the binding to rod opsin. To further demonstrate the specificity of this finding, the effects of two additional mutations in TM4 on the interaction with rod opsin were analyzed. One of the mutated residues was the conserved glutamate at position 276, which was shown in a preceding study to be crucial for the photoreceptor disc morphogenesis (Goldberg *et al.*, 2007). Importantly, changing the glycine residue at position 266 and the glutamate residue at position 276 to the neutral amino acid alanine (G266A and E276A, respectively) did not disrupt the binding to rod opsin.

To confirm the results obtained from FRET measurements in HEK293 cells, co-IP experiments were performed in HEK293 cells co-transfected with rod opsin and WT or mutant peripherin-2 constructs.

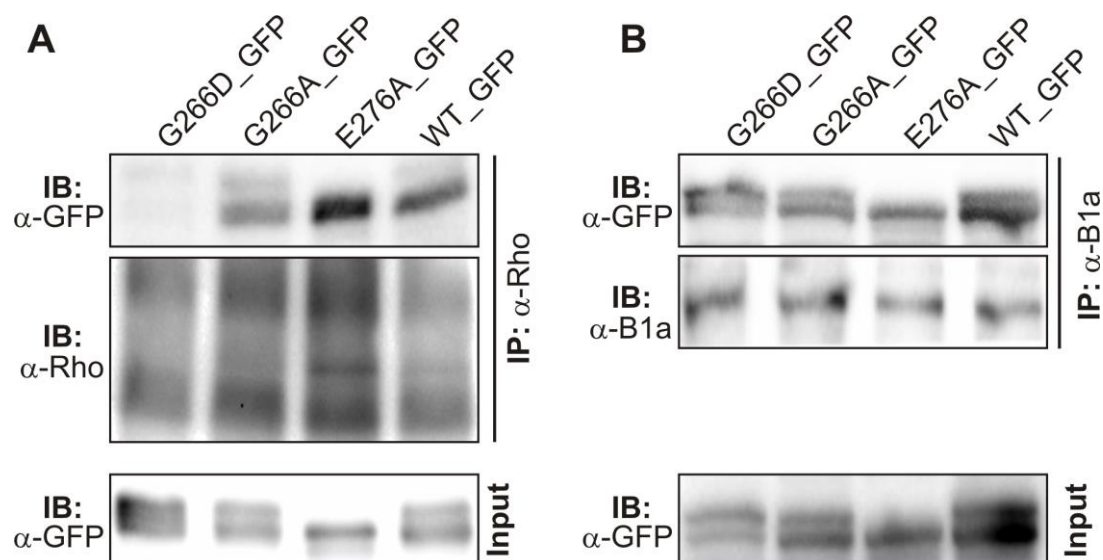


**Figure 3.1.7.2. Co-IP experiments in HEK293 cells confirm the FRET results.** A) Lysates of HEK293 cells co-transfected with rod opsin and GFP-tagged WT or mutant peripherin-2 constructs were immunoprecipitated (IP) with  $\alpha$ -Rho. Immunoblots (IB) were analyzed with  $\alpha$ -GFP and  $\alpha$ -Rho antibodies. B) Lysates of HEK293 cells co-transfected with CNGB1a and GFP-tagged WT or mutant peripherin-2 constructs were immunoprecipitated (IP) with  $\alpha$ -CNGB1a. Immunoblots (IB) were analyzed with  $\alpha$ -GFP and  $\alpha$ -CNGB1a antibodies. The inputs in A and B contain 10 % of the cell lysate used for the IP.

The co-IP experiments presented in Figure 3.1.7.2A also demonstrated that the G266D mutant abolishes the interaction of peripherin-2 with rod opsin. Furthermore, the additional mutants, G266A and E276A showed no effect on the rod opsin binding. A second control co-IP experiment revealed that the interaction of the single peripherin-2 mutations with CNGB1a was not affected (Figure 3.1.7.2B). This indicates that the disrupted binding of the G266D mutant to rod opsin is most likely not due to overall folding efficiency. Importantly, the input controls from the membrane preparations used for the respective co-IPs showed no differences in the membrane expression levels of the mutants compared to WT peripherin-2. This argues against any reduced membrane expression or transport deficits for any of the analyzed peripherin-2 mutants.

### 3.2 Analysis of the peripherin-2 and cone opsin interaction in outer segments of cone photoreceptors

So far, this study demonstrated that peripherin-2 interacts with rhodopsin in rod outer segments. Based on the relatively low homology between rhodopsin and M-opsin (40.9 %) or rhodopsin and S-opsin (43.9 %, see chapter 1.4), it is unclear if peripherin-2 also binds to cone opsins. If there is an interaction between peripherin-2 and cone opsins, it is conceivable that this binding is also mediated by TM4 of peripherin-2. Interestingly, another mutation in TM4 of peripherin-2 (V268I) has been associated with cone defects (Figure 3.2.1.1A). As depicted in Figure 3.2.1.1B, the valine residue at position 268 is highly conserved in mammals as well as in birds. Consequently, using different *in vitro* and *in vivo* approaches, I analyzed if peripherin-2 binds to cone opsins and if the V268I mutation interferes with this interaction. To address these two questions *in vitro*, co-IP and FRET experiments were conducted in HEK293 cells transiently transfected with various combinations of WT and mutant peripherin-2 with S-opsin, M-opsin, and rod opsin.

#### 3.2.1 Interaction analysis of WT and V268I peripherin-2 with cone opsins in HEK293 cells

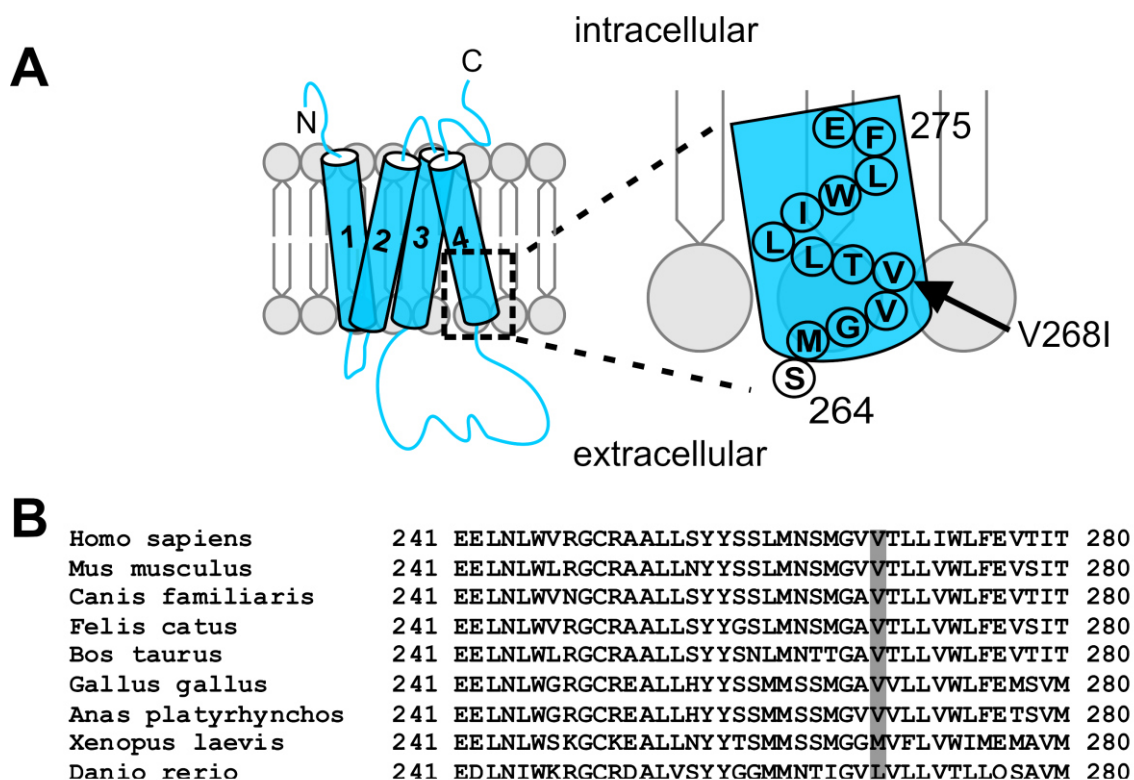


**Figure 3.2.1.1. Localization and conservation of the V268 position in peripherin-2.** A) Schematic illustration of the mutation position within TM4 of peripherin-2 (black arrow). The dashed rectangle on the left depicts the magnified image of the proximal part of TM4 on the right. B) The non-polar amino acid valine is conserved in mammals and birds (grey box). In the African clawed frog, the position is occupied by methionine and in the zebrafish, by leucine. Isoleucine was not found in any of the species at this position.

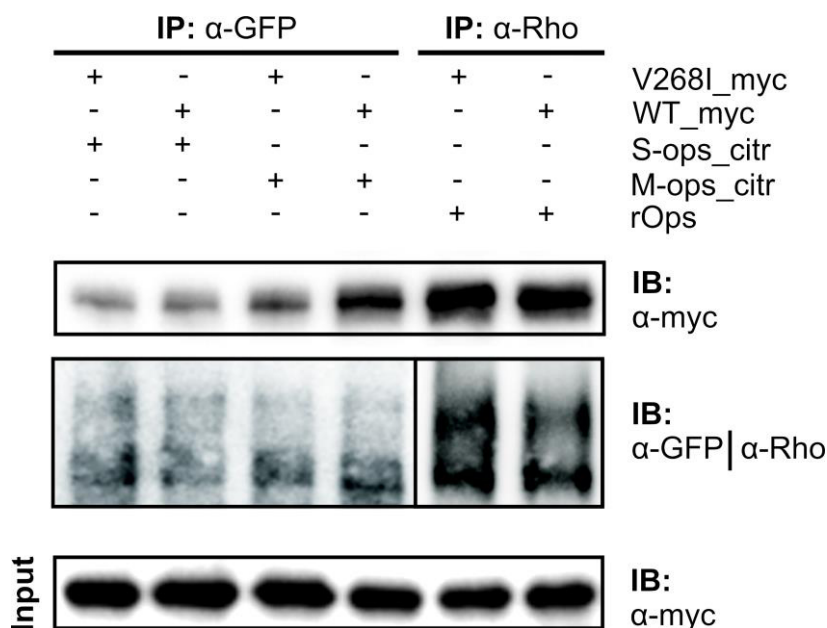


**Figure 3.2.1.2. Peripherin-2 interacts with cone opsins and the V268I mutation selectively impedes the binding to M-opsin.** Co-IPs from HEK293 cells co-expressing either myc-tagged wild-type (WT\_myc) or mutant (V268I\_myc) peripherin-2 with citrine-tagged S-opsin (S-ops\_citr), M-opsin (M-ops\_citr) and tag-free rod opsin (rOps) as indicated. Immunoprecipitation (IP) was performed with anti-GFP antibody ( $\alpha$ -GFP) that recognizes the citrine tag and anti-rod opsin antibody ( $\alpha$ -Rho), respectively. Input controls contain 10 % of total protein lysate used for co-IPs. IB, immunoblotting.

The Western blot analysis in Figure 3.2.1.2 indicates that WT peripherin-2 binds to both cone opsins, albeit their interactions appear to be less strong compared to that of the peripherin-2/rod opsin interaction. Of note, there was also a difference in binding to S-opsin and M-opsin as more peripherin-2 could be co-immunoprecipitated with the latter. Interestingly, the V268I mutant showed a decreased interaction with M-opsin, whereas binding to S-opsin and rod opsin remained unaffected.

To confirm the results from the co-IP experiments and to quantify the protein-protein interactions, FRET measurements were carried out in HEK293 cells transiently co-transfected with WT or mutant peripherin-2 and rod or cone opsins. All FRET partners were C-terminally fused to the FRET fluorophores as indicated in Figure 3.2.1.3A.

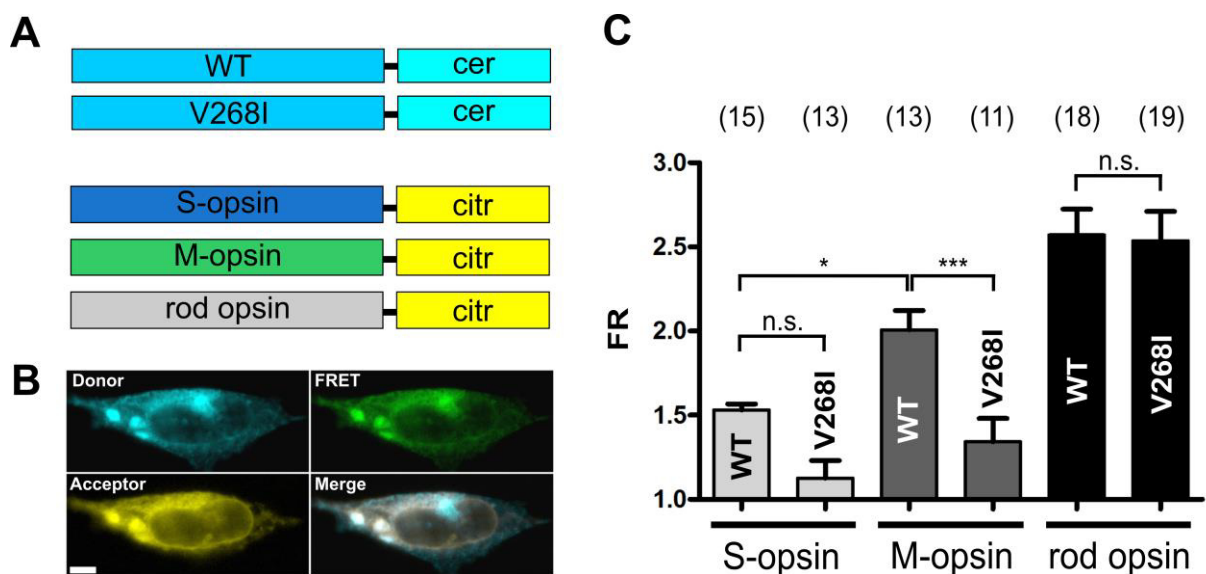


**Figure 3.2.1.3. FRET experiments in HEK293 cells confirm the reduced binding of the V268I peripherin-2 mutant to M-opsin.** A) Schematic representation of wild-type (WT) and mutant (V268I) peripherin-2, S-opsin, M-opsin and rod opsin constructs used for determination of FRET ratios (FR) shown in C. Cerulean (cer) or citrine (citr) was fused to the C-terminus of all transgenes. B) Representative confocal images showing Donor, FRET, Acceptor, and Merge channel of a single HEK293 cell used for the calculation of the FR shown in C. Scale bar represents 3  $\mu$ m. C) FRs of WT and V268I peripherin-2 constructs co-expressed with S-opsin-, M-opsin-, and rod opsin as indicated. Calculated FR of the respective FRET pairs is as follows: WT/S-opsin, FR =  $1.53 \pm 0.04$ ; V268I/S-opsin, FR =  $1.13 \pm 0.10$ ; WT/M-opsin, FR =  $2.00 \pm 0.11$ ; V268I/M-opsin, FR =  $1.34 \pm 0.14$ ; WT/rod opsin, FR =  $2.57 \pm 0.15$ ; V268I/rod opsin, FR =  $2.54 \pm 0.18$ . P value of the compared respective FRs is as follows: WT + S-opsin vs. V268I + S-opsin,  $p = 0.0626$ ; WT + M-opsin vs. V268I + M-opsin,  $p = 0.0002$ ; WT + rod opsin vs. V268I + rod opsin,  $p = 0.8786$ ; WT + S-opsin vs. WT + M-opsin,  $p = 0.0106$ . Numbers of independent measurements (n) are given in brackets.

Consistent with the immunoprecipitation data, FRET signals were detected for WT peripherin-2 in combination with all three opsins (Figure 3.2.1.3B, C). Quantitatively, the strongest FRs were obtained for the peripherin-2/rod opsin interaction followed by the peripherin-2/M-opsin combination. The weakest FRs were measured for the peripherin-2/S-opsin interaction. Importantly, the statistical analysis disclosed that the V268I mutation selectively reduces binding of peripherin-2 to M-opsin (Figure 3.2.1.3C). By contrast, no significant changes between WT and mutant peripherin-2 could be detected for the peripherin-2/S-opsin or the peripherin-2/rod opsin interaction. Overall, the FRET-based measurements are consistent with the results obtained from the co-IPs shown in Figure 3.2.1.2.

### 3.2.2 Analysis of the peripherin-2/cone opsin interaction in WT murine retinas

To confirm the results from HEK293 cells of the peripherin-2/cone opsin interaction *in vivo*, co-IP was performed from membrane preparations of WT mouse retinas (Figure 3.2.2.1).

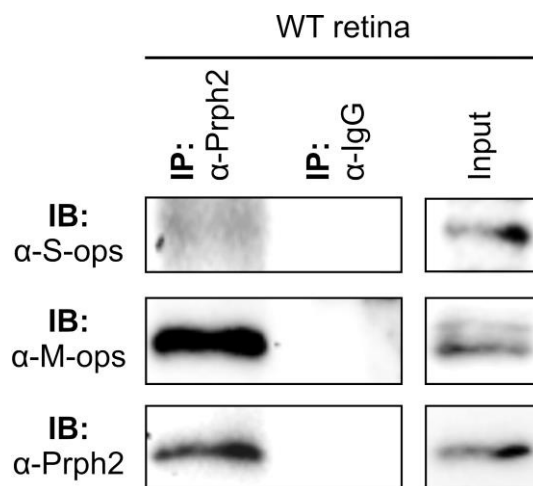


**Figure 3.2.2.1. Peripherin-2 interacts with cone opsins in the murine retina.** Immunoprecipitation (IP) from membrane preparations of WT mouse retinas was performed with anti-peripherin-2 antibody ( $\alpha$ -Prph2) or control antibody ( $\alpha$ -IgG). Immunoblotting (IB) was conducted using antibodies directed against S-opsin ( $\alpha$ -S-ops), M-opsin ( $\alpha$ -M-ops), and  $\alpha$ -Prph2. Input controls contain 10 % of total protein lysate used for co-IPs.

In agreement with the data conducted in HEK293 cells, binding of peripherin-2 to M-opsin appears tighter than that to S-opsin as the intensity of the input band was increased for M-opsin but not for S-opsin after immunoprecipitation using a peripherin-2-specific antibody (Figure 3.2.2.1). Of note, no specific band was detected when a control antibody was used for immunoprecipitation.

To obtain a detailed view on the localization of peripherin-2, S-opsin, and M-opsin in the outer segment of cone photoreceptors, transmission electron microscopy was applied to longitudinal sections of WT mouse retinas (Figure 3.2.2.2). Immunogold particles of different diameters were co-labeled with anti-peripherin-2, anti-S-opsin, and anti-M-opsin antibodies, respectively.

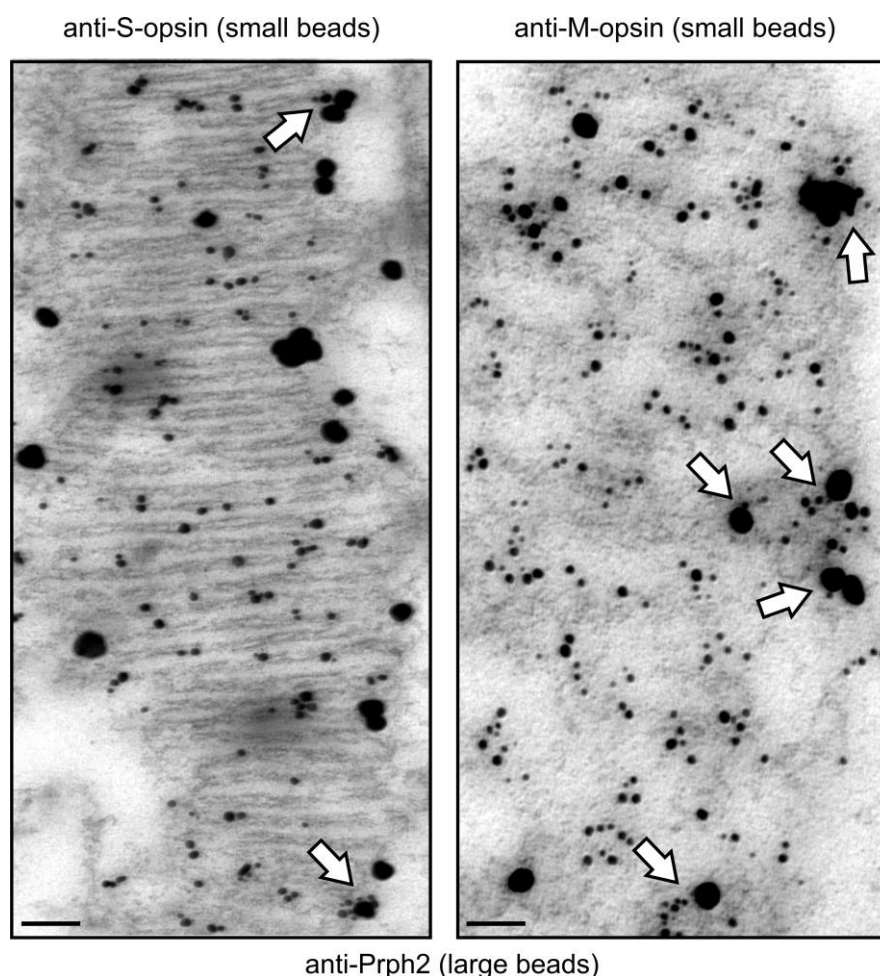


**Figure 3.2.2.2. Peripherin-2 co-localizes with S-opsin and M-opsin in cone outer segments.**

Immunoelectron microscopy images of longitudinal sections of mouse cone outer segments co-stained with small-diameter immunogold beads coupled to anti-S-opsin antibody (left) or anti-M-opsin antibody (right) and large-diameter beads coupled to anti-peripherin-2 (anti-Prph2) antibody. Co-localization of small and large beads is marked by white arrows. Scale bar represents 100 nm.

The transmission electron microscopy images revealed that peripherin-2 partially co-localized with S-opsin and largely co-localized with M-opsin. (Figure 3.2.2.2, left and right panel). This is in line with a more stringent interaction of peripherin-2 and M-opsin, as suggested from the data in Figures 3.2.1.2, 3.2.1.3, and 3.2.2.1.

### 3.2.3 rAAV-mediated expression of the V268I mutant in cones

Despite the fact that no mislocalization of the V268I mutant was observed in HEK293 cells, it is conceivable that this mutant might not be properly transported to the cone outer segment. To exclude this possibility, C-terminally cerulean-tagged V268I mutant was expressed in cones using the murine S-opsin promoter (mSWS) (Figure 3.2.3.1, upper panel). The rAAV

particles were subretinally administered in two week-old (P14) wild-type mice and the retinas were prepared three weeks post injection.

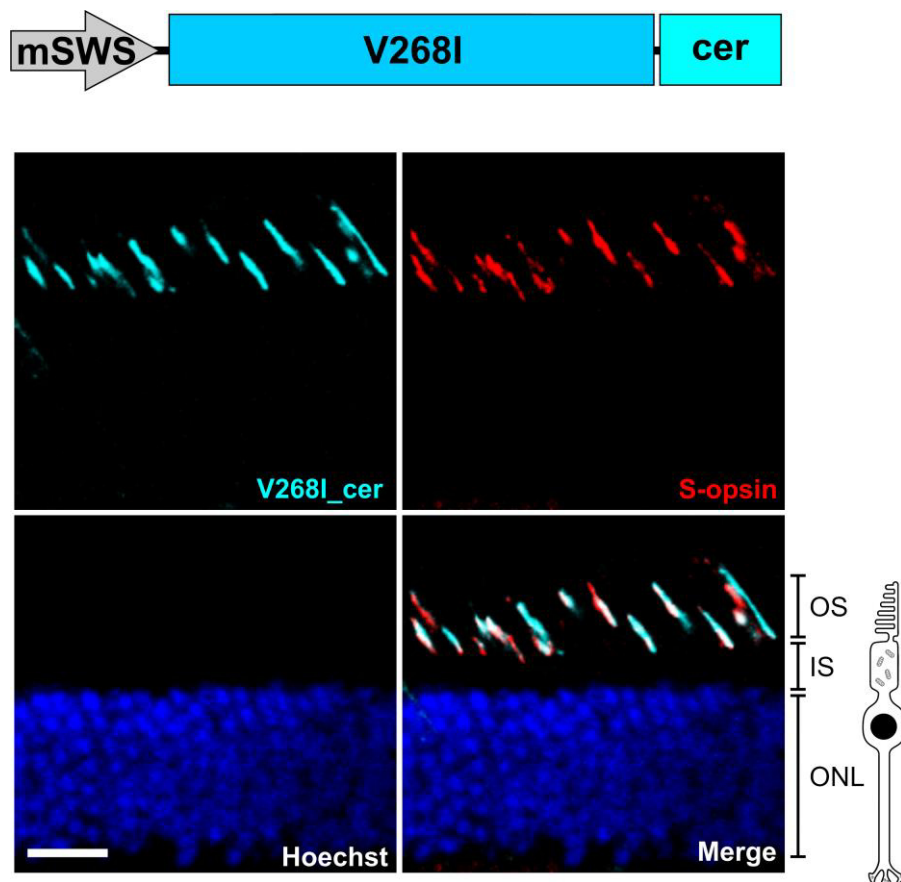


**Figure 3.2.3.1. The V268I mutant is correctly localized in cone outer segments.** Upper panel, the rAAV construct used for transduction of murine cone photoreceptors contains a murine S-opsin promoter (mSWS) for cone-specific expression, the PRPH2 transgene carrying the V268I mutation, and C-terminal cerulean (cer) as a reporter. Lower panel, immunohistological staining of murine retina transduced with V268I-cerulean fusion construct (V268I\_cer). V268I\_cer expression is depicted in cyan. The antibody directed against S-opsin was used as a marker for cone outer segments (red) and Hoechst was used as a nuclear marker (blue). Scale bar represents 20  $\mu\text{m}$ . The schematic illustration of a cone photoreceptor on the right bottom marks the respective layers in the merged image. OS, outer segment; IS, inner segment; ONL, outer nuclear layer.

As shown in Figure 3.2.3.1, the immunohistological images of injected retinas unveiled full co-localization of the V268I mutant and S-opsin. No detectable signal was observed for the mutant outside of the cone outer segments indicating proper localization of the V268I mutant.

### 3.2.4 FRET analysis of the WT and V268I peripherin-2/cone opsin interaction in cone outer segments

The correct localization of the V268I mutant *in vivo* allows for FRET measurement of the constructs shown in Figure 3.2.1.3A in cone outer segments. For this purpose, WT and mutant peripherin-2, S-opsin, and M-opsin were subcloned into an rAAV-vector that contains the mSWS promoter. Three weeks post injection, cone and rod outer segments were isolated using the self-designed quick protocol that was described in chapter 3.1.

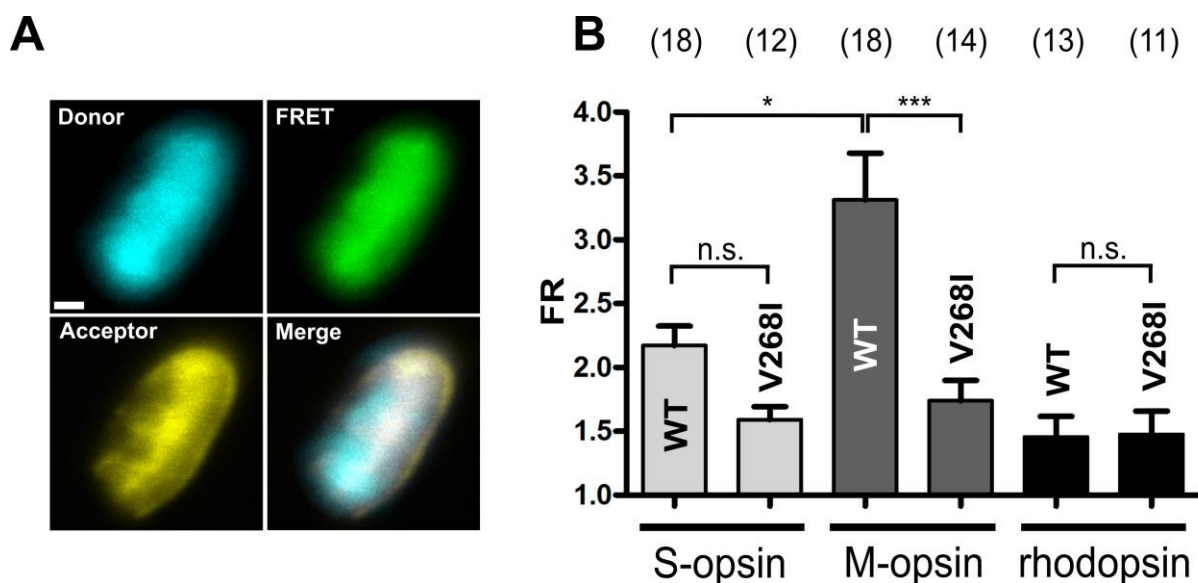


**Figure 3.2.4.1. FRET in isolated cone outer segments from WT mice.** A) Representative confocal image of Donor, FRET, Acceptor, and Merge channel of a single cone outer segment used for FRET measurements in B. Scale bar represents 2  $\mu$ m. B) FRs of WT and V268I peripherin-2-cerulean constructs co-expressed with S-opsin-, M-opsin-, and rhodopsin-citrine as indicated. FRs were determined from the FRET measurements in isolated cone outer segments (for FRET pairs containing S-opsin or M-opsin) and rod outer segments (for FRET pairs containing rhodopsin), respectively. For each FRET pair, the calculated FR is as follows: WT/S-opsin, FR =  $2.17 \pm 0.15$ ; V268I/S-opsin, FR =  $1.59 \pm 0.10$ ; WT/M-opsin, FR =  $3.31 \pm 0.36$ ; V268I/M-opsin, FR =  $1.74 \pm 0.16$ ; WT/rhodopsin, FR =  $1.46 \pm 0.16$ ; V268I/rhodopsin, FR =  $1.48 \pm 0.18$ . P value of the compared respective FRs is as follows: WT + S-opsin vs. V268I + S-opsin,  $p = 0.4263$ ; WT + M-opsin vs. V268I + M-opsin,  $p < 0.0001$ ; WT + rhodopsin vs. V268I + rhodopsin,  $p = 0.9323$ ; WT + S-opsin vs. WT + M-opsin,  $p = 0.0126$ . Numbers of independent measurements (n) are given in brackets.

Overall, the FRET results obtained from rod and cone outer segments are in very good agreement with the findings from HEK293 cells (see Figures 3.2.1.2 and 3.2.1.3). First, for WT peripherin-2, a robust FRET signal could be obtained with both M-opsin and S-opsin

indicating that these proteins indeed interact *in vivo*. Quantitatively, however, the FR of M-opsin/peripherin-2 was significantly higher than that of the S-opsin/peripherin-2 FRET pair.

Second, the FR of the M-opsin/V268I peripherin-2 was significantly attenuated compared to the FR of M-opsin/WT peripherin-2. By trend, but not significantly, such an attenuation was also observed for the S-opsin/V268I peripherin-2 FRET pair.

Third, in rod outer segments, neither tendency nor significant differences could be measured when comparing the FRs between the rhodopsin/WT peripherin-2 and the rhodopsin/V268I peripherin-2 FRET pairs.

Notably, compared to the FRET results from HEK293 cells, the FRs were constantly higher for cone opsin/peripherin-2 interaction, whereas they were lower for the rhodopsin/peripherin-2 FRET pair. The latter finding was already described in chapter 3.1.6. The constantly higher FRs for the cone opsin/peripherin-2 FRET pairs lay further emphasis on the potential importance of the cone opsin/peripherin-2 interaction in cone photoreceptors.

## 4 Discussion

### 4.1 Analysis of the peripherin-2 and rhodopsin interaction in outer segments of rod photoreceptors

The first part of this study shows that peripherin-2 forms a stable protein complex with both rhodopsin and the rod CNG channel in rod outer segments. Several lines of evidence support this conclusion. First, antibodies specific for the rod CNGB1a subunit immunoprecipitated rhodopsin from murine retinal lysates. Similarly, immunoprecipitation with rhodopsin-specific antibodies pulled down CNGB1a. In both sets of experiments, peripherin-2 was identified in the immunoprecipitated complex. Experiments in HEK293 cells revealed that rhodopsin does not directly bind to the CNG channel, but rather requires peripherin-2 as a molecular linker to form a complex with the channel. FRET experiments strongly supported this “bridging” function of peripherin-2. Based on the confocal FRET measurements, the relative binding affinity for the peripherin-2/rhodopsin interaction was in the similar range as for the rhodopsin/rhodopsin homomer. So far, the absolute binding affinity of rhodopsin homomers has not been determined. However, in the co-IP experiments, rhodopsin dimers and oligomers could be detected even under stringent SDS-PAGE and reducing conditions. Based on this, the absolute binding affinity of rhodopsin homomers are expected to be rather high. These results indicate that rhodopsin binds to peripherin-2 with a high affinity that is comparable to that of the rhodopsin homomer. The biochemical and FRET experiments in isolated outer segments strongly support the presence of rhodopsin dimers and oligomers in the native tissue. This is in line with recent studies providing strong evidence for the existence of rhodopsin dimers and oligomers in the native environment (Fotiadis *et al.*, 2003; Suda *et al.*, 2004; Knepp *et al.*, 2012; Koch and Dell'Orco, 2015). In this study, the molecular determinants required for the rhodopsin/peripherin-2 interaction were also identified. Since the major portion of both proteins is residing in the disc membrane of rod outer segments, it seems reasonable to assume that the interaction occurs via the transmembrane helices. In support of such a model, deletion of transmembrane domain 4 (TM4) in peripherin-2 abolished binding to rhodopsin. Moreover, a single glycine to aspartate exchange at the position 266 in the TM4 of peripherin-2 that was previously reported in patients suffering from adRP (Sohocki *et al.*, 2001) resulted in loss of binding to rhodopsin. Importantly, binding to CNGB1a was unaffected in the G266D mutant suggesting that the pathophysiological impact of this mutation relies on the impairment of the interaction with rhodopsin. The functional role of intradiscal and intracellular domains of peripherin-2 was examined in studies (Goldberg,

2006; Stuck *et al.*, 2016). However, only one study addressed the role of a transmembrane domain of this protein showing that the glutamate residue at position 276 in TM4 was crucial for disc morphogenesis (Goldberg *et al.*, 2007). Interestingly, the exchange of this charged amino acid to alanine (E276A) did not affect the interaction with rhodopsin. Similarly, the G266A mutation also had no effects on the peripherin-2/rhodopsin complex formation. These results suggest that introduction of charged residues on position 266 disrupts the binding of peripherin-2 to rhodopsin, whereas neutral amino acids at the same position do not affect this interaction. Taken together, the data point to a key role of TM4 for the peripherin-2/rhodopsin interaction and suggest that impaired binding to rhodopsin may contribute to the pathophysiology of peripherin-2 mutations.

As is evident in Figure 3.1.7.2, two bands for wild-type peripherin-2 are detected in the inputs and co-IP experiments. As the protein samples were deglycosylated prior to SDS-PAGE, the occurring upper band of peripherin-2 is most likely not a result of glycosylation. Intriguingly, the relative intensities of the two bands correlate with the number of negative charges in TM4. In the G266D mutant that contains two negative charges (E276, D266), the upper band possesses a higher signal intensity than the lower band. By contrast, in G266A and wild-type containing one negative charge in TM4 (E276), the signal of the lower band is more intense than that of the upper band. Finally, in the E276A mutant containing no negative charge, only the lower band is visible. A potential effect of charges on the conformation and relative mobility of peripherin-2 would be in agreement with previous findings showing that single mutants can lead to a differential electrophoretic mobility of the corresponding protein (Shi *et al.*, 2012).

Finally, FRET and immunoelectron microscopy were used to directly demonstrate that rhodopsin and CNGB1a are located in close proximity in rod outer segments. Overall, the results are consistent with the model shown in Figure 4.1.1. The novel aspect of this model is that peripherin-2, by binding to both, rhodopsin and the CNG channel, physically couples the most proximal protein of the light transduction cascade (rhodopsin) with the most distal protein (the CNG channel) in a narrow spatial microcompartment encompassing the disc rims and the neighboring plasma membrane. One could imagine two principal scenarios where the supramolecular organization of these proteins might be relevant. First, the complex could play a structural role in the formation and maintenance of rod outer segment structure. Mutations in peripherin-2 as well as in rhodopsin are associated with impaired disc morphogenesis and stability resulting in shortened and deteriorated rod outer segments (Sanyal and Jansen, 1981; Travis *et al.*, 1991; Humphries *et al.*, 1997; Lem *et al.*, 1999). Structural impairments of outer segments are also seen upon mutation of rom-1, another photoreceptor specific protein that binds to peripherin-2 (Clarke *et al.*, 2000), and in CNGB1a knockout mice lacking the peripherin-2-binding GARP domain (Zhang *et al.*, 2009).

Taken together, these findings imply that the integrity of the rhodopsin/peripherin-2/rom-1/CNG channel complex is crucial for morphogenesis and long-term stability of rod outer segments. Loss or functional impairment of any of the constituents of the complex will thus lead to more or less severe structural defects. In support to a structural role of the rhodopsin/peripherin-2 interaction, the addition of rhodopsin to the reconstituted peripherin-2/rom-1 complex in lipid vesicles was recently reported to induce the formation of disc rim-like structures *in vitro* (Kevany *et al.*, 2013).

The second scenario refers to a functional role of the complex in visual transduction. By binding to both, rhodopsin and the CNG channel, peripherin-2 helps to generate a microcompartment in the rim disc region that could have evolved to optimize the sensitivity and precision of light transduction. Recently, it was reported that a substantial portion of the rod phosphodiesterase (PDE6) is located at the disc rims of rod outer segments (Chen *et al.*, 2008). GARP2 that was shown to bind PDE6, peripherin-2, and the CNG channel subunits (Poetsch *et al.*, 2001; Pentia *et al.*, 2006; Michalakis *et al.*, 2011), could serve as an adaptor protein that anchors PDE6 to the disc rim. Another study also reported a physical interaction of PDE6 and the rod CNG channel (Bennett *et al.*, 1989). The proposed complex would be exquisitely efficient because the distance between the light-harvesting rhodopsin, the cGMP-hydrolyzing PDE6, and the channel that translates changes in cGMP in changes of the Na<sup>+</sup>/Ca<sup>2+</sup> flux would be extremely short. In contrast to rhodopsin, the CNG channel and peripherin-2 were reported to be absent in the central disc region (Molday *et al.*, 1987; Cook *et al.*, 1989; Molday *et al.*, 1991). Consequently, in this region, rhodopsin is physically uncoupled from the CNG channel. At the moment, one can only speculate about the exact functional role of the differential microcompartmentalization of rhodopsin in the central and peripheral part of the discs. Due to the shorter diffusion distance for cGMP, however, the disc rim-associated complex is expected to operate at lower light intensities and faster kinetics. Such an optimization could be important in rods which are tailored to detect extremely low light levels. By contrast, in the less light-sensitive cones, coupling of the light sensor to the channel seems less important. In agreement with this hypothesis, the cone CNG channel subunits lack the GARP domain that is required for the interaction with peripherin-2 (Molday and Molday, 1998; Poetsch *et al.*, 2001; Conley *et al.*, 2010).

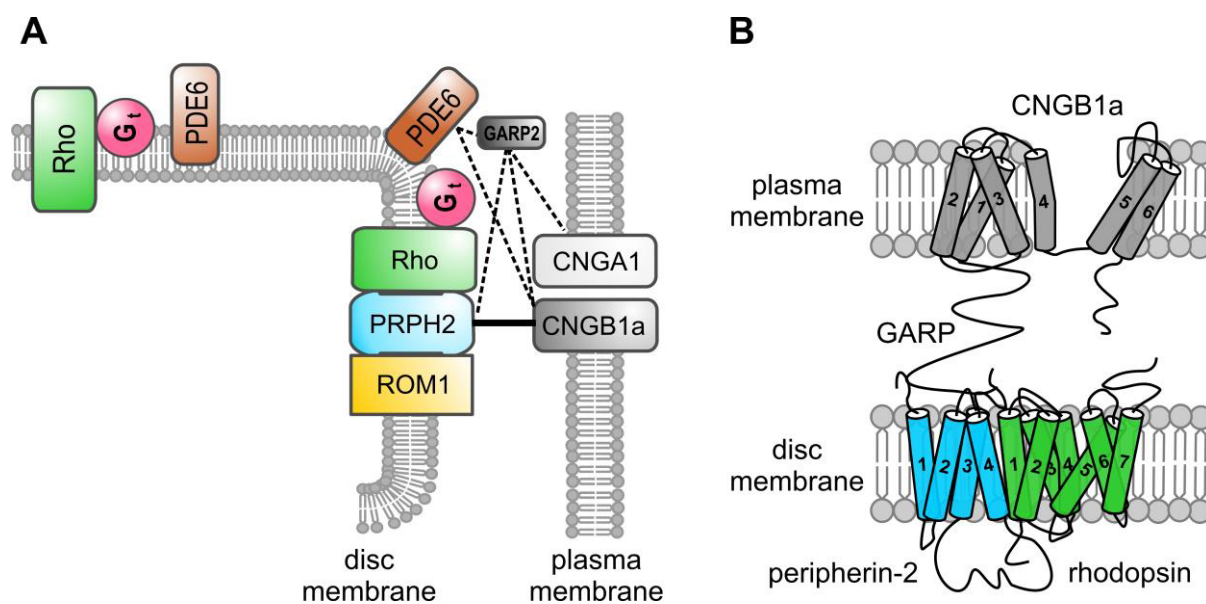


**Figure 4.1.1. Peripherin-2 couples the CNG channel to the phototransduction cascade in rod outer segments.** A) Simplified paradigm of protein-protein interactions in the disc rim region of outer segments. Peripherin-2 simultaneously binds to its homologue rom-1, to CNGB1a, and to rhodopsin. The soluble GARP2 undergoes multiple protein-protein interactions with CNGB1a, CNGA1, PDE6, and peripherin-2 as indicated by the dashed lines. G<sub>t</sub>, transducin. B) Tentative model of the CNGB1a/peripherin-2/rhodopsin complex. Note that the exact portion of rhodopsin that binds to TM4 of peripherin-2 is not known and is only tentatively assigned in this cartoon.

## 4.2 Analysis of the peripherin-2 and cone opsin interaction in outer segments of cone photoreceptors

The second part of this study demonstrates that peripherin-2 interacts with both, S-opsin and M-opsin in cone outer segments. This finding is supported by several methodical approaches including co-IPs, transmission electron microscopy, and quantitative FRET analyses. Both, in transfected HEK293 cells as well as in cone outer segments, the M-opsin/peripherin-2 interaction was shown to be stronger compared to the S-opsin/peripherin-2 interaction. The physiological importance of this differential interaction of peripherin-2 with cone opsins remains unclear. In a recent study, it was shown that M-opsin is severely mislocalized throughout the cone photoreceptor membrane when expressing a peripherin-2 variant that exhibits localization deficits (C150S) in a cone-dominant mouse model (Chakraborty *et al.*, 2010). Similar effects on protein localization were not reported for rhodopsin or S-opsin. One possible explanation for these observations is that the M-opsin/peripherin-2 interaction is specifically required for the concurrent transport of these two proteins to the cone outer segments.

Comparative analysis of FRs from HEK293 cells and rod or cone outer segments revealed an inverse correlation between the rhodopsin/peripherin-2 and cone opsin/peripherin-2 interaction. Whereas the rhodopsin/peripherin-2 FRs were lower in rod outer segments compared to HEK293 cells, the opposite case was observed for the cone opsin/peripherin-2 FRET pairs. One plausible explanation for this finding is that due to the relative rhodopsin/peripherin-2 abundance of approximately 9:1 (Becirovic *et al.*, 2016), most of the labeled rhodopsin molecules are not bound to peripherin-2, quenching the overall FRs. Second, in contrast to rhodopsin, which is reported to be expressed more or less uniformly throughout the discs, peripherin-2 is exclusively found in the disc rim region, where it interacts with CNGB1a (Molday *et al.*, 1987; Poetsch *et al.*, 2001). Thus, only a small portion of rhodopsin is physically able to undergo interactions with peripherin-2. Both restrictions (lower peripherin-2 expression and its physical separation from most part of rhodopsin) are not expected to occur in transfected HEK293 cells, which might explain the higher FRs for the rhodopsin/peripherin-2 interaction obtained in these cells. As described in chapter 1.2, the structure of cone outer segments differs significantly from that of rod outer segments. Moreover, in contrast to rods, no interaction between peripherin-2 and the cone-specific B-subunit of the CNG channel (CNGB3) could be observed as only the rod-specific CNGB1a subunit possesses the GARP domain, which is crucial for the interaction with peripherin-2 (Conley *et al.*, 2010). However, another study showed that, similar to its localization in rod outer segments, peripherin-2 is also mainly expressed in the rim regions of cone outer segments (Arikawa *et al.*, 1992). This result could be confirmed in this study by transmission electron microscopy. Nevertheless, due to the aforementioned facts, the portion of interacting peripherin-2 and cone opsin molecules is expected to be higher than that of interacting peripherin-2 and rhodopsin molecules. Moreover, the mRNA expression levels for peripherin-2 and cone opsins are very similar (Siegert *et al.*, 2012; Becirovic *et al.*, 2016). These findings might explain the relatively high FRs for the peripherin-2/cone opsin interaction in isolated cone outer segments.

The potential physiological relevance of the peripherin-2/M-opsin interaction is further illustrated by the fact that the V268I AVMD-linked mutant in TM4 of peripherin-2 selectively attenuates the binding of peripherin-2 to M-opsin without affecting protein localization. Interestingly, this mutant did not significantly alter the binding to rhodopsin or S-opsin. Given the sequence similarity of the photoreceptor opsins, it is not surprising that their binding to peripherin-2 is mediated by the same domain. However, even though the V268I mutant is in very close proximity to the G266D mutation, only the latter interferes with the peripherin-2/rhodopsin interaction. This finding implies that different molecular determinants within the same domain have evolved to ensure for the specificity of the peripherin-2 binding to rhodopsin and cone opsins. These results provide novel mechanisms which could contribute

to explain the differential penetrance of single peripherin-2 point mutations in rods and cones. Finally, this study also provides a proof-of-principle for FRET measurements in a subcellular compartment in photoreceptors. This approach should be transferrable to other tissues and might help investigating the role of protein-protein interactions under physiological and pathophysiological conditions.

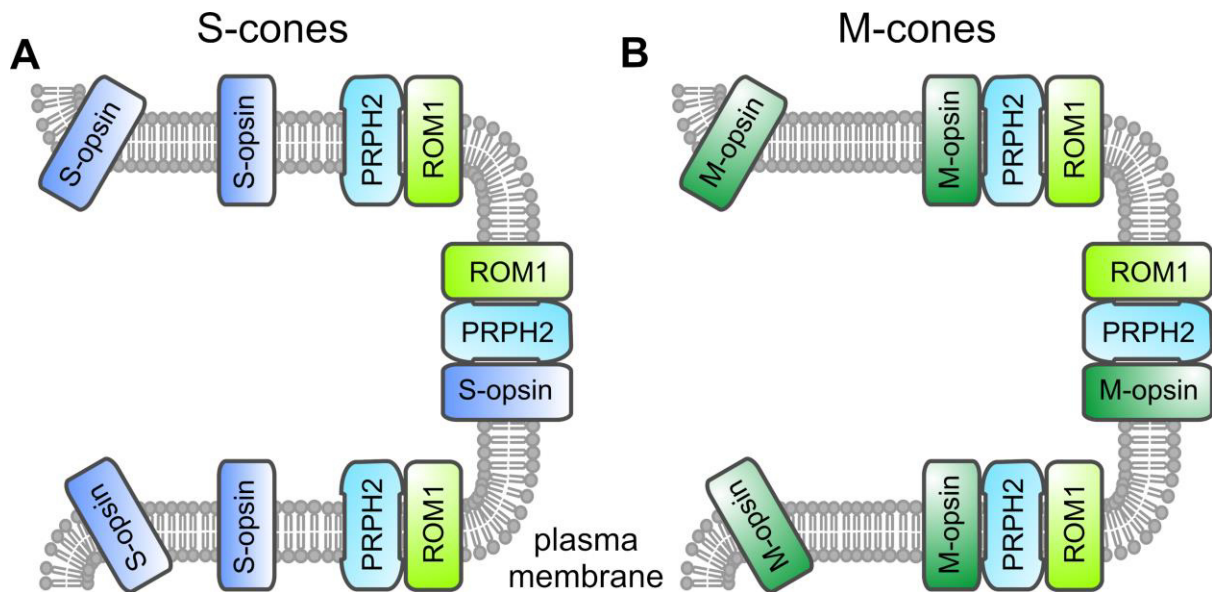


**Figure 4.2.1. Peripherin-2 interacts differentially with S-opsin and M-opsin in the respective cone photoreceptor.** A-B) Simplified illustration of protein-protein interactions in the outer segment plasma membrane of S-cones (A) and M-cones (B). Peripherin-2 simultaneously binds to its homologue rom-1 and to the respective cone opsin. However, interaction between peripherin-2 and M-opsin occurs more frequently than that between peripherin-2 and S-opsin.

## 5 Summary

The tetraspanin peripherin-2 is a glyco-membrane protein exclusively expressed in the outer segments of rod and cone photoreceptors. Mutations in peripherin-2 are associated with retinal disorders characterized by degeneration of rod or cone cells. Previous unpublished work identified peripherin-2 as a potential novel part of the protein complex comprising the B-subunit of the cyclic nucleotide-gated channel (CNGB1a) and the light detector rhodopsin. In the first part of this study, using a combination of protein biochemical and FRET approaches in transfected HEK293 cells and in virally transduced murine rod outer segments, it could be demonstrated that peripherin-2 simultaneously binds to both, CNGB1a and rhodopsin. The interaction between peripherin-2 and rhodopsin was not described in previous studies. The binding domain mediating the peripherin-2/rhodopsin interaction could be narrowed down to the fourth transmembrane domain (TM4) of peripherin-2. Finally, the data revealed that the G266D point mutation in TM4 of peripherin-2 that is linked to a rod degenerative disease selectively disrupts the peripherin-2/rhodopsin interaction.

To analyze if peripherin-2 also binds to cone opsins in the second part of this study, a similar experimental approach was conducted as used for the investigation of the peripherin-2/rhodopsin interaction. In this context, it was unveiled that peripherin-2 binds to both, short wavelength- and medium wavelength-sensitive cone opsin (S-opsin and M-opsin, respectively) in transfected HEK293 cells and in outer segments of transduced murine cones. Co-immunoprecipitation and quantitative FRET analysis revealed that binding of peripherin-2 to M-opsin was stronger than the peripherin-2/S-opsin interaction. This result was supported by transmission electron microscopy studies using gold particles coupled to opsin- and peripherin-2-specific antibodies. Finally, quantitative FRET analysis in transfected HEK293 cells and in transduced cone outer segments demonstrated that the V268I point mutation in TM4 of peripherin-2 associated with a degenerative cone disease significantly attenuates the peripherin-2/M-opsin interaction.

Taken together, this study provides a proof-of-principle for FRET-based analysis of protein-protein interactions in the outer segments of rod and cone photoreceptors. This approach led to the identification of hitherto unknown protein complexes between peripherin-2 and opsins suggesting a novel physiological role of peripherin-2 in rods and cones. Finally, analysis of disease-linked point mutations unveiled the molecular determinants of the peripherin-2/opsin interaction. These results might contribute to understanding the differential penetrance of certain point mutations in rods and cones.

## Zusammenfassung

Das Tetraspanin Peripherin-2 ist ein Glykomembran-Protein, das ausschließlich in den Außensegmenten von Stäbchen- und Zapfen-Fotorezeptoren exprimiert wird. Mutationen in Peripherin-2 sind mit Netzhauterkrankungen assoziiert, die zur Degeneration von Stäbchen oder Zapfen führen. In Vorarbeiten wurde Peripherin-2 als potenzieller neuer Bestandteil des Proteinkomplexes identifiziert, der aus der B-Untereinheit des Zyklonukleotid-gesteuerten Kanals (CNGB1a) und dem Lichtdetektor Rhodopsin besteht.

Im ersten Teil dieser Studie konnte mittels einer Kombination aus proteinbiochemischen und FRET-basierten Untersuchungen in transfizierten HEK293 Zellen sowie in mit viralen Vektoren transduzierten murinen Stäbchen-Außensegmenten gezeigt werden, dass Peripherin-2 gleichzeitig sowohl an CNGB1a als auch an Rhodopsin bindet. Die Interaktion zwischen Peripherin-2 und Rhodopsin wurde bisher in keiner Studie beschrieben. Die Bindungsdomäne, die die Peripherin-2/Rhodopsin Interaktion vermittelt, konnte auf das vierte Transmembransegment (TM4) von Peripherin-2 eingegrenzt werden. Schließlich wurde gezeigt, dass die G266D Punktmutation in TM4 von Peripherin-2, die mit einer degenerativen Stäbchenerkrankung einhergeht, selektiv die Peripherin-2/Rhodopsin Interaktion unterbindet.

Um zu untersuchen, ob Peripherin-2 auch an Zapfenopsine bindet, wurde im zweiten Teil dieser Studie ein ähnlicher experimenteller Ansatz, der bereits für die Analyse der Peripherin-2/Rhodopsin Interaktion verwendet wurde, durchgeführt. In diesem Zusammenhang konnte nachgewiesen werden, dass Peripherin-2 an beide Opsine, das kurzwellige und das mittelwellige Opsin (S-Opsin bzw. M-Opsin) in transfizierten HEK293 Zellen und in Außensegmenten von transduzierten murinen Zapfen bindet. Ko-Immunpräzipitation und quantitative FRET Analyse zeigten ferner, dass die Bindung von Peripherin-2 zu M-Opsin stärker als die zu S-Opsin ist. Dieses Ergebnis wurde durch transmissionselektronenmikroskopische Untersuchungen unter Verwendung von Goldpartikeln, die an Opsin- und Peripherin-2-spezifische Antikörper gekoppelt waren, unterstützt. Zuletzt zeigte die quantitative FRET-Analyse in transfizierten HEK293 Zellen und in transduzierten murinen Zapfen-Außensegmenten, dass die V268I Punktmutation in TM4 von Peripherin-2, die mit einer degenerativen Zapfenerkrankung assoziiert ist, signifikant die Peripherin-2/M-Opsin Interaktion vermindert.

Zusammenfassend konnte im Rahmen dieser Studie die FRET-basierte Analyse zur Untersuchung von Protein-Protein Interaktionen in Außensegmenten von Stäbchen- und Zapfen-Fotorezeptoren etabliert werden. Des Weiteren führte dieser Ansatz zur Identifizierung von bisher unbekanntem Proteinkomplexen bestehend aus Peripherin-2 und

den Opsinen, was auf eine neue physiologische Rolle von Peripherin-2 in Stäbchen und Zapfen schließen lässt. Schließlich konnten mittels Analyse von krankheitsassoziierten Punktmutationen die molekularen Determinanten der Peripherin-2/Opsin Interaktion erfasst werden. Die Ergebnisse dieser Studie tragen schließlich auch zum besseren Verständnis der molekularen Mechanismen bei, die der unterschiedlichen Penetranz bestimmter Punktmutationen in Stäbchen- und Zapfen-Fotorezeptoren zu Grunde liegen.

## 6 Literature

### 6.1 Cited publications

- Allocca, M., Mussolino, C., Garcia-Hoyos, M., Sanges, D., Iodice, C., Petrillo, M., Vandenberghe, L. H., Wilson, J. M., Marigo, V., Surace, E. M., *et al.* (2007). Novel adeno-associated virus serotypes efficiently transduce murine photoreceptors. *Journal of virology* 81(20): 11372-11380.
- Ammann, F., Klein, D. and Franceschetti, A. (1965). Genetic and epidemiological investigations on pigmentary degeneration of the retina and allied disorders in Switzerland. *Journal of the neurological sciences* 2(2): 183-196.
- Andreu, Z. and Yanez-Mo, M. (2014). Tetraspanins in extracellular vesicle formation and function. *Frontiers in immunology* 5: 442.
- Arikawa, K., Molday, L. L., Molday, R. S. and Williams, D. S. (1992). Localization of peripherin/rds in the disk membranes of cone and rod photoreceptors: relationship to disk membrane morphogenesis and retinal degeneration. *The Journal of cell biology* 116(3): 659-667.
- Ayuso, C., Garcia-Sandoval, B., Najera, C., Valverde, D., Carballo, M. and Antinolo, G. (1995). Retinitis pigmentosa in Spain. The Spanish Multicentric and Multidisciplinary Group for Research into Retinitis Pigmentosa. *Clinical genetics* 48(3): 120-122.
- Barnes, S. (1994). After transduction: response shaping and control of transmission by ion channels of the photoreceptor inner segments. *Neuroscience* 58(3): 447-459.
- Baylor, D. A., Lamb, T. D. and Yau, K. W. (1979). Responses of retinal rods to single photons. *The Journal of physiology* 288: 613-634.
- Becirovic, E., Bohm, S., Nguyen, O. N., Riedmayr, L. M., Koch, M. A., Schulze, E., Kohl, S., Borsch, O., Santos-Ferreira, T., Ader, M., *et al.* (2016). In Vivo Analysis of Disease-Associated Point Mutations Unveils Profound Differences in mRNA Splicing of Peripherin-2 in Rod and Cone Photoreceptors. *PLoS genetics* 12(1): e1005811.
- Bennett, N., Ildefonse, M., Crouzy, S., Chapron, Y. and Clerc, A. (1989). Direct activation of cGMP-dependent channels of retinal rods by the cGMP phosphodiesterase. *Proceedings of the National Academy of Sciences of the United States of America* 86(10): 3634-3638.
- Berson, E. L., Rosner, B., Sandberg, M. A., Hayes, K. C., Nicholson, B. W., Weigel-DiFranco, C. and Willett, W. (1993). A randomized trial of vitamin A and vitamin E supplementation for retinitis pigmentosa. *Archives of ophthalmology* 111(6): 761-772.

- Boesze-Battaglia, K., Kong, F., Lamba, O. P., Stefano, F. P. and Williams, D. S. (1997). Purification and light-dependent phosphorylation of a candidate fusion protein, the photoreceptor cell peripherin/rds. *Biochemistry* 36(22): 6835-6846.
- Boesze-Battaglia, K., Lamba, O. P., Napoli, A. A., Jr., Sinha, S. and Guo, Y. (1998). Fusion between retinal rod outer segment membranes and model membranes: a role for photoreceptor peripherin/rds. *Biochemistry* 37(26): 9477-9487.
- Boesze-Battaglia, K., Song, H., Sokolov, M., Lillo, C., Pankoski-Walker, L., Gretzula, C., Gallagher, B., Rachel, R. A., Jenkins, N. A., Copeland, N. G., *et al.* (2007). The tetraspanin protein peripherin-2 forms a complex with melanoregulin, a putative membrane fusion regulator. *Biochemistry* 46(5): 1256-1272.
- Boon, C. J., den Hollander, A. I., Hoyng, C. B., Cremers, F. P., Klevering, B. J. and Keunen, J. E. (2008). The spectrum of retinal dystrophies caused by mutations in the peripherin/RDS gene. *Progress in retinal and eye research* 27(2): 213-235.
- Boughman, J. A., Conneally, P. M. and Nance, W. E. (1980). Population genetic studies of retinitis pigmentosa. *American journal of human genetics* 32(2): 223-235.
- Boughman, J. A. and Fishman, G. A. (1983). A genetic analysis of retinitis pigmentosa. *The British journal of ophthalmology* 67(7): 449-454.
- Bradford, M. M. (1976). A rapid and sensitive method for the quantitation of microgram quantities of protein utilizing the principle of protein-dye binding. *Analytical biochemistry* 72: 248-254.
- Bunker, C. H., Berson, E. L., Bromley, W. C., Hayes, R. P. and Roderick, T. H. (1984). Prevalence of retinitis pigmentosa in Maine. *American journal of ophthalmology* 97(3): 357-365.
- Carter-Dawson, L. D. and LaVail, M. M. (1979). Rods and cones in the mouse retina. I. Structural analysis using light and electron microscopy. *The Journal of comparative neurology* 188(2): 245-262.
- Carter-Dawson, L. D. and LaVail, M. M. (1979). Rods and cones in the mouse retina. II. Autoradiographic analysis of cell generation using tritiated thymidine. *The Journal of comparative neurology* 188(2): 263-272.
- Chakraborty, D., Conley, S. M., Stuck, M. W. and Naash, M. I. (2010). Differences in RDS trafficking, assembly and function in cones versus rods: insights from studies of C150S-RDS. *Human molecular genetics* 19(24): 4799-4812.
- Chen, C. K., Burns, M. E., Spencer, M., Niemi, G. A., Chen, J., Hurley, J. B., Baylor, D. A. and Simon, M. I. (1999). Abnormal photoresponses and light-induced apoptosis in rods lacking rhodopsin kinase. *Proceedings of the National Academy of Sciences of the United States of America* 96(7): 3718-3722.

- Chen, J., Yoshida, T. and Bitensky, M. W. (2008). Light-induced translocation of cyclic-GMP phosphodiesterase on rod disc membranes in rat retina. *Molecular vision* 14: 2509-2517.
- Choe, H. W., Kim, Y. J., Park, J. H., Morizumi, T., Pai, E. F., Krauss, N., Hofmann, K. P., Scheerer, P. and Ernst, O. P. (2011). Crystal structure of metarhodopsin II. *Nature* 471(7340): 651-655.
- Clarke, G., Goldberg, A. F., Vidgen, D., Collins, L., Ploder, L., Schwarz, L., Molday, L. L., Rossant, J., Szel, A., Molday, R. S., *et al.* (2000). Rom-1 is required for rod photoreceptor viability and the regulation of disk morphogenesis. *Nature genetics* 25(1): 67-73.
- Cohen, A. I. (1960). The ultrastructure of the rods of the mouse retina. *The American journal of anatomy* 107: 23-48.
- Conley, S. M., Ding, X. Q. and Naash, M. I. (2010). RDS in cones does not interact with the beta subunit of the cyclic nucleotide gated channel. *Advances in experimental medicine and biology* 664: 63-70.
- Connell, G. J. and Molday, R. S. (1990). Molecular cloning, primary structure, and orientation of the vertebrate photoreceptor cell protein peripherin in the rod outer segment disk membrane. *Biochemistry* 29(19): 4691-4698.
- Cook, N. J., Molday, L. L., Reid, D., Kaupp, U. B. and Molday, R. S. (1989). The cGMP-gated channel of bovine rod photoreceptors is localized exclusively in the plasma membrane. *The Journal of biological chemistry* 264(12): 6996-6999.
- Eckmiller, M. S. (1987). Cone outer segment morphogenesis: taper change and distal invaginations. *The Journal of cell biology* 105(5): 2267-2277.
- Edrington, T. C. t., Yeagle, P. L., Gretzula, C. L. and Boesze-Battaglia, K. (2007). Calcium-dependent association of calmodulin with the C-terminal domain of the tetraspanin protein peripherin/rds. *Biochemistry* 46(12): 3862-3871.
- Epstein, G. A. and Rabb, M. F. (1980). Adult vitelliform macular degeneration: diagnosis and natural history. *The British journal of ophthalmology* 64(10): 733-740.
- Fain, G. L., Matthews, H. R., Cornwall, M. C. and Koutalos, Y. (2001). Adaptation in vertebrate photoreceptors. *Physiological reviews* 81(1): 117-151.
- Farjo, R., Skaggs, J. S., Nagel, B. A., Quiambao, A. B., Nash, Z. A., Fliesler, S. J. and Naash, M. I. (2006). Retention of function without normal disc morphogenesis occurs in cone but not rod photoreceptors. *The Journal of cell biology* 173(1): 59-68.
- Felbor, U., Schilling, H. and Weber, B. H. (1997). Adult vitelliform macular dystrophy is frequently associated with mutations in the peripherin/RDS gene. *Human mutation* 10(4): 301-309.

- Ferrari, S., Di Iorio, E., Barbaro, V., Ponzin, D., Sorrentino, F. S. and Parmeggiani, F. (2011). Retinitis pigmentosa: genes and disease mechanisms. *Current genomics* 12(4): 238-249.
- Fotiadis, D., Liang, Y., Filipek, S., Saperstein, D. A., Engel, A. and Palczewski, K. (2003). Atomic-force microscopy: Rhodopsin dimers in native disc membranes. *Nature* 421(6919): 127-128.
- Gardner, J. C., Webb, T. R., Kanuga, N., Robson, A. G., Holder, G. E., Stockman, A., Ripamonti, C., Ebenezer, N. D., Ogun, O., Devery, S., *et al.* (2010). X-linked cone dystrophy caused by mutation of the red and green cone opsins. *American journal of human genetics* 87(1): 26-39.
- Goldberg, A. F. (2006). Role of peripherin/rds in vertebrate photoreceptor architecture and inherited retinal degenerations. *International review of cytology* 253: 131-175.
- Goldberg, A. F. and Molday, R. S. (1996). Subunit composition of the peripherin/rds-rom-1 disk rim complex from rod photoreceptors: hydrodynamic evidence for a tetrameric quaternary structure. *Biochemistry* 35(19): 6144-6149.
- Goldberg, A. F., Moritz, O. L. and Molday, R. S. (1995). Heterologous expression of photoreceptor peripherin/rds and Rom-1 in COS-1 cells: assembly, interactions, and localization of multisubunit complexes. *Biochemistry* 34(43): 14213-14219.
- Goldberg, A. F., Ritter, L. M., Khattree, N., Peachey, N. S., Fariss, R. N., Dang, L., Yu, M. and Bottrell, A. R. (2007). An intramembrane glutamic acid governs peripherin/rds function for photoreceptor disk morphogenesis. *Investigative ophthalmology & visual science* 48(7): 2975-2986.
- Goschnick, M. W., Lau, L. M., Wee, J. L., Liu, Y. S., Hogarth, P. M., Robb, L. M., Hickey, M. J., Wright, M. D. and Jackson, D. E. (2006). Impaired "outside-in" integrin  $\alpha$ IIb $\beta$ 3 signaling and thrombus stability in TSSC6-deficient mice. *Blood* 108(6): 1911-1918.
- Graham, F. L. and van der Eb, A. J. (1973). A new technique for the assay of infectivity of human adenovirus 5 DNA. *Virology* 52(2): 456-467.
- Griesbeck, O., Baird, G. S., Campbell, R. E., Zacharias, D. A. and Tsien, R. Y. (2001). Reducing the environmental sensitivity of yellow fluorescent protein. Mechanism and applications. *The Journal of biological chemistry* 276(31): 29188-29194.
- Gruning, G., Millan, J. M., Meins, M., Beneyto, M., Caballero, M., Apfelstedt-Sylla, E., Bosch, R., Zrenner, E., Prieto, F. and Gal, A. (1994). Mutations in the human peripherin/RDS gene associated with autosomal dominant retinitis pigmentosa. *Human mutation* 3(3): 321-323.

- Gunkel, M., Schoneberg, J., Alkhalidi, W., Irsen, S., Noe, F., Kaupp, U. B. and Al-Amoudi, A. (2015). Higher-order architecture of rhodopsin in intact photoreceptors and its implication for phototransduction kinetics. *Structure* 23(4): 628-638.
- Hamel, C. (2006). Retinitis pigmentosa. *Orphanet journal of rare diseases* 1: 40.
- Han, Z., Anderson, D. W. and Papermaster, D. S. (2012). Prominin-1 localizes to the open rims of outer segment lamellae in *Xenopus laevis* rod and cone photoreceptors. *Investigative ophthalmology & visual science* 53(1): 361-373.
- Hartong, D. T., Berson, E. L. and Dryja, T. P. (2006). Retinitis pigmentosa. *Lancet* 368(9549): 1795-1809.
- Hemler, M. E. (2005). Tetraspanin functions and associated microdomains. *Nature reviews. Molecular cell biology* 6(10): 801-811.
- Humphries, M. M., Rancourt, D., Farrar, G. J., Kenna, P., Hazel, M., Bush, R. A., Sieving, P. A., Sheils, D. M., McNally, N., Creighton, P., *et al.* (1997). Retinopathy induced in mice by targeted disruption of the rhodopsin gene. *Nature genetics* 15(2): 216-219.
- Hunt, D. M., Dulai, K. S., Cowing, J. A., Julliot, C., Mollon, J. D., Bowmaker, J. K., Li, W. H. and Hewett-Emmett, D. (1998). Molecular evolution of trichromacy in primates. *Vision research* 38(21): 3299-3306.
- Jay, M. (1982). On the heredity of retinitis pigmentosa. *The British journal of ophthalmology* 66(7): 405-416.
- Kevany, B. M., Tsybovsky, Y., Campuzano, I. D., Schnier, P. D., Engel, A. and Palczewski, K. (2013). Structural and functional analysis of the native peripherin-ROM1 complex isolated from photoreceptor cells. *The Journal of biological chemistry* 288(51): 36272-36284.
- Khattree, N., Ritter, L. M. and Goldberg, A. F. (2013). Membrane curvature generation by a C-terminal amphipathic helix in peripherin-2/rds, a tetraspanin required for photoreceptor sensory cilium morphogenesis. *Journal of cell science* 126(Pt 20): 4659-4670.
- Knepp, A. M., Periole, X., Marrink, S. J., Sakmar, T. P. and Huber, T. (2012). Rhodopsin forms a dimer with cytoplasmic helix 8 contacts in native membranes. *Biochemistry* 51(9): 1819-1821.
- Koch, K. W. and Dell'Orco, D. (2015). Protein and Signaling Networks in Vertebrate Photoreceptor Cells. *Frontiers in molecular neuroscience* 8: 67.
- Koch, S., Sothilingam, V., Garcia Garrido, M., Tanimoto, N., Becirovic, E., Koch, F., Seide, C., Beck, S. C., Seeliger, M. W., Biel, M., *et al.* (2012). Gene therapy restores vision and delays degeneration in the CNGB1(-/-) mouse model of retinitis pigmentosa. *Human molecular genetics* 21(20): 4486-4496.

- Korschen, H. G., Beyermann, M., Muller, F., Heck, M., Vantler, M., Koch, K. W., Kellner, R., Wolfrum, U., Bode, C., Hofmann, K. P., *et al.* (1999). Interaction of glutamic-acid-rich proteins with the cGMP signalling pathway in rod photoreceptors. *Nature* 400(6746): 761-766.
- Lem, J., Krasnoperova, N. V., Calvert, P. D., Kosaras, B., Cameron, D. A., Nicolo, M., Makino, C. L. and Sidman, R. L. (1999). Morphological, physiological, and biochemical changes in rhodopsin knockout mice. *Proceedings of the National Academy of Sciences of the United States of America* 96(2): 736-741.
- Loewen, C. J. and Molday, R. S. (2000). Disulfide-mediated oligomerization of Peripherin/Rds and Rom-1 in photoreceptor disk membranes. Implications for photoreceptor outer segment morphogenesis and degeneration. *The Journal of biological chemistry* 275(8): 5370-5378.
- Loewen, C. J., Moritz, O. L. and Molday, R. S. (2001). Molecular characterization of peripherin-2 and rom-1 mutants responsible for digenic retinitis pigmentosa. *The Journal of biological chemistry* 276(25): 22388-22396.
- Manes, G., Guillaumie, T., Vos, W. L., Devos, A., Audo, I., Zeitz, C., Marquette, V., Zanlonghi, X., Defoort-Dhellemmes, S., Puech, B., *et al.* (2015). High prevalence of PRPH2 in autosomal dominant retinitis pigmentosa in france and characterization of biochemical and clinical features. *American journal of ophthalmology* 159(2): 302-314.
- Michalakis, S., Muhlfriedel, R., Tanimoto, N., Krishnamoorthy, V., Koch, S., Fischer, M. D., Becirovic, E., Bai, L., Huber, G., Beck, S. C., *et al.* (2010). Restoration of cone vision in the CNGA3<sup>-/-</sup> mouse model of congenital complete lack of cone photoreceptor function. *Molecular therapy : the journal of the American Society of Gene Therapy* 18(12): 2057-2063.
- Michalakis, S., Zong, X., Becirovic, E., Hammelmann, V., Wein, T., Wanner, K. T. and Biel, M. (2011). The glutamic acid-rich protein is a gating inhibitor of cyclic nucleotide-gated channels. *The Journal of neuroscience : the official journal of the Society for Neuroscience* 31(1): 133-141.
- Molday, R. S., Hicks, D. and Molday, L. (1987). Peripherin. A rim-specific membrane protein of rod outer segment discs. *Investigative ophthalmology & visual science* 28(1): 50-61.
- Molday, R. S. and Molday, L. L. (1998). Molecular properties of the cGMP-gated channel of rod photoreceptors. *Vision research* 38(10): 1315-1323.
- Molday, R. S., Molday, L. L., Dose, A., Clark-Lewis, I., Illing, M., Cook, N. J., Eismann, E. and Kaupp, U. B. (1991). The cGMP-gated channel of the rod photoreceptor cell characterization and orientation of the amino terminus. *The Journal of biological chemistry* 266(32): 21917-21922.

- Mustafi, D., Engel, A. H. and Palczewski, K. (2009). Structure of cone photoreceptors. *Progress in retinal and eye research* 28(4): 289-302.
- Nathans, J., Thomas, D. and Hogness, D. S. (1986). Molecular genetics of human color vision: the genes encoding blue, green, and red pigments. *Science* 232(4747): 193-202.
- Neitz, J. and Neitz, M. (2011). The genetics of normal and defective color vision. *Vision research* 51(7): 633-651.
- Nickell, S., Park, P. S., Baumeister, W. and Palczewski, K. (2007). Three-dimensional architecture of murine rod outer segments determined by cryoelectron tomography. *The Journal of cell biology* 177(5): 917-925.
- Okano, T., Kojima, D., Fukada, Y., Shichida, Y. and Yoshizawa, T. (1992). Primary structures of chicken cone visual pigments: vertebrate rhodopsins have evolved out of cone visual pigments. *Proceedings of the National Academy of Sciences of the United States of America* 89(13): 5932-5936.
- Pentia, D. C., Hosier, S. and Cote, R. H. (2006). The glutamic acid-rich protein-2 (GARP2) is a high affinity rod photoreceptor phosphodiesterase (PDE6)-binding protein that modulates its catalytic properties. *The Journal of biological chemistry* 281(9): 5500-5505.
- Petrs-Silva, H., Dinculescu, A., Li, Q., Deng, W. T., Pang, J. J., Min, S. H., Chiodo, V., Neeley, A. W., Govindasamy, L., Bennett, A., *et al.* (2011). Novel properties of tyrosine-mutant AAV2 vectors in the mouse retina. *Molecular therapy : the journal of the American Society of Gene Therapy* 19(2): 293-301.
- Petrs-Silva, H., Dinculescu, A., Li, Q., Min, S. H., Chiodo, V., Pang, J. J., Zhong, L., Zolotukhin, S., Srivastava, A., Lewin, A. S., *et al.* (2009). High-efficiency transduction of the mouse retina by tyrosine-mutant AAV serotype vectors. *Molecular therapy : the journal of the American Society of Gene Therapy* 17(3): 463-471.
- Poetsch, A., Molday, L. L. and Molday, R. S. (2001). The cGMP-gated channel and related glutamic acid-rich proteins interact with peripherin-2 at the rim region of rod photoreceptor disc membranes. *The Journal of biological chemistry* 276(51): 48009-48016.
- Puech, B., Kostrubiec, B., Hache, J. C. and Francois, P. (1991). [Epidemiology and prevalence of hereditary retinal dystrophies in the Northern France]. *Journal francais d'ophtalmologie* 14(3): 153-164.
- Renner, A. B., Tillack, H., Kraus, H., Kohl, S., Wissinger, B., Mohr, N., Weber, B. H., Kellner, U. and Foerster, M. H. (2004). Morphology and functional characteristics in adult vitelliform macular dystrophy. *Retina* 24(6): 929-939.

- Ritter, L. M., Khattree, N., Tam, B., Moritz, O. L., Schmitz, F. and Goldberg, A. F. (2011). In situ visualization of protein interactions in sensory neurons: glutamic acid-rich proteins (GARPs) play differential roles for photoreceptor outer segment scaffolding. *The Journal of neuroscience : the official journal of the Society for Neuroscience* 31(31): 11231-11243.
- Rizzo, M. A., Springer, G. H., Granada, B. and Piston, D. W. (2004). An improved cyan fluorescent protein variant useful for FRET. *Nature biotechnology* 22(4): 445-449.
- Sanyal, S. and Jansen, H. G. (1981). Absence of receptor outer segments in the retina of rds mutant mice. *Neuroscience letters* 21(1): 23-26.
- Sanyal, S. and Zeilmaker, G. H. (1984). Development and degeneration of retina in rds mutant mice: light and electron microscopic observations in experimental chimaeras. *Experimental eye research* 39(2): 231-246.
- Shi, Y., Mowery, R. A., Ashley, J., Hentz, M., Ramirez, A. J., Bilgicer, B., Slunt-Brown, H., Borchelt, D. R. and Shaw, B. F. (2012). Abnormal SDS-PAGE migration of cytosolic proteins can identify domains and mechanisms that control surfactant binding. *Protein science : a publication of the Protein Society* 21(8): 1197-1209.
- Siegert, S., Cabuy, E., Scherf, B. G., Kohler, H., Panda, S., Le, Y. Z., Fehling, H. J., Gaidatzis, D., Stadler, M. B. and Roska, B. (2012). Transcriptional code and disease map for adult retinal cell types. *Nature neuroscience* 15(3): 487-495, S481-482.
- Sohocki, M. M., Daiger, S. P., Bowne, S. J., Rodriguez, J. A., Northrup, H., Heckenlively, J. R., Birch, D. G., Mintz-Hittner, H., Ruiz, R. S., Lewis, R. A., *et al.* (2001). Prevalence of mutations causing retinitis pigmentosa and other inherited retinopathies. *Human mutation* 17(1): 42-51.
- Stefano, F. P., Krouse, J., Marta, P. and Boesze-Battaglia, K. (2002). Heterologous expression of WT and mutant photoreceptor peripherin/rds in Madin Darby canine kidney cells: an assessment of fusogenic function. *Experimental eye research* 74(2): 267-283.
- Stuck, M. W., Conley, S. M. and Naash, M. I. (2016). PRPH2/RDS and ROM-1: Historical context, current views and future considerations. *Progress in retinal and eye research*.
- Suda, K., Filipek, S., Palczewski, K., Engel, A. and Fotiadis, D. (2004). The supramolecular structure of the GPCR rhodopsin in solution and native disc membranes. *Molecular membrane biology* 21(6): 435-446.
- Sung, C. H. and Chuang, J. Z. (2010). The cell biology of vision. *The Journal of cell biology* 190(6): 953-963.
- Travis, G. H., Sutcliffe, J. G. and Bok, D. (1991). The retinal degeneration slow (rds) gene product is a photoreceptor disc membrane-associated glycoprotein. *Neuron* 6(1): 61-70.

- Vandenberghe, L. H. and Auricchio, A. (2012). Novel adeno-associated viral vectors for retinal gene therapy. *Gene therapy* 19(2): 162-168.
- Vos, W. L., Vaughan, S., Lall, P. Y., McCaffrey, J. G., Wysocka-Kapcinska, M. and Findlay, J. B. (2010). Expression and structural characterization of peripherin/RDS, a membrane protein implicated in photoreceptor outer segment morphology. *European biophysics journal* : EBJ 39(4): 679-688.
- Wells, J., Wroblewski, J., Keen, J., Inglehearn, C., Jubb, C., Eckstein, A., Jay, M., Arden, G., Bhattacharya, S., Fitzke, F., *et al.* (1993). Mutations in the human retinal degeneration slow (RDS) gene can cause either retinitis pigmentosa or macular dystrophy. *Nature genetics* 3(3): 213-218.
- Wu, C. and Lu, Y. (2007). Inclusion of high molecular weight dextran in calcium phosphate-mediated transfection significantly improves gene transfer efficiency. *Cellular and molecular biology* 53(4): 67-74.
- Xu, J., Dodd, R. L., Makino, C. L., Simon, M. I., Baylor, D. A. and Chen, J. (1997). Prolonged photoresponses in transgenic mouse rods lacking arrestin. *Nature* 389(6650): 505-509.
- Zacharias, D. A., Violin, J. D., Newton, A. C. and Tsien, R. Y. (2002). Partitioning of lipid-modified monomeric GFPs into membrane microdomains of live cells. *Science* 296(5569): 913-916.
- Zhang, Y., Molday, L. L., Molday, R. S., Sarfare, S. S., Woodruff, M. L., Fain, G. L., Kraft, T. W. and Pittler, S. J. (2009). Knockout of GARPs and the beta-subunit of the rod cGMP-gated channel disrupts disk morphogenesis and rod outer segment structural integrity. *Journal of cell science* 122(Pt 8): 1192-1200.

## 6.2 Own publications

**Nguyen O. N. P.**, Böhm S., Gießl A., Butz E. S., Wolfrum U., Brandstätter J. H., Wahl-Schott C., Biel M. and Becirovic E. (2016). Peripherin-2 differentially interacts with cone opsins in outer segments of cone photoreceptors. Accepted in Human molecular genetics.

Becirovic, E., Böhm, S., **Nguyen, O. N. P.**, Riedmayr, L. M., Koch, M. A., Schulze, E., Kohl, S., Borsch, O., Santos-Ferreira, T., Ader, M., *et al.* (2016). In vivo analysis of disease-associated point mutations unveils profound differences in mRNA splicing of peripherin-2 in rod and cone photoreceptors. PLoS genetics 12(1): e1005811.

Becirovic, E.\*, **Nguyen O. N. P.\***, Paparizos, C., Butz, E. S., Stern-Schneider, G., Wolfrum, U., Hauck, S. M., Ueffing, M., Wahl-Schott, C., Michalakis, S., *et al.* (2014). Peripherin-2 couples rhodopsin to the CNG channel in outer segments of rod photoreceptors. Human molecular genetics 23(22): 5989-5997.

\*contributed equally

Publications in preparation:

Becirovic E.\*, **Nguyen O. N. P.\***, Butz E. S., Schulze E., Paparizos C., Wahl-Schott C., Biel M. and Michalakis S. FRET-based analysis of protein-protein interactions and binding characteristics in murine rod outer segments.

\*contributed equally

## 7 Appendix

### 7.1 List of primers used for cloning and sequencing

Primers for cloning of truncated Prph2 constructs	
Prph2_ΔCT_NotI_R	GATCGCGGCCGCGAGTCCGGCAGTGATGCTCAC
Prph2_toTM4_F	CAGCAGCCTCATGAATTCCTAGGGCGTCGTCACACTTCTCG
Prph2_toTM4_R	CGAGAAGTGTGACGACGCCCTAGGAATTCATGAGGCTGCTG
Primers for introduction of mPrph2 or hPRPH2 mutations	
mPrph2_G266D_F	CTCATGAATTCCATGGACGTCGTCACACTTCTC
mPrph2_G266D_R	GAGAAGTGTGACGACGTCCATGGAATTCATGAG
mPrph2_G266A_F	CTCATGAATTCCATGGCCGTCGTCACACTTCTC
mPrph2_G266A_R	GAGAAGTGTGACGACGCCATGGAATTCATGAG
mPrph2_E276A_F	CTCGTCTGGCTCTTTGCGGTGAGCATCACTGCC
mPrph2_E276A_R	GGCAGTGATGCTCACCCCAAAGAGCCAGACGAG
mPrph2_V268I_F	GAATTCCATGGGCGTCATCACACTTCTCGTCTG
mPrph2_V268I_R	CAGACGAGAAGTGTGATGACGCCCATGGAATTC

Introduced point mutations are marked in red.

## 7.2 List of CNGB1a-binding proteins identified via LC-MS/MS

Protein/peptide name
Hbb-b2 MGI (curated) Hemoglobin subunit beta-1
<b>Cnga1 MGI (curated) cGMP-gated cation channel alpha-1</b>
<b>Cngb1 MGI (curated) Cngb1 protein Fragment</b>
<b>Rho MGI (automatic) Rhodopsin</b>
AC164613.3 Clone-based
Rpl10a MGI (curated) 60S ribosomal protein L10a
Rpl7 MGI (curated) 60S ribosomal protein L7
Rps11 MGI (automatic) 40S ribosomal protein S11
Rpl6 MGI (curated) 60S ribosomal protein L6
<b>GARP BC016201 MGI (automatic) hypothetical protein LOC234586</b>
Rpl37a MGI (automatic) 60S ribosomal protein L37a
Rps8 MGI (curated) 40S ribosomal protein S8
Rpl35a MGI (curated) 60S ribosomal protein L35a
Purb MGI (curated) Transcriptional activator protein Pur-beta
Rpl8 MGI (automatic) 60S ribosomal protein L8
Glul MGI (curated) Glutamine synthetase
Rpl13 MGI (curated) 60S ribosomal protein L13
Rps18 MGI (automatic) 40S ribosomal protein S18
AC147018.4 Clone-based
Rps23 MGI (automatic) 40S ribosomal protein S23
Rpl27a MGI (curated) ribosomal protein L27a
Rpl36a MGI (curated) 60S ribosomal protein L36a
Rpl10 MGI (curated) 60S ribosomal protein L10
Rpl38 MGI (curated) 60S ribosomal protein L38
Vdac1 MGI (curated) Voltage-dependent anion-selective channel protein 1
Atp1a3 MGI (curated) Sodium/potassium-transporting ATPase subunit alpha-3
<b>Prph2 MGI (automatic) Peripherin-2 (Retinal degeneration slow protein)</b>
Syt1 MGI (curated) Synaptotagmin-1
Rpl22 MGI (curated) 60S ribosomal protein L22
AC155934.2-1 Clone-based

Shown are the first 30 hits from the analysis. Proteins used for subsequent analyses are marked in red.

### 7.3 Abbreviations

$\alpha$	anti-
adRP	autosomal-dominant retinitis pigmentosa
ALAS	aminolevulinic acid synthase
Amp <sup>R</sup>	ampicillin resistance gene
APS	ammonium persulfate
B1-/-	CNGB1 knockout
B1a	CNGB1a channel subunit
2x BBS	2x BES buffered saline
BES	<i>N,N</i> -bis[2-hydroxyethyl]-2-aminoethanesulfonic acid
BGH	bovine growth hormone
bp	base pairs
CaCl <sub>2</sub>	calcium chloride
cAMP	cyclic adenosine monophosphate
cap	packaging gene
cGMP	cyclic guanosine monophosphate
cm	centimeter
CMV	cytomegalovirus
CNBD	cyclic nucleotide-binding domain
CNG	cyclic nucleotide-gated
CO <sub>2</sub>	carbon dioxide
ColE1	colicinogenic factor
co-IP	co-immunoprecipitation
C <sub>p</sub>	crossing points value
cP-mg	cone-specific promoter minigene
dk	donkey
DS	splice donor site
DTT	dithiothreitol
EDTA	ethylenediaminetetraacetic acid
ESE	exonic splice enhancer
ESS	exonic splice silencer
F	phenylalanine
f1	filamentous phage
FACS	fluorescence-activated cell sorting

FBS	fetal bovine serum
FRET	Förster/fluorescence resonance energy transfer
g	gram
<i>g</i>	gravity
GCAPs	guanylate cyclase-activating proteins
GCL	ganglion cell layer
GARP	glutamic acid-rich protein
gt	goat
GC-E	guanylyl cyclase E
GC-F	guanylyl cyclase F
GPCR	G protein-coupled receptor
h	hour
H <sub>2</sub> O	water
HCl	hydrochloric acid
hRHO	human rhodopsin promoter
INL	inner nuclear layer
IPL	inner plexiform layer
ITR	inverted terminal repeat
kb	kilobase pairs
KCl	potassium chloride
KO	knockout
l	liter
L-opsin	long wavelength-sensitive cone opsin
MCS	multiple cloning site
µg	microgram
MgCl <sub>2</sub>	magnesium chloride
min	minute
ml	milliliter
µl	microliter
µm	micrometer
M-opsin	medium wavelength-sensitive cone opsin
ms	mouse
msec	millisecond
mSWS	murine short-wavelength opsin promoter
mV	millivolt
MW	molecular weight

Neo <sup>R</sup>	neomycin resistance gene
ng	nanogram
nm	nanometer
NMD	nonsense-mediated mRNA decay
ONL	outer nuclear layer
OPL	outer plexiform layer
ori	origin of replication
OS	outer segments
pA	polyadenylation signal
PAGE	polyacrylamide gel electrophoresis
PB	phosphate buffer
PBS	phosphate buffered saline
PCR	polymerase chain reaction
PDE6	cGMP phosphodiesterase 6
PFA	paraformaldehyde
PMMA	Poly(methyl methacrylate)
Prph2/PRPH2	peripherin-2
PVDF	polyvinylidene fluoride
qRT-PCR	quantitative real-time PCR
rAAV	recombinant adeno-associated virus
rb	rabbit
rep	replication gene
Rh*	metarhodopsin II
Rho	rhodopsin
rpm	rounds per minute
rP-mg	rod-specific promoter minigene
RT	room temperature
SDS	sodium dodecylsulfate
SE	standard error
sec	second
S-opsin	short wavelength-sensitive cone opsin
SV40	simian virus
TBE	tris buffered EDTA
TEMED	tetramethylethylenediamine
TM4	fourth transmembrane domain
UV	ultraviolet

V	volt
v/v	volume concentration
W	watt
WPRE	woodchuck hepatitis virus posttranscriptional regulatory element
WT	wild-type
w/v	mass concentration
Y	tyrosine
YF	mutation substituting tyrosine with phenylalanine

## 7.4 Danksagung

Mein größter Dank gilt meiner Familie, insbesondere meiner lieben Mutter, die mich immerzu unterstützt hat. Ihre anspornende, zugleich hingebungsvolle Art und auch ihre fabelhaften Kochkünste haben mich durch Schule und Studium begleitet und nicht zuletzt meinen bisherigen wissenschaftlichen Werdegang ermöglicht. Ich hoffe, dass ich in Zukunft diese großartige Unterstützung meiner Familie wieder zurückgeben kann.

Auch möchte ich meinem Betreuer Elvir Becirovic von ganzem Herzen danken, dass er mir immer, in guten wie in schwierigen Zeiten, mit seiner Expertise wie auch mit seinen aufbauenden Worten beistand. Die Zusammenarbeit war eine ausnahmslos positive Erfahrung für mich, ich hatte viel Spaß an den Projekten, mir wurde sehr viel experimentelles Know-how vermittelt, und ich gewöhnte mir mit der Zeit einen besonderen Sinn für Humor an, mit dem man immer noch über tausend negative Klone lachen konnte (einer geht noch!). Wer kann außerdem behaupten, dass Witze an der Laborbench zur täglichen Basis gehören und der Betreuer einen mit einem unverkennbaren Klang (Phuooong!!!) herbeiruft. In diesem Sinne nochmals danke dir, Elvir für die unvergessliche Zeit hier.

Herrn Professor Biel möchte ich herzlich für die wissenschaftlichen Ratschläge und insbesondere für die Möglichkeit danken, meine Arbeit in seinem Arbeitskreis anfertigen zu dürfen. Ferner gilt mein Dank auch Verena Hammelmann, Christian „Schöni“ Schön, Stylianos „Stelios“ Michalakis und Christian „Prakti“ Gruner, die mir viele Versuchsmethoden vermittelt haben. Des Weiteren möchte ich Herrn Andreas Gießl für die Anfertigung der schönen TEM-Bilder sowie Frau Stefanie Hauck für die LC-MS/MS Daten vielmals danken.

Ebenfalls danken möchte ich auch Sybille für das harmonische Teamwork bei den vielen gemeinsamen Experimenten und Projekten. Ich bin mir absolut sicher, dass du und Lisa weiterhin mit Elvir ein grandioses Team bildet und gemeinsam spannende Projekte auf Papier bannen werdet. Euch beiden wünsche ich viel Erfolg für die weitere PhD Zeit. Mein besonderer Dank gilt auch Berit, die mich stets bei meinen Experimenten unterstützt hat. Die Zeit, die wir im Labor Rücken an Rücken verbracht haben, werde ich sehr vermissen.

Im Großen und Ganzen hat die gemeinsame Zeit mit meinen Kollegen einen stets positiven Einfluss auf meine bisherige Arbeit gehabt, das erheiternde und oftmals witzige Klima war der Grund, weshalb ich selbst nach auslaugenden Experimenten meinen Optimismus nicht

verloren habe und mit einem Lächeln den nächsten Versuch angehen konnte. Der rege Ideenaustausch und die lustigen After-Work-Unternehmungen, wie etwa unsere kulinarischen Entdeckungstouren und (Kinder-) Punchabende in der Teeküche, werden mir gut in Erinnerung bleiben. Zu guter Letzt möchte ich mich herzlich bei allen Arbeitskollegen für die wirklich schöne Zeit bedanken und auch, dass sie meinen oftmals schrägen und rauen Humor gut aufgenommen haben. Euch wünsche ich weiterhin alles Gute für die Zukunft.